NEUROLOGICALLY BASED CONTROL FOR

QUADRUPED WALKING

by

ALEXANDER JACOB HUNT

Submitted in partial fulfillment of the requirements

for the degree of Doctor of Philosophy

Department of Mechanical and Aerospace Engineering

CASE WESTERN RESERVE UNIVERSITY

January, 2016

CASE WESTERN RESERVE UNIVERSITY

SCHOOL OF GRADUATE STUDIES

We hereby approve the dissertation of

Alexander Jacob Hunt

candidate for the degree of **Doctor of Philosophy***.

Committee Chair

Dr. Roger Quinn (EMAE)

Committee Member

Dr. Joseph Mansour

Committee Member

Dr. Kiju Lee

Committee Member

Dr. Hillel Chiel

Date of Defense

September 24 2015

*We also certify that written approval has been obtained

for any proprietary material contained therein.

Contents

List of Tables

List of Figures

Acknowledgments

I would like to thank my family, first and foremost for always pushing me to be better and work harder. This includes my parents Dan and Maggi, my brothers Jeff and Tyler, and sister Emily. Also my new, immediate family of Liz and Amelia, pushing me to finish as fast as possible!

A big thank you and acknowledgment to my partner in crime, Nicholas Szczecinski. Not only did he contribute the backbone to the low level control chapter by building the optimization routines which I used, but his parallel work in insect systems proved to be invaluable, and my project would have taken on a very different shape without him. Our (almost daily) discussions and musing on the organization of the neural system and purpose of different pathways led me to a much deeper understanding of how animals (both insects and mammals) walk, and allowed me to explore and apply numerous different ideas I would never have come up with on my own.

Not just Nick, but the entire biorobotics lab has been extremely helpful, and the collaborative environment has made this dissertation at least 10x better and more useful than it would have been otherwise. Beginning this project with the other member of the 'A Team': Alex Lonsberry, Vickie Webster, and Brian Mirletz and working the parallel tracks with them, being able to bounce ideas off them, learn interesting new facts about larger spiking networks, muscles and the physical systems, and adaptive CPG control, simulations, and optimization along different routes.

List of Acronyms

CO chordotonal organ.

CPG central pattern generator.

CS campaniform sensilla.

RG rhythm generating.

Neurologically Based Control For Quadruped Walking

Abstract

by

ALEXANDER JACOB HUNT

Current robotic control methods take advantage of high computing power to compute trajectories and perform optimal movements for a given task, yet these robots still fall far short of their animal counterparts when interacting with the environment. Animals dynamically adapt to varying terrain and small perturbations almost effortlessly. In order to improve our robotic systems and build better control methods, it makes sense to look more closely at how animals solve this interaction. In this work, I developed a control model of mammalian walking with models grounded in neuroscience and computational neuroscience. First, I developed a neuromechanical model of a rat with 14 degrees of freedom and 28 muscles, and I explored how hypothesized neural architectures can be used to coordinate four limbs in a walking gait for a rat. Additionally, through simulated ablation experiments, I developed hypotheses on how inter-leg pathways work together to maintain limb timing. After this, I developed a procedure to train the neural system to produce dynamic walking in both a rat simulation and a robot named Puppy. This method works by first using a model of the system (rat or robot) to determine required motor neuron activations to produce stable walking. For the robot, this required building a force-length-pressure model of the McKibben actuators to enable accurate force control. Parameters in the neural system are then set such that it produces similar activations to the desired pattern. I applied the same training procedure to both the simulated rat and the robot and show that it is capable of producing continuous, self-supported stepping in both systems.

Chapter 1

Introduction

To anyone who watched the recent DARPA Robotics Challenge (DRC), it is very apparent that roboticists still have a long way to go before we can get robots to robustly walk in dynamic situations. Controlling complex robots using traditional control methods with on-line optimization and 'single brain' control becomes increasingly difficult and computationally intensive as more degrees of freedom and more points of contact are added. This is in stark contrast with the animal kingdom, in which high redundancy is the norm, and complex interactions with the environment are often accomplished with ease. For example, having more feet on the ground makes an individual animals' control and balance easier, rather than harder. Big or small, it takes little mental effort on the part of the animal to change from fast speeds to slow speeds, change gaits, start turning, step over an object, respond to a ground slip, or move from concrete to loose dirt.

Unfortunately, animals are immensely complex, and the majority of our current robots barely resemble any animals in the world today. Instead of muscles for actuation, our most agile robots use electric motors [Seok et al., 2015] or hydraulics [Raibert et al., 2008, Semini, 2010]. For determining body states and sensing the world, they rely on a few strategically placed sensors instead of an animal's wide net of somatic

sensory neurons spread across its whole body. For control, instead of a highly distributed and hierarchical network of neurons, a single algorithm is often used to calculate the exact position of each joint needs to maintain stability and provide locomotion.

All this is beginning to change however, as researchers are uncovering how neural systems provide advantages to moving around in the world. The compliant nature of muscles can automatically reject perturbations and significantly reduce the burden on the control system [Loeb et al., 1999, Jindrich and Full, 2002]. Researchers are beginning to build actuators which add compliance and greater control of force [Schilling et al., 2013b, Thorson and Caldwell, 2011, Pratt and Williamson, 1995, Rollinson et al., 2013] . The large number of sensory neurons allow for both high specificity in knowing exactly where a contact occurs and how strong it is, and redundancy, so that if a sensor were to malfunction and give incorrect information for a time, it can be ignored. The distributed nature of the neural control is capable of rapidly compiling all the sensory information to build a picture of the world and adjust control actions at any level of the hierarchy to reject perturbations and continue with the overall goals of the system. To this end, more distributed control networks capable of overcoming significant changes to the system have been developed [Rutter et al., 2011, von Twickel et al., 2011, Schilling et al., 2013a].

However, these controllers are based on studies of insects, and to build more effective, dynamic robot controllers, it may be useful to look at creatures which are approximately the same size as the robots we are building. Animals such as rats, cats, and dogs have two major differences that separate their locomotion strategies compared to that of insects. First, cockroaches and other insects have a wide stance relative to their bodies, and a minimum of three legs on the ground stabilizing their bodies during normal locomotion [Ting et al., 1994], while larger animals walk with legs underneath the body to take advantage of better energetics; however, the more

upright posture makes balance more difficult [Biewener, 2005]. Second, insect muscles are highly damped, making inertial forces from the leg small by comparison, requiring different control strategies and activation patterns than in mammals [Hooper, 2012, Zakotnik et al., 2006].

Though modeling of vertebrate systems is more limited, significant headway is being made. Rats, mice, and cats are often studied for their genetic manipulability and convenient size. Models of these animals include those of muscles [Zajac, 1989, Johnson et al., 2008], kinematic and dynamic movements [Andrada et al., 2013, Witte et al., 2001], the behavior and connectivity of the neural systems involved in locomotion [Zhong et al., 2012], and network pathways which influence stepping transitions of a neuromechanical simulation [Ekeberg and Pearson, 2005]. However, animals are both neural and mechanical walking systems, and before this work, there was not yet a model which combined both a full neural model with a full mechanical model or physical robot to test theories in mammalian locomotion and build better walking machines.

This work expanded upon these modeling efforts and tested the validity of using neural control for use in dynamic robotics. This was done by using neural models of mammalian locomotion systems to control simulations of a rat as well as a dog shaped robot. While doing this work, I attempted to use as much of the neural connectivity that is known in mammalian systems, and then trained the parameters of the system to produce the desired output: forward walking.

Chapter 2 provides a background for the developed models and systems. I outline what is known about the connectivity and sensory influences for walking in mammals and how these sensory influences work together to produce steps and a stable gait. I also discuss the different modeling environments and robot system which were explored in this work. This chapter concludes with the different modeling decisions made and what effect these decisions may have on the results.

Chapter 3 discusses the first leg of the journey, in which network architecture for producing walking in a four legged animal is explored. The connectivity networks were developed based on behavioral and reduced preparation experiments on mice and cats. This connectivity network proved to be sufficient for producing stepping motions in the model by coordinating 14 joints in a rat model into a walking gait. With this model, I explored how changes in these inter-leg pathways could affect gait behavior. This work won 'best paper' at Living Machines 2014 [Hunt et al., 2014] and was expanded upon in an invited paper to Bioinspiration and Biomimetics [Hunt et al., 2015a].

However, this work required hand tuning of individual parameters, and as it progressed it became apparent that new tools and methods needed to be developed to speed development and produce more reliable behavior. The first problem to solve is what exactly is our network trying to output? Chapter 4 outlines the development of motor neuron (MN) activations for two systems, a rat simulation and the lab's Puppy robot. Determining MN activations for the simulated rat was relatively straightforward; I directly used kinematic and dynamic data collected from rats and applied them to a carefully constructed rat model. Determining MN activations for the robot however required developing my own kinematic and torque data and developing my own model and control system of the Festo artificial muscle.

With the developed MN activation patterns, I needed to train the networks to mimic the desired activations. Chapter 5 describes the training methods used to set parameters to produce walking motions instead of hand tuning. The backbone of the developed training and optimization methods was produced by Nicholas Szczecinski while I worked to determine the proper training procedure which would ensure reliable results in a network that can be trained off-line to produce walking in a vertebrate or robot model. The results of using this training procedure for the rat was presented at Living Machines 2015 [Hunt et al., 2015b].

Chapter 6 presents results of the walking simulation and robot. I show how the networks trained with the developed routines produce walking in the rat simulation as well as with Puppy. The developed procedure is useful regardless of kinematic and actuator types. I analyze these results and differences between desired and real-time MN activations, tensions, and kinematics. Finally, I summarize the work and develop ideas for future research with the simulation and robot.

Chapter 2

Background

2.1 Neurobiology and Modeled Animal Systems

The neural circuits which accomplish stable standing and walking are difficult to understand because they reside in complex hierarchies which oscillate and interact with each other at different time scales, integrate extraordinary amounts of feedback from sensory information, and control complex, self-exciting motor neurons [ElBasiouny et al., 2010]. The prevailing theory in neurobiology is that hierarchies in the central nervous system sub-divide complex tasks into sub-tasks [Bicanski et al., 2013]. With the brain at the top and motor neurons at the bottom, each level relies on level-appropriate sensory information to predict outcomes at different time-scales and act on the levels below [Kiebel et al., 2008]. Neurological experimentation suggests that a large set of neurons involved in steady state walking are located in the thoracic ganglia for arthropods [Büschges et al., 1995], and the spinal cord for vertebrates [Brown, 1914].

2.1.1 Central Pattern Generators and Control of Repetitive Movements

Subcircuits located in the spinal cord which are responsible for repetitive behaviors such as walking and breathing are central pattern generators (CPGs). These CPGs are capable of oscillating and providing a patterned output either with or without external input. CPGs coordinate complex muscle activations to help the animal achieve proper timing to accomplish a given task. They have been found to be involved in a large variety of movement behaviors including the leech heartbeat [Arbas and Calabrese, 1987], human breathing and gasping [Tryba et al., 2006], lobster digestion [Meyrand et al., 1994], turtle scratching [Mortin and Stein, 1989], and locomotion in stick insects [Bässler and Büschges, 1998], lamprey [Cohen et al., 1992], cats [Brown, 1914], and mice [Hägglund et al., 2013].

Modeling of these circuits show that CPGs can coordinate multiple segments into predictable patterns during locomotion. For example, a set of CPGs that are coupled similarly to that of a lamprey have been shown to produce a traveling wave along the body that provides forward locomotion [Ekeberg, 1993]. This wave can be easily modified by sensory feedback to allow the model to adapt to its surroundings and produce more robust waves [Ekeberg and Grillner, 1999, Ijspeert et al., 1999]. It has also been shown how this CPG system can be expanded to the salamander and produce adaptable locomotion strategies for both water and land [Bicanski et al., 2013].

Experimental evidence in stick insects and crickets show that each joint in these animals has its own individual CPG that coordinates flexion and extension for the joints [Bässler and Büschges, 1998]. To coordinate walking, these CPGs are likely not directly coupled, however their relative timing is coordinated through sensory influences in the muscles and other sensors distributed throughout the leg [Akay and Büschges, 2006]. Models of stick insect walking show how despite no direct coupling

between the CPGs, coordinated walking which is robust to perturbations can be achieved [Ekeberg et al., 2004].

These models are expandable beyond the forward walking models. Increasing the importance of different sensory pathways over others can effectively 'reorganize' the neural system to produce different gaits [Daun-Gruhn, 2010], turning behaviors [Szczecinski et al., 2013], and even step backwards [Tóth et al., 2012]. These modeling efforts have shown how this neural reorganization need be nothing more than changes in the activity level of a single or set of neurons from a higher command center [Tóth et al., 2012, Szczecinski et al., 2013].

Less is known about mammalian CPG organization than insect organization. Early theories hypothesized the existence of a single CPG per leg, driving transitions between stance and swing [Brown, 1914]. However, more recent models utilize multiple oscillating circuits at multiple hierarchical levels [McCrea and Rybak, 2008] supported by recent neurological data [Zhong et al., 2012]. Mammalian CPG systems may look more similar to those in insects than previously hypothesized [Büschges and Borgmann, 2013]. A model of a CPGs coordinated through sensory feedback pathways has been shown to successfully replicate many behaviors in mammalian systems [Markin et al., 2010].

There are still many unanswered questions concerning CPG systems however. How can CPGs provide specific patterned output for walking? How are they organized to correctly time all the muscle activations of the entire leg? How and where do specific sensory signals modify the CPG output?

2.1.2 Sensory Influences on Walking

There is an insufficient amount of scientific data on how sensory neural signals affect walking in the animal kingdom to build a complete model of neural control of walking. It is very difficult to record from individual neurons of live, intact animals as they move

freely in the world, and reduced in vitro preparations effectively eliminate natural sensory feedback. Nevertheless, details of neural organization and sensory feedback pathways for a few animals have begun to emerge, the most prominant of which are the stick insect, cat, and mouse. Because of their evolutionary differences and the amount of data in the field, it can be very useful to compare and contrast the control strategies that emerge in these systems.

Two major categories of sensory nerves have been shown to influence muscle activations in insects and mammals: load detectors and stretch receptors. Load detectors in insects consist of campaniform sensilla (CS) mostly arranged on the proximal portion of each leg segment (where strain is greatest) [Zill et al., 2004]. The CS are able to detect the direction of load and send signals up into the thoracic ganglia. Load is detected in mammals through Ib sensory feedback emanating from Golgi organs within the tendon system of each muscle, effectively recording the amount of force each muscle is experiencing [Jami, 1992]. Chordotonal organ (CO) are stretch receptors attached to the exoskeleton in insects and detect joint positions and velocities [Bässler, 1974]. Again, the mammalian analog is built into the muscular system instead of the skeletal system. Primary and secondary muscle spindles (Ia and II) are parallel to the muscle fibers and detect velocity and length respectively [Boyd, 1980].

Load detection has been found to be very important for initiating changes between stance and swing in insects and mammals. Increased load detected by CS in the femur and trochanter segments of the stick insect encourage stance muscles to activate, while decreased load encourages swing muscles to activate [Akay et al., 2001, Akay et al., 2004]. Trochanter CS coordinate the thoracic-coxa joint while femur CS coordinate the femur-tibia joint. Similarly, it has been found that decreased load in cat legs will encourage swing muscles to activate [Duysens and Pearson, 1980]. However, unlike the stick insect, all joints are coordinated by the golgi tendon organ in the calf muscles.

Load detection influences more than timing. It also affects strength of muscle activation. Tests on stick insects and cockroaches have found that increased strain detected by CS cause higher muscle activations in distal joint extensors and proximal flexors [Zill et al., 2004]. In contrast, type Ib feedback in mammals has state dependent magnitude control. In non-moving animals type Ib feedback has an inhibitory effect on muscles [Duysens et al., 2000]. However, when walking begins Ib feedback becomes excitatory, creating a positive feedback loop [Prochazka et al., 1997].

The femur CO in the stick insect are also important for encouraging joint transitions between extension and flexion and back again [Bässler, 1988, Bucher et al., 2003, Hess and Büschges, 1999]. Similarly in mammals, muscle spindles in the hip joint are responsible for affecting joint transitions in all joints, with increased stretching of hip flexors encouraging the initiation of swing, and increased stretching of extensors encouraging stance initiation [McVea et al., 2005, Pearson, 2008, Akay et al., 2014].

Positive and negative feedback control derived from joint velocity and length feedback also play an important part in activation strength. Flexion sensed in the femur-tibia CO encourages flexion of the coxa-trochanter joint while extension of the femur-tibia CO encourages extension of the coxa-trochanter joint [Hess and Büschges, 1999, Bucher et al., 2003]. However, negative feedback from movement in the coxa-trochanter joint activate muscles opposing the movement [Schmitz, 1986].

Feedback associated with muscle spindles affecting motor neuron activations in mammalian systems is less well understood. Muscles spindles innervate a number of interneurons which are also innervated by many other interneurons, higher level centers, and tendon organs [Jankowska, 1992]. In one verified pathway, Ia feedback from an inactive muscle provides inhibition to antagonistic muscles, reducing activation and slowing movement [Jankowska, 2008].

Models of walking in which sensory signals cause transitions in CPGs or CPG-

like structures have been created for both insects [Ekeberg et al., 2004, Rutter et al., 2011, Schilling et al., 2013a] and cats [Pearson, 2008, Ekeberg and Pearson, 2005]. Some of these models have even been applied to robots. However, no model has combined all these single leg feedback pathways of mammalian locomotion into a single stepping model yet. Before this work, it was unclear whether or not these known pathways are sufficient to produce coordinated stepping within the animal. There was also no model of stepping in the front legs for a mammalian system before this work.

2.1.3 Inter-leg Pathways in Locomotion

To successfully navigate through varied terrain, not only must the joints within a leg be coordinated into stepping motions with proper activations, but individual limbs must be coordinated together as well. Both insects and mammals have neural coordination pathways which directly couple CPG networks together as well as coordination mechanisms which rely on sensory information from other legs. These inter-leg pathways tend to be an order of magnitude weaker than intra-leg connections [Cruse, 1990], and are dominated by local coordination rules when there is conflict [Borgmann et al., 2009].

Most coordination pathways in the stick insect act caudally [Daun-Gruhn, 2010]. This helps ensure that corrections taken by forward legs help influence stepping behavior in the hind legs. What started out as a set of rules based on behavioral observations [Cruse, 1990] has turned into attempts at describing some of these connections with more detailed neurological layouts [Daun-Gruhn and Tóth, 2010]. CPGs are connected by weak inhibitory and excitatory connections which are enhanced by the sensory feedback within the leg. Contralateral connections between legs in the stick insect are significantly weaker, and are dominated by mechanical couplings [Borgmann et al., 2009].

Neuronal connections between contralateral legs in mammals are much more dominant. Commissural interneurons which have been found in mice [Talpalar et al., 2013] and cats [Jankowska, 2008] coordinate front legs in antiphase with one another. These same neurons can be manipulated in mice to coordinate the front legs in phase with each other in a hopping motion as well [Talpalar et al., 2013]. Recent efforts have worked to described these connections with detailed neural modeling [Rybak et al., 2013].

Ipsilateral inter-leg connections have been hypothesized from behavioral mammalian experiments. Akay et al. [Akay et al., 2006] postulate three main coordinating influences between fore and hind legs. Influence 1) Foreleg extension reduces onset of the hind limb hip flexor. Influence 2) The end of activation of the hind limb hip flexor advances activation of forelimb swing. Influence 3) Activation of the forelimb elbow flexors contributes to inhibiting hind limb hip flexors.

Though models of inter-leg pathways have been built for insects, before this work, there was no system to test whether these inter-leg pathways are sufficient to coordinate walking in a four legged mammalian system.

2.2 Rattus norvegicus

The main animal studied and modeled in this work is the Rattus norvegicus, or brown rat. Kinematic and dynamic data were collected by our collaborators in Jena, Germany at the Friederich-Schiller-Universität Jena: Manuela Schmidt, Emanuel Andrada, and Martin Fischer. They took high speed x-ray video and force plate measurements of walking animals; Fig. 2.1 shows a still frame from the x-ray video.

Within each frame, joint positions are marked and angles are measured to produce a kinematic detail of movements during both stance and swing. More details of this process can be found in Appendix A and [Niderschuh et al., 2015]. My collaborators
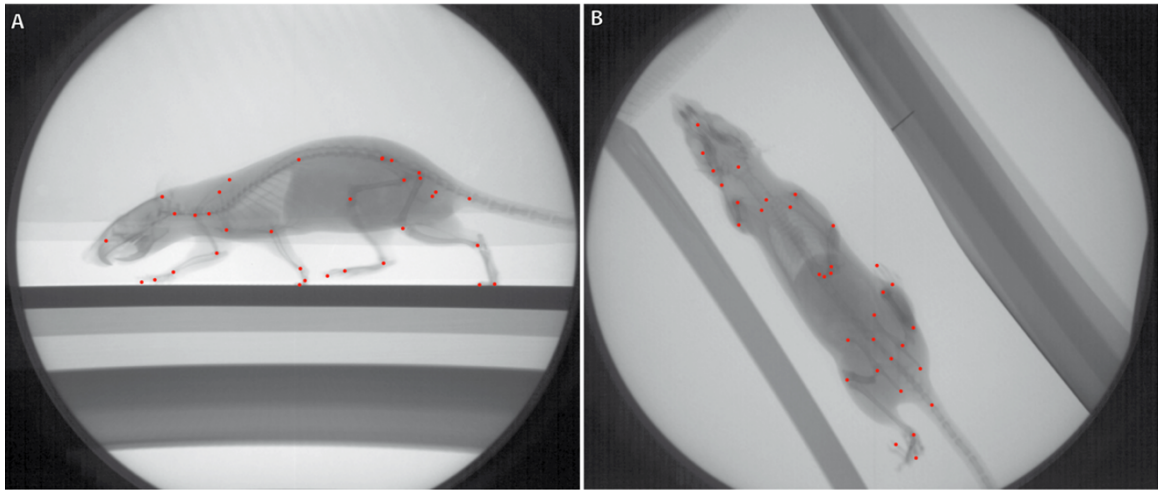
Figure 2.1: Side and overhead view of a walking rat on a treadmill. Joints are marked with red markers and are used to measure the joint angles for each frame.

also combined stance kinematics and force plate data to produce an estimate of the joint torques [Andrada et al., 2013].

2.3 Simulations and Modeling

Many of these neurological measurements suggest hypothetical circuits, and modeling is a useful tool to test how controllers based on these circuits can affect desired behavior [Pearson et al., 2006]. To fully test the system, the model must contain a neural system as well as a mechanical system. Two major simulation environments were pursued in this work: Animatlab (versions 1 and 2), and OpenSim in conjunction with Simulink. Ultimately, the OpenSim/Simulink path was discarded as the physical simulation of the system. Although it is more detailed, simulations ran too slow and did not allow for fast enough turnaround in manipulating variables. Efforts regarding OpenSim and Matlab are described in Appendix B.

2.3.1 Animatlab

Simulation and control were done with Animatlab and Animatlab 2. The simulation is conducted in the Vortex physics engine (CM Labs, Montreal, Quebec) implemented by Animatlab [Cofer et al., 2010]. Rigid body dynamics, ground contact, body collisions, and friction are all simulated. Both the physics and neural system are simulated every 0.1 ms using single step forward Euler integration. The inertia of a solid body is determined by the shape of a triangulated mesh and a given density.

Animatlab 2 added several major features utilized in this work. The first major feature was the ability to export and manipulate standalone simulation files. This allows Matlab to initiate a simulation run, read in relevant information from the developed model, run analysis on the simulation, adjust parameters and repeat. That is, we could build an optimization routine in Matlab which used the simulation engine of Animatlab.

The second major feature is communication with external hardware. Animatlab 2 offers external communication with different hardware systems including Firmata protocols for Arduino communication, XBee Commander for remote control, and a general serial communication protocol. This allowed me to set up communication with the sbRIO and control Puppy using the neural control system developed in Animatlab.

2.3.2 Neural Modeling

The goal of the research was to better understand walking in mammalian systems and be able to apply this knowledge to a four legged, mammal-like robot. To understand mammalian walking I wanted to build a neural system which is able to capture important dynamic characteristics of the nervous system. The use of dynamic neurons provides useful time-based filtering capabilities, and conductance based neural models enable the addition of ion channels that produce more dynamic and interesting

behaviors.

This work is built on the dynamics of a leaky integrator. The leaky integrator captures the most basic behavior of neurons and allows more complex behaviors to be built on top of it. It is capable of modeling individual non-spiking interneurons, the firing rate of a population of neurons, or a single spiking neuron after a spiking threshold is included. My work is not concerned with the specifics on how action potentials are generated and have left out Hodgkin-Huxley sodium and potassium currents, though this type of neuron could be injected into the middle of the system without modification to the modeling environment. Instead, I was concerned with how signals propagate through the network, and how individual neurons and populations of neurons activate, deactivate, and contribute to network behavior. Each neuron is governed by the equation:

$$C_m \frac{dV}{dt} = g_L \cdot (E_L - V) + I_{ext} + I_{ions} \tag{2.1}$$

where V is the membrane potential, C_m is the membrane capacitance, E_L is the leak potential, g_L is the leak conductance, I_{ext} are the external synaptic and injected current inputs and I_{ions} are additional ionic currents that can be added to increase the complexity of behaviors of particular neurons (e.g. the calcium or sodium current in the rhythm generating neurons in equation 2.4). Constants such as C_m, g_L, and E_L are based on typical spinal cord interneuron values, but may be more directly implemented with known values when knowledge of them is made available. This limits the number of free parameters in the network and allows us to focus on the strength and types of connections between neurons. When the neuron voltage goes up, it becomes more active and transmits more information to 'downstream neurons' via synapses. The synapse model is:

$$I_{syn} = g_{syn} \cdot (E_{syn} - V_{post}) \tag{2.2}$$

where E_{syn} is the potential of the synapse, and V_{post} is the postsynaptic membrane potential. When E_{syn} is above V_{post}, it is said to be an excitatory synapse and drives the voltage of the neuron higher and less negative. When E_{syn} is below V_{post}, it is said to be an inhibitory synapse and drives the voltage of the neuron lower and more negative. All E_{syn} values in this model are set such that they are either excitatory or inhibitory at all times. The value g_{syn} is a piecewise linear activation function defined as

$$g_{syn} = g_{max} \cdot min\left(max\left(\frac{V_{pre} - E_{lo}}{E_{hi} - E_{lo}}, 0 \right), 1 \right) \qquad (2.3)$$

where g_{max} is a user defined maximum conductance, V_{pre} is the presynaptic membrane potential, and E_{lo} and E_{hi} are the two user-defined voltage threshold values that define the piecewise-linear function where $E_{lo} < E_{hi}$. The above model is also capable of representing the activation of a population of neurons with the same type of synapse where the population activity varies between 0 when $V_{pre} < E_{lo}$ and g_{max} when $V_{pre} = E_{hi}$. Most neurons used in this model are used in this way and represent average voltage values of a population, similar to those of other networks that model mammalian walking behaviors [Markin et al., 2010, Daun-Gruhn, 2010].

This neural model offers many advantages. Because the model is biologically based, it is expandable and not limited to the currently modeled system. Known neural pathways and ionic currents that influence locomotor behavior can be implemented directly into the model, several of which are described in Chapter 3. These additional currents and properties that present a significant impact on the behavior of a particular area of the neural system may be added to individual neurons appropriately without further increasing the complexity of the rest of the system. One particular area of relevance to our study is how a set of neurons can produce a pattern generating behavior. During initial work with the network architecture experimentation, I included calcium channels in the rhythm generating (RG) neurons

that contribute to active bursting phases. Continued work revised this model to that of persistent sodium ion channels based on work done with the mouse locomotory system [Zhong et al., 2012]. The sodium and calcium currents, I_{Ion}, are defined as:

$$I_{Ion} = g_{Ion} \cdot m\left(V\right) \cdot h\left(V\right) \cdot \left(E_{Ion} - V\right) \tag{2.4}$$

$$\frac{dm}{dt} = \frac{m_\infty(V) - m}{\tau_m(V)} \qquad \frac{dh}{dt} = \frac{h_\infty(V) - h}{\tau_h(V)} \tag{2.5}$$

where E_{Na} is the equilibrium channel voltage for the particular ion, g_{Ion} is the conductance and $\tau_m(V) = \phi_m \sqrt{\epsilon_m(V)}$ and $\tau_h(V) = \phi_h \sqrt{\epsilon_h(V)}$. The functions $m_\infty(V) = \frac{1}{1+\epsilon_m(V)}$ and $h_\infty(V) = \frac{1}{1+\epsilon_h(V)}$ are sigmoids, where $\epsilon_m(V) = exp(-S_m \cdot (V_m - V))$ and $\epsilon_h(V) = exp(-S_h \cdot (V_h - V))$. $\phi_m, \phi_h, S_m, S_h, V_m$ and V_h are constants. For each instance of ion use, m_∞ and h_∞ values were adjusted to match with other CPG models developed in the field [Daun-Gruhn and Büschges, 2011, Markin et al., 2010]. By starting with a relatively simple model, I was able to lay out the basic structure of the network in a tractable manner and through the use of biologically based neurons the complexity could be increase where necessary. Higher levels of complexity can lead to the emergence of more capable and dynamic behaviors [Daun-Gruhn and Büschges, 2011].

2.3.3 Animal Modeling

The biomechanical model was constructed with scans of rat bones which were digitally matched to a rat walking up a rope using 3D x-ray high speed video. The model reconstruction was limited to motion in the sagittal plane, resulting in a total of 14 degrees of freedom, four for each front leg (scapula, shoulder, elbow, and wrist) and three for each hind leg (hip, knee, and ankle). To reduce the control problem to systems which coordinate the joints and match the experimental setup in which
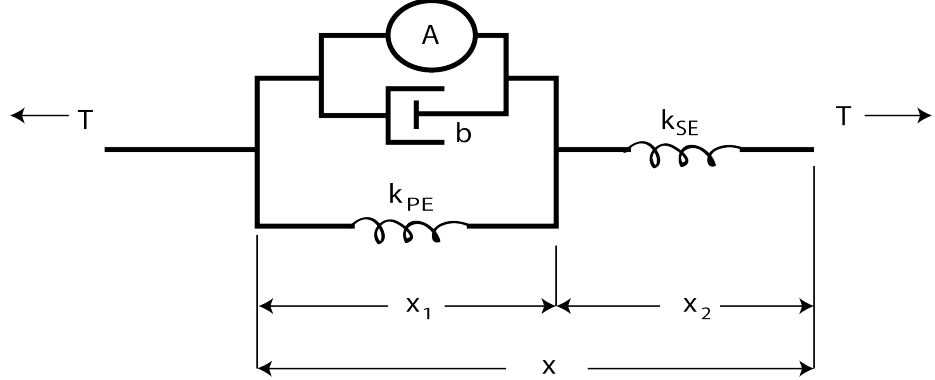
Figure 2.2: Hill Muscle Model

the ipsilateral coordination rules were developed [Akay et al., 2006], body weight is supported at the hip, which is kept 6.5 cm above the ground. A linear Hill muscle model generates forces about each joint within the rat model [Cofer et al., 2010] and is illustrated in Figure 2.2.

Tension, T, is developed in the muscle according to:

$$\frac{dT}{dt} = \frac{k_{se}}{b}\left(k_{pe}x + b\dot{x} - \left(1 + \frac{k_{pe}}{k_{se}}\right) \cdot T + A\right) \tag{2.6}$$

where x is the muscle length, k_{se} and k_{pe} are the series and parallel stiffness, b is the damping element, and A is the activation level of the muscle described by:

$$A = A_m * A_l \tag{2.7}$$

where A_m is the sigmoid adapter equation

$$A_m = \frac{F_{max}}{1 + e^{C(V_o - V)} + B} \tag{2.8}$$

where F_{max} is the maximum muscle force, C describes the slope of the sigmoid, V is the membrane voltage of the motor neuron, and V_o and B describe the V and F

offsets of the sigmoid. A_l is the length-tension relationship described by

$$A_l = 1 - \frac{(l - l_{rest})^2}{l_{width}^2} \tag{2.9}$$

where l_{rest} describes the length at which the muscle can provide the most force and l_{width} describes the length from l_{rest} at which the muscle can provide no force.

Muscles are chosen as the activation method for two main reasons. First, it is likely that some aspects of the control system are tuned directly to the mechanical properties inherent in muscles. For example, the length-tension relationship promotes stability of positive force feedback pathways [Prochazka et al., 1997]. Other properties which could prove important are self-limiting velocity-tension, and physiological delays in tension development. Second, actuator compliance is an important part of achieving robust motions that can reject perturbations passively. To reduce the control problem, each joint is actuated by two antagonistic muscles and biarticular muscles are omitted. Biarticular muscles act mainly to counterbalance gravity [Fischer, 1999, Goslow et al., 1981] and serve to reduce energy consumption [Kuznetsov, 1995]. Their addition to the model would add complexity with little benefit to studying pathways that affect intra- and inter-limb timing but their inclusion in future models could prove beneficial. Muscle properties were set to produce the desired torques calculated by Witte et al. while maintaining stability of motion [Witte et al., 2002].

Sensory feedback in the model is similar to types Ia, Ib, and II in mammalian systems, and although simplified representations of nature, they contain important elements.

$$\text{Ia} = k_a x_2 \qquad \text{Ib} = k_b T \qquad \text{II} = k_c x_1 \tag{2.10}$$

where k_a, k_b, and k_c are gain parameters set by the user to act as injected current into a neuron. The series elastic spring length, x_2, is sensitive to velocity as well as

total muscle length because the dashpot in the parallel element causes the parallel element to change lengths at a slower rate than the series spring. The length of the series spring is used to stimulate Ia feedback, known to be dependent on both length and velocity in animals. Ib feedback is dependent on the tension developed in the muscle, and type II feedback is dependent on length through measurement of the parallel elastic element x_1. The gains were experimentally adjusted to produce an injected current which gives usable information through a sensory neuron across the full range of muscle lengths and contractions.

Muscle parameters are approximated based on data from rats when available, and otherwise from other mammals. Muscle attachments are based on the main antagonistic muscles that actuate each joint [Johnson et al., 2008]. The resting length x_{rest} is set to the maximum length of each muscle, causing muscles to get stronger as they elongate [Zajac, 1989], and x_{width} is set such that the muscles exert 70% of their maximum force when fully contracted [Pearson et al., 2006]. Maximum muscle force A_{max} is set by finding maximum foot forces for several positions of the foot during a step cycle from the full muscled Johnson model [Johnson et al., 2008], and performing inverse analysis to find maximum joint torques. Muscle attachments in our model are then used to find the muscle forces needed to apply these maximum joint torques. Muscle damping c is set to the ratio between maximum muscle force and maximum muscle velocity [Johnson et al., 2008]. Series stiffness is set according to data from [Pearson et al., 2006], and parallel stiffness is set such that the muscle deflects 4% of its total length under maximum load [Meijer et al., 1998].

2.4 Robot Control

2.4.1 Bioinspired Walking Robot Controllers

Ever since there were mobile robots, researchers have been taking inspiration from neurobiology to control them [Walter, 1950]. However, it was not until the early 1990s that neural control systems were effectively used to control walking robots, when it became evident that distributed control systems offered significant robustness and reduced complexity compared to more classic control systems [Brooks, 1989]. Robot I from the Biorobotic's lab at Case Western Reserve University was one of the first robots to use a distributed neural control system [Beer et al., 1992]. The controller for this robot was capable of producing a variety of different walking gaits and was robust to a variety of sensory and central lesions [Beer et al., 1989, Chiel and Beer, 1989]. The distributed nature of this control system allowed it to generate a large variety of gaits more continuously than other robot controllers [Beer et al., 1992]. Additionally, another walking controller for this robot was produced by use of a genetic algorithm, evolving the control system as has occurred with natural selection in the real world [Beer and Gallagher, 1992, Gallagher et al., 1996].

Robot II, built on the same control system ideals as Robot I, added an additional degree of freedom per leg and specific local leg reflexes such as an elevator reflex and ground searching [Espenschied et al., 1996]. These additional reflexes garnered from neuroethology enabled the robot to more dynamically respond to its environment, overcoming obstacles and responding to mechanical perturbations in a decidedly animal-like way. This controller was readily expandable to an eight legged robot, K^2T, and the addition of a 'free stroke' reflex and posture control enabled more efficient energy transfer between legs and better locomotion over rough terrain [Flannigan et al., 1998].

For some time after this, biologically inspired controllers tended to simplify the

neural aspects, attempting to draw more inspiration from behavior than the structure of the neural systems underlying them. Simplified CPGs which were more tractable to manipulate than the pacemaker neurons of the above systems became more common as they were used to control swimming and walking robots. Ijspeert has an excellent review on the growth of CPG use in robotics [Ijspeert, 2008]. The Ijspeert lab has successfully implemented adaptive CPG-like controllers for walking on a salamander robot [Ijspeert, 2001] as well as a small quadruped robot [Buchli and Ijspeert, 2008]. Controllers utilizing CPGs and reflexive pathways have been shown to robustly adjust to perturbations by maintaining locomotion rhythms and improving control at different speeds when compared to purely reflexive controllers [Klein and Lewis, 2012, Dzeladini et al., 2014].

Non-dynamic CPGs acting as finite state controllers have also produced adaptive walking rhythms. Walknet, one such simplified controller, is composed of a modular artificial neural network in which the CPGs act as gating mechanisms which switch low level control between target swing or stance [Schilling et al., 2013a]. The CPGs are gated by different sensory feedback parameters and the different neurons are characterized by piecewise linear activation functions and dynamic properties are added into the system as needed. The decentralized architecture of Walknet has been succesfully implemented on the robot Hector, where it enables the robot to walk across uneven terrain, reflexively step onto a platform, and maintain body height over different terrain heights [Paskarbeit et al., 2015]. LegConNet or SCASM, developed in the Biorobotics Lab at Case Western Reserve University in conjunction with collaborators at the University of Cologne, uses sensory signals and timeout procedures to reflexively adjust stepping behavior to different terrains as well [Rutter et al., 2007]. This work also demonstrated how descending commands can be used to create smooth behavioral transitions with this modular architecture [Rutter et al., 2011].

The first robot to use a sensory modulated CPG based neural control system built

of dynamic, spiking neurons to control a walking robot is Achilles, built at the Robotic and Neural Systems lab at the University of Arizona [Klein and Lewis, 2012]. This robot uses a two neuron CPG model for each leg, and shows how the CPG is entrained to the natural walking cycle of the leg. They show how the neural system is sufficient for producing steps and the CPG helps the system reject external perturbations.

2.4.2   Festo Air Muscles

Though muscles are inefficient compared to most robot actuators (electric motors, hydraulic cylinders, etc.) [Alexander, 2003], animal control of muscles has resulted in more efficient and agile locomotion over a wide variety of terrains than any legged robot to date. Although muscles are not efficient by themselves, in combination with tendons, they create a compliant actuation system with many advantages. Compliance allows energy to be stored and returned to the system during repetitive tasks such as walking. Joints with built in compliance are also able to conform to the surrounding environment. This makes them safer than non-compliant actuators without complex control by absorbing inaccuracies within the compliance. The compliant structure of the muscular system also requires less energy to maintain stability when suddenly perturbed [Jindrich and Full, 2002, Loeb et al., 1999]. Series elastic actuators are one such actuator that has been effectively used on many walking robots to simplify control and produce more robust walking [Pratt and Williamson, 1995].

Another advantage to muscular systems is that this compliance can be varied by activating antagonistic muscles [Blickhan, 1989]. This variable compliance allows joints to be tuned to work more effectively for a variety of speeds [McMahon and Cheng, 1990] ground stiffnesses [Farley et al., 1998], and changes in environment [Ferris et al., 1999]. This has led to the development of several variably compliant actuator systems [Colbrunn and Nelson, 2001, Ham et al., 2009, Webster et al., 2014].

Biological control systems (neural systems) evolved in tandem with muscles to

effectively control them. With advances in neurobiology, research into biologically and neurologically derived controllers has increased significantly in recent years [Gay et al., 2013, Hunt et al., 2014, Schilling et al., 2013a, Szczecinski et al., 2014, Tóth et al., 2012]. Many of these control systems take advantage of the compliant nature of the tendon-muscular system. To fully test these control theories, robots with biomechanical properties similar to animals need be developed [Tytell et al., 2011].

Braided pneumatic actuators (BPAs) are an actuator that has been explored in the robotic community for many decades [Gaylord, 1958] and offer some similar properties to those of muscles. BPAs are similar to muscles in that they are compliant and they can only effectively pull to provide force, requiring at least two antagonistic actuators to be positioned on each joint to provide torque in either direction. These actuators can be operated independently, like muscles, and their operation can provide variable joint compliance around a joint. Modeling efforts have led to characterization of length-tension-pressure relationships of the muscles [Chou and Hannaford, 1996, Colbrunn et al., 2001], spurring their use on several legged robots [Aschenbeck et al., 2006, Kingsley et al., 2006, Vanderborght et al., 2008, Nakatsu et al., 2014, Berns et al., 2001]. However, these properties lead to a lack of precision, and these robots largely underperform compared to their hydraulic or electric counterparts. Additionally, length-pressure-force relationships of stiffer, BPAs that use liquids are even more complex and not fully characterized. Hysteresis and creep can alter output force by 10% [Minh et al., 2012, Tondu and Lopez, 2000]. This makes feed-forward control of pressure to produce desired positions or torques not easy to compute. Additionally, in order to control a single joint, at least two parallel actuators must be controlled, compounding problems in uncertainty.

To avoid this complexity, many controllers use joint angle feedback transformed into valve control [Ahn and Thanh, 2005, Caldwell et al., 1995, Colbrunn and Nelson, 2001, Van Damme et al., 2009]. However, these control methods can suffer signif-

icantly from delays and are unable to respond quickly enough for robust robotic systems. Modeling BPAs and creating feed-forward controllers has resulted in more responsive systems capable of achieving speeds that more closely match animal movements [Andrikopoulos and Nikolakopoulos, 2014, Hošovský and Havran, 2012, Sarosi, 2012, Szepe, 2011]. However, these models have parameters which must be found experimentally for each actuator, and in some cases, different parameters are found between filling and emptying the same actuator with compressed air. This lack of generalizability makes it difficult to build a new system and begin testing new biological and other control systems without significant startup time and cost. This work produces a model in which only the resting length and the shortest length of a new actuator (maximum no-load contraction) need to be experimentally determined to provide feed-forward control of pressure from the desired length and force of a range of different length actuators. I then use this model for low level control on the Puppy Robot in our lab.

Chapter 3

Network Architecture

3.1 Developing Network Connectivity Diagram

3.1.1 Intra-Leg Network

Developing and testing network architecture required building a tractable system which could be easily adjusted to produce new results. The use of dynamic neurons creates a highly non-linear system in which changes to a single section have (often unpredictable) ripple effects across the entire system. My main concern while developing the architecture was to determine how sensory feedback can be used to coordinate all the joints in successful stepping motions. Because the focus is on coordination and not force production, I could support the body in simulation and make design decisions which enabled some reasonable isolation of the different components.

The first of such decisions was to isolate each joint with its own CPG and joint controller. The exact nature of how the nervous system controls muscle activation is not known [Brownstone and Bui, 2010]. For simplicity, the first iteration of our muscle control system was tuned for position based control, and leaves out the effect of Renshaw cells, Ia feedback, and other known motor neuron influences. Tension develops in the muscle based on type II afferent feedback (stretch receptors) modu-
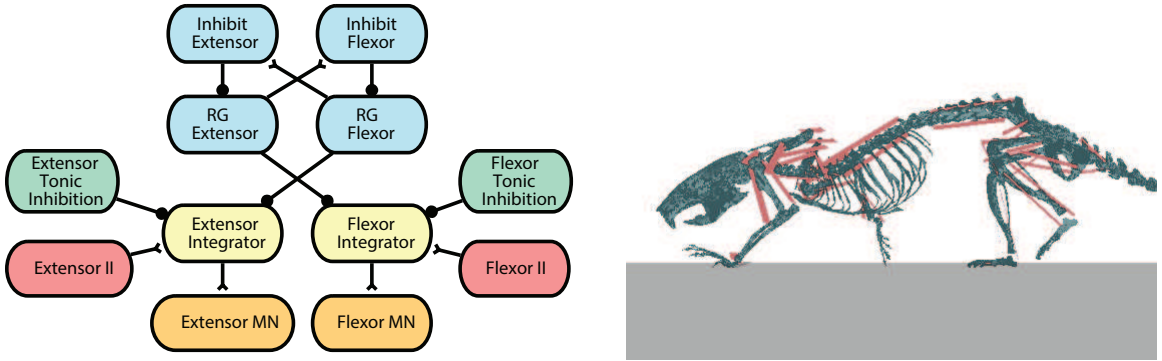
Figure 3.1: Left: Single leg joint controller. Circular ends represent inhibitory synapses while triangular ends represent excitatory synapses. CPGs are composed of two rhythm generating (RG) neurons with calcium channel dynamics which mutually inhibit each other via less dynamic interneurons. Each motor neuron is excited by type II (red) feedback unless inhibited by a CPG half-center (blue). Each motor neuron is also inhibited through an adjustable tonic inhibition (green). Right: Animatlab model of rat. Model reconstruction was done using bone matching of high speed, 3D x-ray video.

lated by a constant inhibiting neuron and is illustrated in Fig. 3.1. As the muscle gets closer to its desired length, excitation of the motor neuron decreases. This acts similar to low gain position control. We use kinematic data [Fischer et al., 2002] and recently collected unpublished data to determine these endpoint positions and tuned the low level controllers to reach these angles. This joint control system was later replaced with a network which does include Renshaw cells, Ia feedback, and Ib feedback when I focused more on force production (in later chapters).

The second major design decision was to build in an integrator layer of interneurons which filter the sensory signals, allowing easy change of threshold levels and combining of sensory signals before affecting the CPG systems. There is very little known about how the sensory signals are routed to affect the CPG and MN systems, however there is significant evidence of nonspiking neurons in spinal cords and thoracic ganglia which could play a similar role.

Most intra-leg network pathways in the model are developed directly from proposed mechanisms in mammalian literature, which is focused almost exclusively on

the hind leg. Stance-to-swing transition is the most studied phenomenon, and it occurs from both reduced firing in Ib Golgi tendon afferents, and increased firing from hip flexor stretching [Pearson, 2008]. This integration of signals is shown in Fig. 3.2 and can be visually followed with the purple dashed synapses; the "Load Release neuron is inhibited by ankle extensor Ib feedback and excited by hip flexor Ia feedback via the "Hip Angle Back" neuron. When the "Hip Angle Back" and "Load Release" neurons becomes sufficiently active, they inhibit hip, knee, and ankle extensor activations causing a switch from stance to swing. Positive force feedback [Prochazka et al., 1997] also plays a role in the network. This load feedback (blue pathway) can initiate stance if the leg is not already in this state, as well as increase muscle activation (not shown). Experiments have shown that stance is initiated by reduced firing of the hip flexor type II afferents or increased firing of hip extensor type II afferents [McVea et al., 2005, Akay et al., 2014]. This indicates that the hip is forward and causes contraction of the hip and ankle extensors and can be followed by the brown pathways. Using only these theories initially proved difficult in developing a walking model that is able to step stably, and one notably absent piece to the puzzle is the initiation of contraction in the knee extensor muscles. I hypothesize that knee extensor contraction is initiated by stretching of the hip extensor muscle during the swing phase (black lines in Fig. 3.2). This causes the knee extensor to start contracting part way through swing, as can be determined through analysis of the kinetic data [Witte et al., 2002].

The sensory triggers for a step cycle for the hind leg is as follows: The hip, knee, and ankle extensors are active during stance. During this time, the 'Ankle Extensor Ib' neuron is active, stimulating the 'Load Feedback' neuron and inhibiting the 'Load Release' neuron. As the leg moves further back, the sensory neuron 'Hip Flexor Ia' becomes more active and begins to stimulate the 'Hip Angle Back' neuron. As this neuron becomes more active, it stimulates the 'Load Release' neuron. When the

Intra-leg network for the rear rat leg model
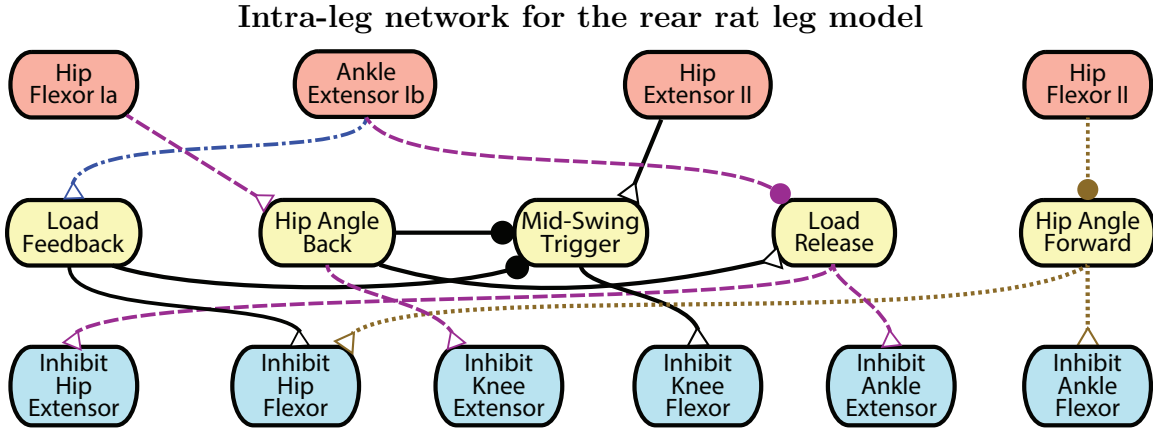
Figure 3.2: Three joints are controlled in this diagram: hip, knee, and ankle. All blocks are a single integrator neuron as described in Eq. 2.1. Sensory information is transduced to current and injected into the sensory neurons (top). Feedback is filtered by a layer of interneurons (middle) and is used to coordinate the CPGs (bottom). Coordinating pathways are inhibitory (circle end) or excitatory (triangle end). Pathways inspired through previous biological research can be followed as dashed purple [Pearson, 2008], dot-dashed blue [Prochazka et al., 1997], and dotted brown [McVea et al., 2005, Akay et al., 2014] lines. The pathways in black are hypothesized as a result of this work.

'Hip Angle Back' is sufficiently active, it excites the 'Inhibit Knee Extensor' neuron, causing the knee to switch from extension to flexion. As the load drops in the ankle, and the leg continues to move backwards, the 'Load Release' neuron becomes more active and excites 'Inhibit Hip Extensor' and 'Inhibit Ankle Extensor', causing the leg to fully enter swing as all flexor muscles are now active. Midway through swing, as the hip extensor muscle stretches, the sensory neuron 'Hip Extensor II' become more active. This neuron excites the 'Mid-Swing Trigger' neuron (which is inhibited during stance by the 'Load Feedback' nueron), which in turn excites the 'Inhibit Knee Flexor' neuron, causing the knee to switch from flexion to extension. As the hip continues to swing forward, the 'Hip Flexor II' neuron becomes less active, and inhibits the 'Hip Angle Forward' neuron less. As this neuron becomes more excited, it excites the 'Inhibit Hip Flexor' and 'Inhibit Ankle Flexor' neurons, causing the leg to switch to stance again. Additionally, if load feedback occurs earlier, this can cause the hip to enter stance earlier.

Intra-leg coordination for the front rat leg model
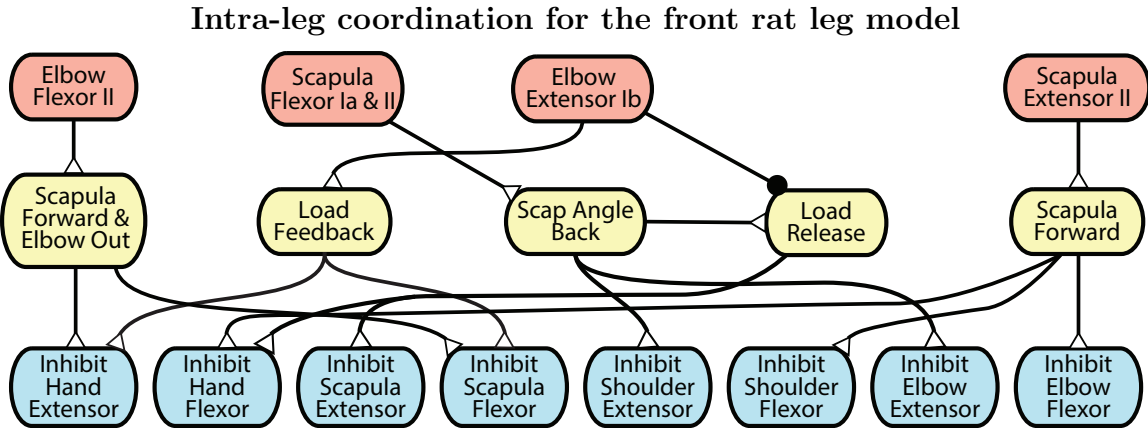
Figure 3.3: Four joints are controlled in this diagram: scapula, shoulder, elbow, and wrist. Coordination pathways were developed using analogous pathways to that of the known hind leg pathways.

Though the foreleg has an extra joint, analysis of several of the joints show nearly identical trajectories during stance and swing movements of the hind-leg. Scapula movement, like the hip, extends during stance and flexes during swing. The shoulder and elbow movements have the same bimodal shape and relative peaks with the knee, and ankle, respectively. The front leg network is built on the hypothesis that these joints are controlled with analogous sensory pathways (Fig. 3.3). Therefore, the extra joint in the front leg which requires additional control is the wrist. Elbow extensor Ib feedback is used in parallel with ankle extensor Ib feedback for load detection. Continued elbow extensor Ib feedback inhibits swing for the highest and lowest joints, and when load is detected, it ensures those joints are in stance. Scapula flexor Ia and II feedback are used to determine when the leg is at the end of stance, and causes the shoulder and elbow joints to enter flexion. Scapula extensor II excitatory feedback is used to indicate when the leg is in the middle of swing analogous to hip extensor II excitatory feedback used for the hind leg. This feedback causes the elbow and shoulder to begin extending. Elbow flexor II feedback initiates stance of the scapula and wrist comparable to how hip flexor II feedback is used to initiate stance in the hip and ankle.

3.1.2   Inter-Leg Network

Inter-leg connections are based on behavioral mammalian experiments. They are an order of magnitude weaker than intra-leg connections [Cruse, 1990]. Akay et al. [Akay et al., 2006] postulate three main coordinating influences between fore and hind legs. Influence 1) Foreleg extension reduces onset of the hind limb hip flexor. Influence 2) The end of activation of the hind limb hip flexor advances activation of forelimb swing. Influence 3) Activation of the forelimb elbow flexors contributes to inhibiting hind limb hip flexors. The influences are based on behavioral experiments in cats and have been implemented as network connections in the following ways: C1) Activation of the elbow extensor motor neuron applies inhibition to the hip flexor motor neuron. C2) Reduced activation of the hip flexor motor neuron allows the "Side Interneuron" to escape and excite the "Init Swing" neuron of the front leg for a short period. C3) Activation of the elbow flexor motor neuron depolarizes the "Hip Angle Forward" neuron on the hind legs, helping to initiate stance. These can be followed with the green pathways and labels in Fig. 3.4.

Coordination between the two front legs is tested in two ways. The first is based on observations of the animal, in which it is seen that rats primarily move in a symmetrical gait with both front legs 50% out of phase with each other. These connections can be seen in Fig. 3.4. If one leg is in swing, the contralateral leg is encouraged to either enter stance if it is in swing, or continue in stance. Additionally, we have implemented the connection that if a leg is in stance then the contralateral leg is encouraged to enter swing. Kinematic and coordination data are shown from these connections. In addition to behavioral based connections, we have run some preliminary experiments with direct connections using commissural interneurons as has been tested in mice [Talpalar et al., 2013] and cats [Jankowska, 2008], and further described with neural modeling [Rybak et al., 2013]. With these connections, because we do not have a single CPG for each leg, the scapula joint CPGs are connected

Inter-leg behavioral network
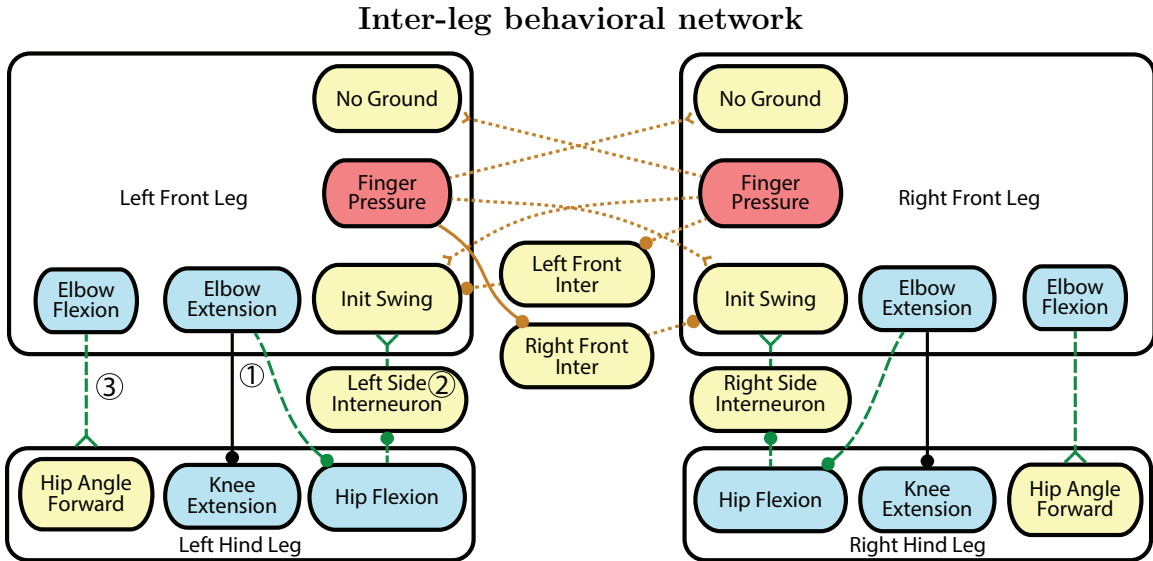
Figure 3.4: These connections are weaker than connections coordinating intra-limb movement. Contralateral connections encourage only one front foot to be on the ground at a time and can be followed with the orange dotted lines. Ipsilateral legs are coordinated based on research performed on cats, can be followed with the green dashed lines, and are numbered according to the influences determined by Akay et al. [Akay et al., 2006].

with inhibitory and excitatory commisseral internerons (CINi and CINe), and the rest of the CPGs remain unconnected. These pathways are set such that the CINi pathways provide three times as much inhibition as the CINe provides excitation, similar to [Rybak et al., 2013]. These connections can be seen in Fig. 3.5. Parameters were tuned to encourage coordination within a few steps of model initiation, but not impose coordination immediately.

3.2 Results from connectivity networks

3.2.1 Model Testing

Several tests were run on the model to determine its effectiveness. In all tests, the model was dropped from a short height with limbs in a walking configuration similar to that at the beginning of stance. The hip joints were constrained to a minimum of 5.83

Front leg commissural neural network
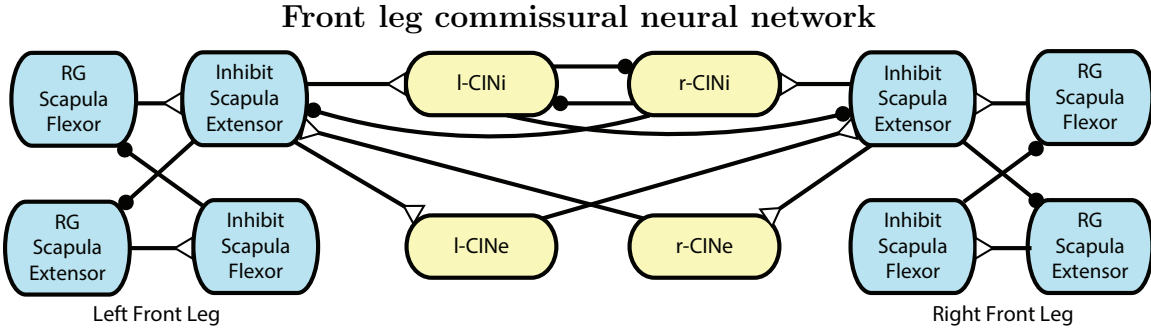
Figure 3.5: Scapula flexor activation both inhibits opposite leg scapula flexion (CINi neurons) and excites opposite leg flexion (CINe neurons), but at one third the strength of inhibition.

cm from the ground and uniform random noise of 0.1 mV was inserted into the CPG-RG level to encourage different starting neural configurations (which joints begin in flexion, and which in extension) and to keep the system from settling on unstable equilibrium during testing. The tests varied the inter-leg connections between fore and hind legs. Inter-leg connection tests consisted of 1) fully connecting system as described above (C123), 2) removal of connection 1 (C23) 3) removal of connection 2 (C13) and 4) removal of connections 1 & 2 (C3). Attempts without connection 3 never resulted in a coordinated walking gait and are therefore not presented. Tests were recorded for 5s and analyzed from 1.5-5s (after the model had time to initialize and develop coordination). Each configuration was run 40 times. Kinematic data were collected for fore and hind legs during C123. Mean and standard deviation of step timing was taken for all tests that gained symmetrical coordination within the first 1.5s. Simulation files of the rat, raw data collected, and videos of the walking rat simulation are posted on-line at http://biorobots.case.edu/hunt-dissertation-files/.

3.2.2 Intra-leg Coordination and Kinematics

The network is capable of producing stepping motions for both front and hind legs. Most joint kinematics match well, and many trends which are observed in the animal data are also captured in the simulation. The mean and one standard deviation for
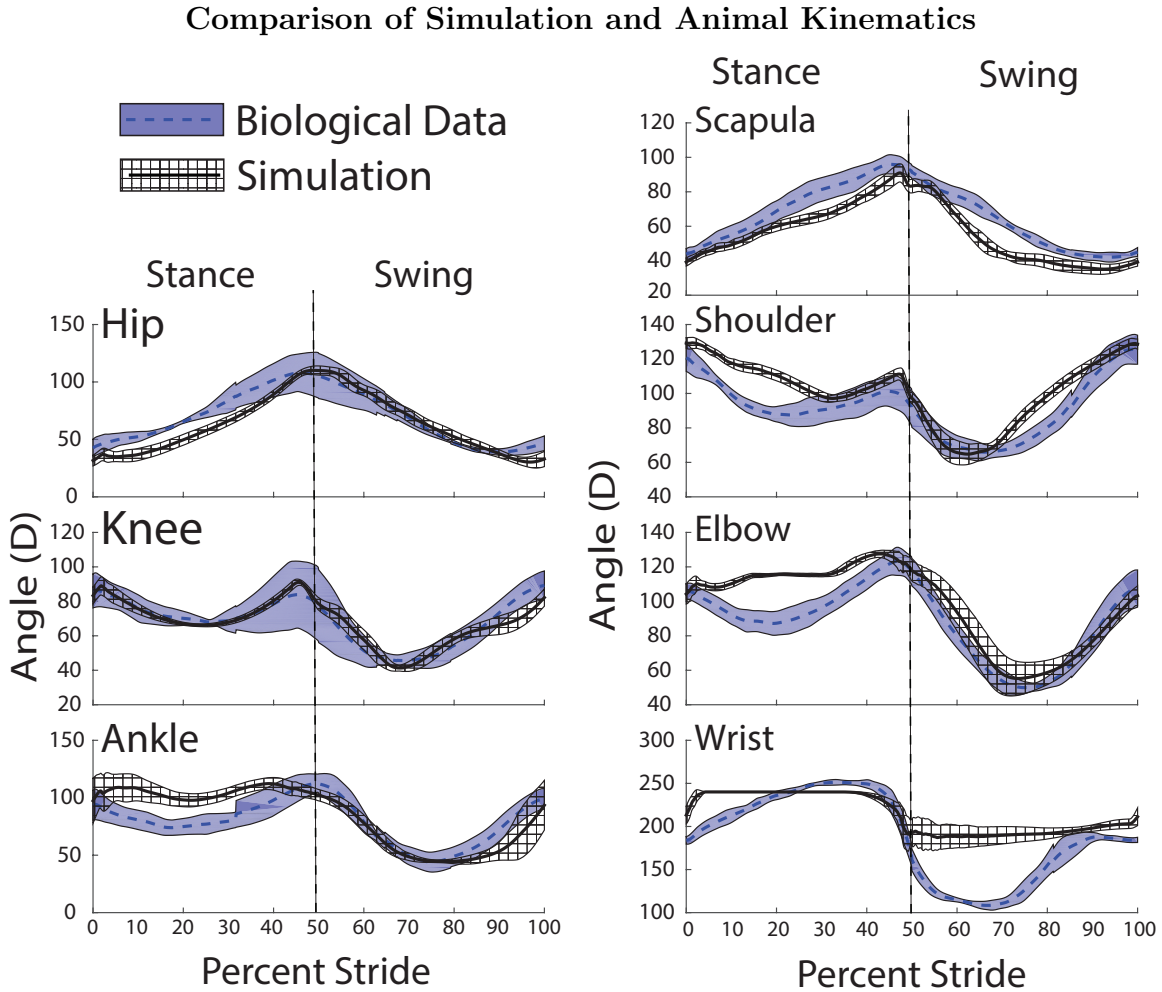
Figure 3.6: Comparison of averaged biological recordings with results of the simulation for a single stride over multiple trials. Mean data for each is shown with the dashed and solid lines and one standard deviation is shown shaded or hashed around it. Stride is broken into stance from 0%-50% and swing 50%-100%.

animal and simulation data are plotted in Fig. 3.6. The hip joint of the model moves more slowly at the beginning of stance but catches up at the end of stance, while swing is well matched. The knee joint movement is within one standard deviation of the animal for both stance and swing including the double extension and flexion phases visible in the animal. The ankle joint also matches the double extension and flexion phases of the animal, though flexion during stance is less pronounced in the simulation due to external support of the body. Ankle flexion and extension of the model during swing are also mostly within one standard deviation of animal movement.

Using network connections derived from the hind limb, the front limb is capable of producing steps which also share many of the same characteristics with the animal. The scapula extends and flexes with the same timing to that of the animal for stance and swing with only slight differences in speed, moving slower than the animal near the transition from swing to stance, and faster than the animal near the transition from stance to swing. The shoulder shows the double extension and flexion phases visible in the animal, though flexion during stance is more limited than in the animal. The elbow does not undergo flexion during stance, which is likely due to the support of the body, similar to its analogous joint in the hind leg, the ankle. One standard deviation of elbow in the model overlaps with the animal during the entire swing phase. The wrist is unable to achieve the same range of motion as the animal, though it does undergo extension and flexion in the same phases.

3.2.3 Inter-leg Coordination

Not all of the trials resulted in coordination by the 1.5s mark. C123 produced coordination 80% of the time. C23 produced coordination 53%, C13 produced coordination 75%, and C3 produced coordination 65% of the time. The p values associated with comparing the different data sets using an N-1 two proportion test are in Table 3.1. There is no statistical difference in the ability of the simulation to develop coordination when connection 2 is removed from the system, however there is significant difference when connection 1 is removed from the system (p<.05).

The resulting coordination with original weights is timed within a about two percent as what was recorded by Górska et al. [Górska et al., 1999]. However it contains some distinct differences when compared to recent data taken in the Fischer lab. In all instances, homologous limbs (both front, or both hind) are directly out of phase, touching down halfway through the stride of the opposing leg. For ipsilateral legs, the simulation matches data recorded by Górska et al., hind limbs touch down
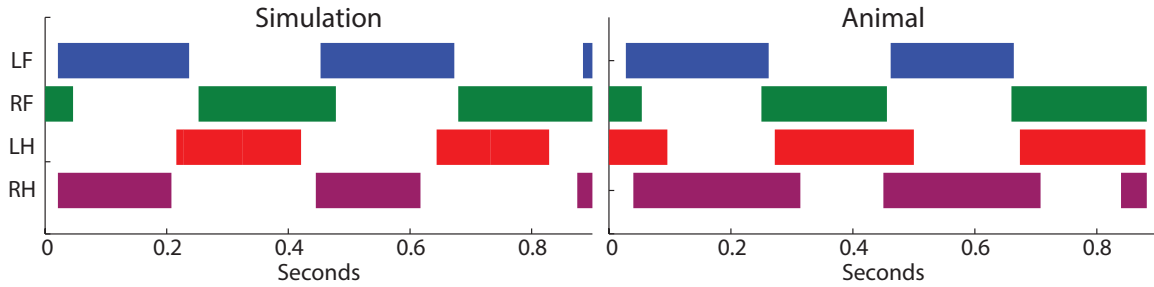
Figure 3.7: Footfall diagram of simulation compared with animal data taken at FSU Jena. Solid bars indicate stance of a particular foot. A single step cycle is approximately 450ms long for both the live animal and simulation. For the symmetric gait, front legs alternate stance and swing and are approximately 50% out of phase. When compared to the live animal, the hind legs' phase of the simulation is shifted forward by 20%, which can be corrected by changing the strength of connection 1 of the inter-leg network.

40% of the way through the stride of the ipsilateral forelimb. This is about 20% out of phase compared to the data collected in the Fischer lab, in which the hind limbs touch down 60% through the phase of the preceding limb. Coordination is extremely tight for the walking animals, with standard deviations of 3-8% of the stride. Simulation coordination with the C123 network is within a couple percent of the original coordination, with standard deviation from previous coordination of 3-8%. C23 also has standard deviations of 3-7% on the same order of the animal. C13 still results in coordination, however standard deviations increase to 10-17%, and C3 results in ranges from 9-20%.

Using the proposed front leg inter-leg connectivity in which CPGs are directly

Table 3.1: P values for probabilities of different networks developing coordination within 1.5 seconds of start. There is no statistical difference in the ability of the simulation to develop coordination when connection 2 is removed from the system, however there is significant difference when connection 1 is removed from the system (p<.05).

	C3	C23	C13
C123	0.129	0.014	0.346
C13	0.248	0.045	
C23	0.209		

Table 3.2: Comparison of footfall timing in biological data collected by Górska et al. [Górska et al., 1999] and data collected in the Fischer lab at FSU Jena with simulation experiments. A value of 0.00 represents steps which fall at the same time, and 0.50 represents steps which fall 50% out of phase with each other. The $\pm$ 0.05 represents one standard deviation of variation for the timing at 5% of the total step time.

	Homologous			
Test	LF→RF	RF→LF	RH→LH	LH→RH
Górska et al. [Górska et al., 1999]	0.48 ± 0.05	0.52 ± 0.05	0.51 ± 0.04	0.49 ± 0.05
Jena Data	0.49 ± 0.07	0.53 ± 0.03	0.53 ± 0.05	0.49 ± 0.04
C123	0.53 ± 0.08	0.46 ± 0.05	0.47 ± 0.04	0.53 ± 0.04
C23	0.54 ± 0.04	0.46 ± 0.06	0.45 ± 0.05	0.54 ± 0.05
C13	0.51 ± 0.17	0.48 ± 0.16	0.48 ± 0.17	0.51 ± 0.16
C3	0.51 ± 0.20	0.48 ± 0.19	0.45 ± 0.19	0.55 ± 0.19

	Diagonal		Homolateral	
Test	RH→LF	LH→RF	LF→LH	RF→RH
Górska et al. [Górska et al., 1999]	0.11 ± 0.05	0.08 ± 0.05	0.40 ± 0.05	0.41 ± 0.06
Jena Data	-0.10 ± 0.08	-0.13 ± 0.04	0.65 ± 0.06	0.60 ± 0.05
C123	0.04 ± 0.06	0.10 ± 0.04	0.43 ± 0.03	0.43 ± 0.04
C23	0.04 ± 0.07	0.11 ± 0.04	0.42 ± 0.03	0.43 ± 0.04
C13	-0.01 ± 0.17	0.08 ± 0.15	0.41 ± 0.12	0.42 ± 0.10
C3	-0.02 ± 0.16	0.07 ± 0.15	0.43 ± 0.11	0.40 ± 0.09

Table 3.3: Coordination of forelimbs in the developed model using behavioral rules, connections based on neural studies of wild type animals, and connections based on neural studies of Netrin-1 Knock Out (KO) animals. Phase timing of limbs are correlated as a fraction of the period of another limb. Behavioral rules and wild type neural connections both produce symmetric walking with front legs, while Netrin-1 KO rules produce in phase bounding. In all scenarios, the ipsilateral coordination is minimally affected.

| | Diagonal | | Homolateral | |
Test	LF→RF	RF→LF	LF→LH	RF→RH
Behavioral	0.51	0.49	0.61	0.63
Wild Type	0.50	0.50	0.61	0.63
Netrin-1 KO	-0.01	0.01	0.57	0.57

coupled also produces coordination in the front legs. Using strengths with similar proportionality as that for wild type mice in Rybak et al. [Rybak et al., 2013], we produced alternating stepping patterns which match that of the walking animal (Table 3.3). When the strength of the inhibitory connection is adjusted to 10% or lower of the original strength (CINi to Inhibit Scapula Extensor, Fig. 3.5), the model begins bounding in a similar manner to Netrin-1 Knock Out (KO) mice [Rybak et al., 2013].

After these results were produced, I attempted to see if I could modify the network to more closely match the data collected by Jena. Adjustments to the strength of one connection in the model (C1, Fig. 3.4), is able to effectively alter the timing between fore and hind limbs such that both sets of animal data can be matched. Higher connection strengths cause the phase timing of the hind leg touchdown compared to foreleg liftoff to shift backwards (Table 3.4). A strength of 1.5 uS of conductance in C1 creates an average phase timing of 0.62 for hind limb touchdown when compared to forelimb touchdown, which is similar to the phase timing of the data collected at FSU Jena. When this connection is weakened to a value of 0.2 uS, the phase is reduced to an average of 0.475, with the hind foot touching down before forelimb liftoff, and matching the data collected by Górska et al. more closely.

Table 3.4: Comparison of biological data collected in the Fischer lab at FSU Jena, data collected by Górska et al. [Górska et al., 1999], and the simulation experiments. Phase timing of limbs are correlated as a fraction of the period of another limb. Standard deviation for all data sets is between 4-8%. For all animals and simulation, homologous limbs were 50%±3% out of phase with each other. Discrepancies between diagonal and homolateral limbs of the different rat data were mostly accounted for by a modification of the strength of C1.

	Diagonal		Homolateral	
Test	RH→LF	LH→RF	LF→LH	RF→RH
Górska	0.11	0.08	0.40	0.41
Jena Data	-0.10	-0.13	0.65	0.60
C1 = 0.2 uS	0.01	0.04	0.46	0.49
C1 = 1.5 uS	-0.14	-0.10	0.61	0.63

3.3 Discussion

3.3.1 Intra-leg Coordination and Kinematics

The neural system is capable of producing forward walking motions of the rat simulation. Hind leg movements have the same shape and magnitude as those made by the animal, including the presence of joint flexion during the beginning of stance while the extensors are activated. A reliance on purely kinematic data would not capture the eccentric muscle contractions occurring at this time, but data of the dynamics and knowledge of the neural systems involved informed the formulation of a simplified neural controller capable of producing these results. The front leg also produces steps, despite being developed mainly from hind leg connectivity properties.

There is room for improvement, however, as there are still some issues in kinematic matching. First, limits in the joint range of motion cause poor matching in the wrist. Methods for better designing muscle attachments to achieve greater ranges of motion could improve this, however without simulation capability which can actively wrap muscles around joints and update force directions, it is unlikely the same range of motion can be achieved in simulation as is seen in the animal.

Second, external support of the body reduces the joint torques, especially at the

beginning of stance. Development of local motor control networks which can produce the proper torque profiles required for walking would eliminate the need for this external support. Exploration of better joint control begins in Chapter 4.

Though more detailed network construction may lead to better fitting of the biological data, most of phase transition and joint amplitudes are mimicked by the model. These results support the validity of the developed neural network and model and serve as a useful tool for testing the network connectivity through means such as pathway deletions and strength modulation.

3.3.2 Inter-leg Coordination

The data for coordination suggest several conclusions. The developed inter-leg network has no connection between hind legs, and coordination is maintained by connections between the fore and hind legs. Using the mechanisms postulated by Akay et al. the developed network is able to produce a stable symmetrical gait. The data of this gait is within 5% of the data collected by Górska et al., and supports this as a potential means of coordination for mammals. Not only is the timing between foot touchdowns nearly identical, but the network keeps the timing as closely coupled as that of the animal. These data contrast with recently collected data on locomoting rats and previously collected data on locomoting cats [Cruse and Warnecke, 1992], in which stance of the hind leg occurs after swing of the foreleg begins. However, changes in a single connection strength (C1) is capable of shifting the timing between fore and hind limbs to more closely match data collected by the Jena group.

In the model network, an additional pathway was added to connection 1 to slow down movement of knee extension in addition to hip flexion. This connection could be further tested in the animal to determine if knee extension is indeed affected by elbow flexion during the hind limb swing phase.

Performing ablation tests of the inter-leg network indicates the roles of each con-

nection in producing tight, coordinated movement. Connection 3 is sufficient and necessary to produce coordination in the proposed scheme. It is the only connection that affects the timing signals of the hind legs based on front leg activity. This connection's influence is such that whenever the front leg is off the ground (elbow flexion activity), the hind leg enters stance. This helps ensure that there is not significant time in which both legs are off the ground and the animal does not fall to the side.

Connection 2 only acts rostrally and is not sufficient for producing coordination because the hind legs are not coupled contralaterally. Although connection 2 is not sufficient for producing coordination, removal of the connection from the network (C13) reduces the likelihood of walking coordination. This is because this connection perturbs network timing opposite that of connection 3. When the hind leg enters stance, as evidenced by no longer having any hip flexion, then the front leg is encouraged to enter swing. Therefore connections 2 and 3 are working together to ensure that hind leg stance and front leg swing occur at approximately the same time.

Although connection 1 influences hind leg behavior, it does not directly influence phase and only affects motor neuron activation. Like connection 2, connection 1 is not capable of producing symmetrical coordination by itself. In fact, it often causes front and hind legs to fall into phase with each other, producing the opposite of the desired effect. Perhaps because of this, connection 1 is important to the relative timing of hind leg touchdown to foreleg liftoff. Removal of this connection causes much larger deviations in timing, and changing the strength of the connection changes the phase timing between the fore and hind legs.

Phase timing of ipsilateral and diagonal legs in the range tested is shifted by up to 17% by adjusting the strength of C1. Increasing the strength of C1 slows down the swing of the hind leg more when the front leg is in stance, causing it to reach its forward position later. Coordination as a result of higher connection strengths in C1 match that of the Jena data while coordination results with lower

connection strengths match the data collected by Górska et al. (Table 3.4) With the data collected by Górska et al., rat hind legs touched down before liftoff of the front legs. With the Jena data, the hind legs touched down after the front legs lifted off. Both these outcomes are achievable with the implemented network, and these varied outcomes are produced by adjusting the strength of a single connection. In this study, changes of synapse strength in a single connection generated a continuum of coordination gaits. Such a mechanism may account for behavioral differences in gaits between animals.

When the direct neural connections as have been found by research in mice and cats [Talpalar et al., 2013, Rybak et al., 2013, Jankowska, 2008] are implemented, an alternating stable gait emerges. This occurs even though only the scapula CPGs were influencing each other, and no other joints were involved in the coordination between the front legs. Additionally, coordination is maintained even though the scapula joints were receiving coordinating influences from within the leg to keep the joints coordinated in a walking motion, as well as coordinating influence from the hind legs to maintain ipsilateral coordination.

Ipsilateral coordination is also maintained when changes in the front leg coordination occurs. When the inhibiting synapses are weakened in the same manner as to what occurs in Netrin-1 KO mice, the front legs begin to coordinate together in a bound. Because the hind legs receive all their coordination cues with the ipsilateral foreleg, their coordination with the front legs is maintained and the hind legs fall into phase with each other as well, producing a well coordinated bound. It would be interesting to see if animals which regularly switch between trotting and bounding are able to modulate this connection via descending commands or some other means.

The developed network successfully coordinates four limbs of a walking rat model using neural pathways which have been hypothesized with behavioral and neurological research on animals. However, the building and parameter tuning of this network

was done by hand, which was painstaking and slow. If this network is to be used on robotic systems with different kinematics and dynamic demands, a more effective way of setting parameters must be found. The next two chapters will outline the process I developed to set parameters in the neural network to produce walking for two completely different systems: a rat simulation and a hardware robot.

Chapter 4

Calculating MN activations

Any system which moves in a world (real or simulated) must do so through the application of forces (real or simulated). For systems purposefully moving in these worlds, these forces are produced by the application of torques about different joints in the body which produce forces at the contact point between the system and the world. In order to fully describe how the system is moving, the torques must be described, and any controller and actuator which moves the system must have some way of developing these torques.

In animals (and some robots now), the controller is the nervous system, and the actuators are muscles. Motor neurons (MNs) act as the interface between the control developed by the nervous system and the muscles producing forces and torques in the animal. In order to develop a controller to activate the muscular system of an animal, we must first determine what torques, muscle forces, and MN activity the animal (or robot) require to produce walking behavior.

4.1   Rat Simulation

4.1.1   Joint Torques and Kinematic Motions

Stance joint torques and kinematics were calculated by Dr. Emanuel Andrada, our collaborator working with Martin Fischer in Jena, Germany using inverse dynamics based on force plate and kinematic data of rats walking on level ground. [Andrada et al., 2013]. Kinematic data for swing was the same data collected by Manuela Schmidt also working in Dr. Fischer's lab.

I developed a full hind leg inertial model with joint friction in Simulink-SimMechanics based on the model in Animatlab. This model can be found in the posted material on the website. By inputing the kinematic motion SimMechanics calculates the torques using the equations of motion. The stance data and swing data were concatenated together assuming a 50% duty cycle and smoothed non-linearly to remove discontinuities at the edges. This code can be found in the files posted on-line at http://biorobots.case.edu/hunt-dissertation-files/.

4.1.2   Calculating Muscle Tension and MN Activation

Desired muscle tension was calculated using joint torques and the kinematic model. A unique solution was obtained by assuming only one muscle per joint actively contracts at any time [Hooper et al., 2009]. The active muscle must produce the previously calculated torques as well as overcome torques created by the passive forces produced in each muscle.

Passive forces were calculated using Eq. 2.6 with $A = 0$. Muscle length (x) and muscle velocity ($\dot{x}$) were calculated using model geometry and kinematic data. The derivative was discretized and T was solved for at the next time step based on the

previous tension:

$$T_{i+1} = T_i + \Delta t \cdot \frac{k_{se}}{c} \left(k_{pe} x_i + c \dot{x}_i - \left(1 + \frac{k_{pe}}{k_{se}} \right) \cdot T_i \right) \tag{4.1}$$

Starting with $T = 0$ and repeating this process for several step cycles produces a periodic tension profile which counteracts the ground-force and dynamic torques. A bisection root-finder solves for the active muscle tension required to produce the necessary torques and each muscle's tension was numerically differentiated to find its rate of change. Equations 4.1 and 2.7 were solved with a bisection root-finder to find the motor neuron voltage. The code for this resides within the design_kinematic_organism.m code written by Nick Szczecinski and is available in the posted folder.

4.2 Puppy Robot

Developing the MN activation curves for Puppy was less straightforward. First, we did not have data for desired kinematic trajectories and joint torques for fore and hind legs produced during walking in an equally proportioned dog (though Martin Fischer's group at Jena is currently working on this). Additionally, though the Festo actuators have many properties that are similar to muscles, there are many differences as well. Finally, what is controlled on Puppy is air muscle pressure level, not activation level and therefore some new mapping between MN activation and pressure within the robot muscles must take place.

4.2.1 Joint Torques and Kinematic Motions

To develop kinematic and dynamic motions for the robot, I developed three models in Simulink-SimMechanics: hind leg swing, foreleg swing and hind and foreleg stance 4.1. Puppy has three controllable degrees of freedom per leg. For desired kinematics, I fit a cubic spline to predetermined angles and duty cycles for touchdown, midstance,

liftoff, and midswing. The touchdown, midstance, and liftoff were gathered from data on walking whippets, a species of dog with similar limb proportions and body mass to Puppy [Fischer and Lilje, 2011]. A midswing value was chosen to ensure the foot would achieve ground clearance while in swing. For the fore legs, the scapula and shoulder angle were combined to one angle of progression (θ_S), and the elbow angle (θ_E) was adjusted based on what the angle would be between the new combined scapula-humerus limb and the original ulna orientation.

Hind leg and foreleg swing torques were calculated in the same way as the rat's in section 4.1.1 by adding friction to the joints and doing forward dynamic analysis. The calculation of stance torques was less straightforward because ground reaction forces of walking whippets are not yet available. During a trot, one front leg and one hind leg are on the ground, holding the body up and propelling it forward. Building a closed chain system with a fore and hind leg on the ground at one time and performing inverse dynamic analysis as is done with the swing kinematics results in an extra control parameter; there are 5 independent degrees of freedom and 6 controllable
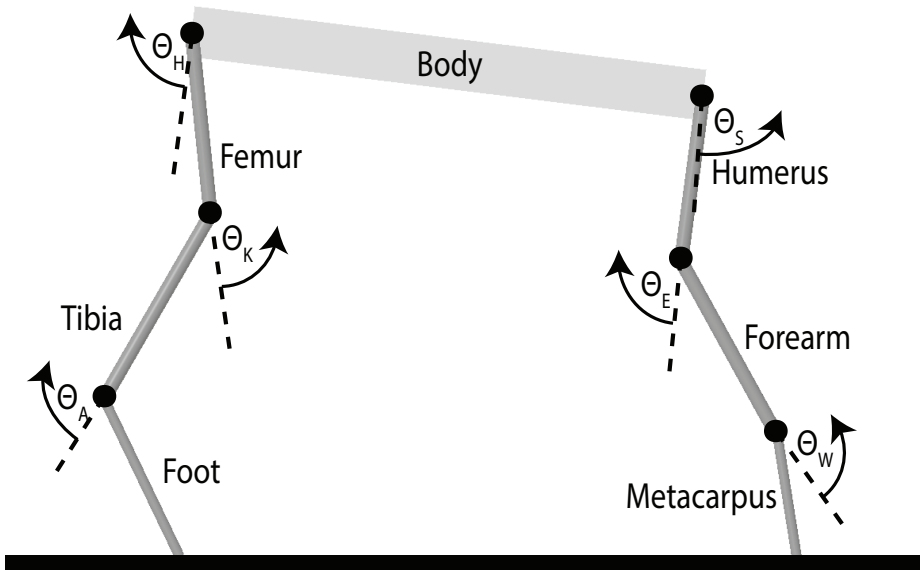
Figure 4.1: Kinematic diagram of Puppy Robot in SimMechanics. There are 7 bodies with 6 controllable planar joints. Extension of a joint is labeled as positive rotation while flexion is labeled as negative rotation.

joints.

$$(7\,Bodies * \frac{3\,DoF}{Body}) - (8\,Pin\,Joints * \frac{2\,Constraints}{Pin\,Joint}) = 5\,Degrees\,of\,Freedom \quad (4.2)$$

This redundancy in control makes for an infinite number of possible torque combinations to produce the desired forward kinematics.

To solve this problem, a proportional-derivative (PD) controller was applied to the stance model. This controller reads in the desired kinematic trajectory, and for each time step, produces a torque on each joint which is proportional to the error in that joint angle and the derivative of the angle. Determining the best proportionality constants took some finesse (like most PD controllers). First, even when initial joint velocities were input to the model, unstable, high torques would often result at the beginning. Therefore the model was made to settle on the initial configuration before being controlled through the desired trajectory. High stiffness control followed the trajectory with little error, but the resultant torques were much higher than has been reported in the greyhound [Colborne et al., 2006], and could be unstable at times (Fig. 4.2 left). Additionally, several joints produced torques which were backwards to the motion of the simulation. Too low of stiffness had trouble following the trajectory. The best found PD control which were within 20% of peak torques recorded in the greyhound consisted of k_P values scaled to overall joint torque between 20 and 40 and k_D values between .7 and 1 ([Fig. 4.2 right]) [Colborne et al., 2006]. The initial resultant desired torques saturated the desired torque outputs and MN controller, so the weight of the robot was lowered from 4.5 kg to 3 kg and a counterweight was added to the robot. The kinematics which resulted from these torques were recorded as the new desired kinematic trajectory for the robot. Similar to the rat, the final kinematic and dynamic profiles were smoothed together to form the final
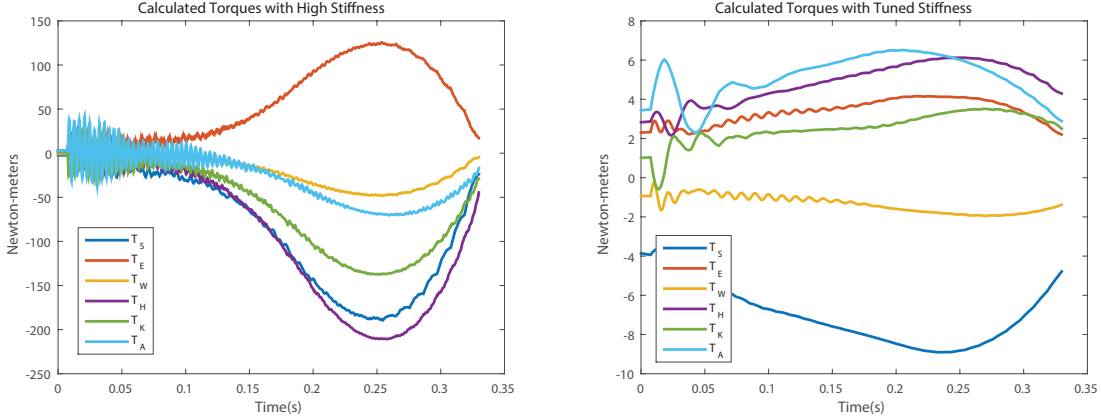
Figure 4.2: Comparison of high and low stiffness controllers in providing the desired kinematic trajectory for the SimMechanics version of Puppy. The high stiffness controller was very unstable at the beginning of the trajectory and resulted in very high torques at the joints. A lower stiffness did not follow the trajectory exactly, but produced scaled hind leg torques which were on the same order as those which had been recorded in the literature [Colborne et al., 2006].
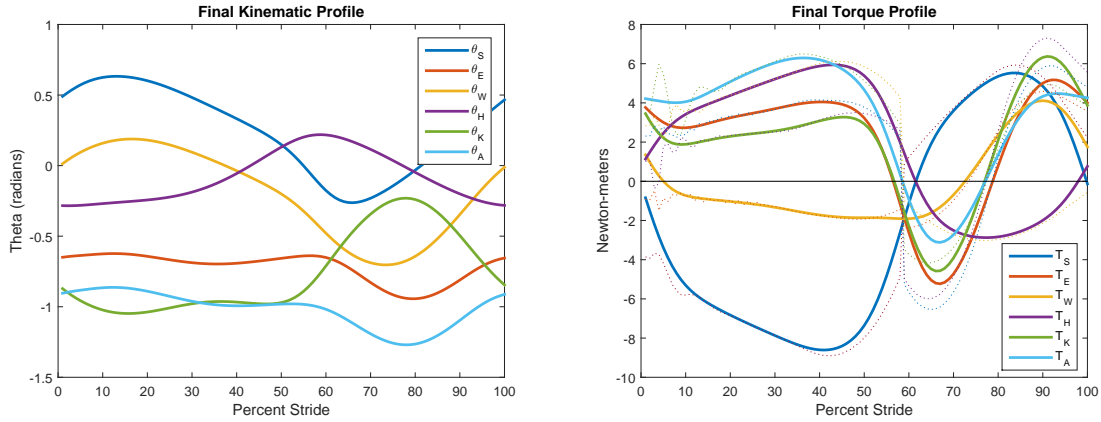
Figure 4.3: Final kinematic and torque profiles for the puppy robot which were used to produce training data for the neural system.

profiles 4.3. The code for this can be found posted with the on-line material at http://biorobots.case.edu/hunt-dissertation-files/.

4.2.2 Modeling Festo Air Muscle Actuators

Determining muscle forces and activation profiles for the robot first require a model of how the actuators produce force. This model must therefore provide a relationship
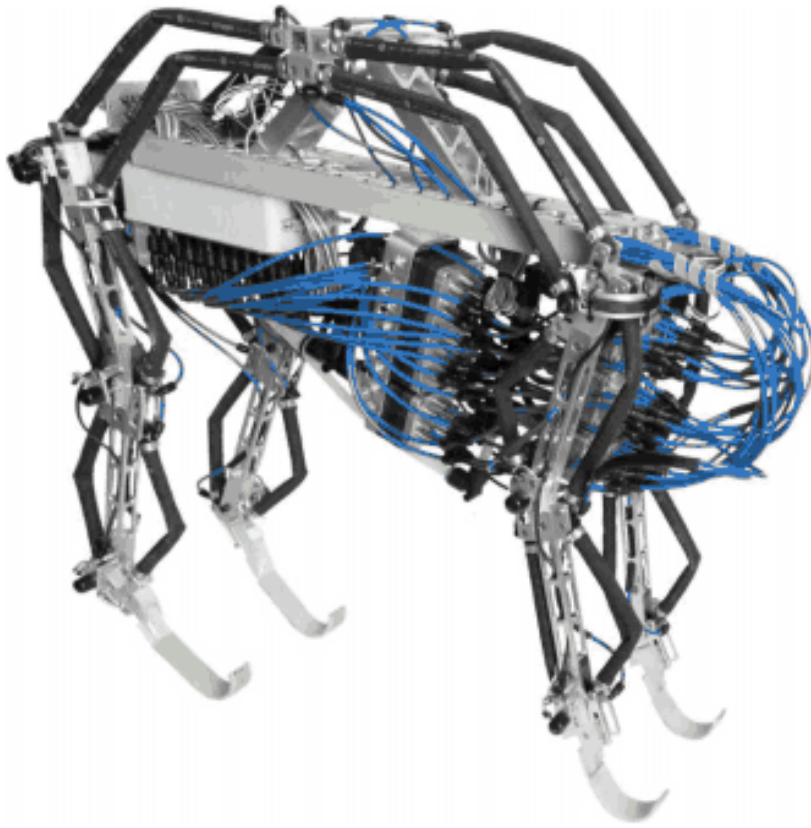
Figure 4.4: Puppy robot with Festo actuators. Over time, permanent kinks have developed in the actuators which result in poor modeling under combined low load and low pressure conditions. Modeling and model testing was performed using actuators in the front right leg.

between the activation variable, pressure, and the force that is produced at a particular length. There are many models of the Festo actuator already available (see section 2.4.2, for a review), however my work with the actuators shows a clear relationship to original actuator length which is not captured in any of these models. Therefore, I collected data on the actuators from Puppy's front right leg and developed a Pressure-Force-Length relationship model which takes in to account original actuator length as well as how the actuator is attached (the end fittings). This process is detailed next.

Data Collection

Data was collected on 6 actuators. These actuators are 10 mm Festo MXAM-10-AA and have resting lengths of 15.31, 18.28, 18.94, 19.50, 27.27, and 28.09 cm from attachment point to attachment point. Each actuator was secured on a vertical test stand (Fig. 4.5) with the top fixed and the bottom on a weighted moving slider. Length data was collected by a Vishay Spectrol 140-0-0-103 potentiometer connected to the moving plate via Kevlar thread wrapped around a 3.18 cm shaft. Pressure was measured using a Freescale gauge pressure sensor. Data was collected with Labview 2014 via a sbRIO-9602 and processed in Matlab 2014b.
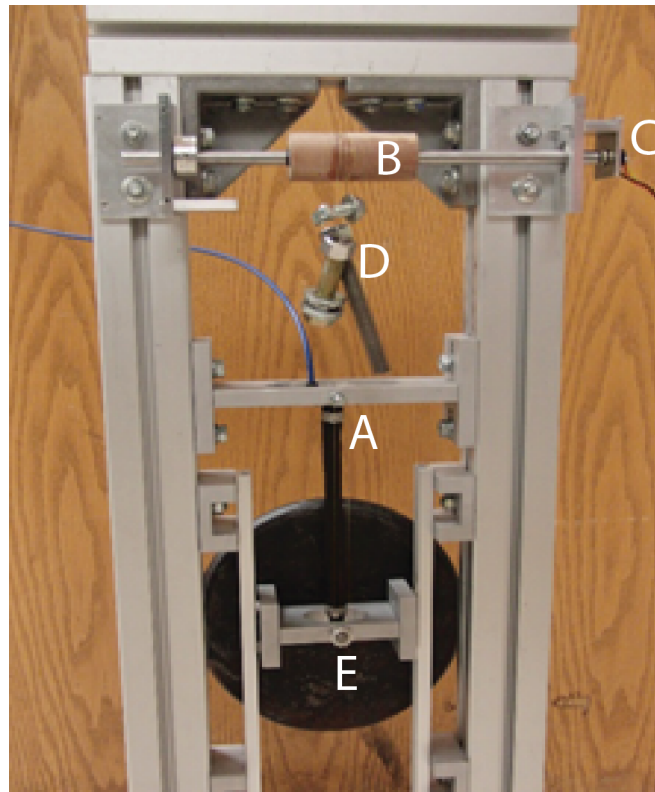
Figure 4.5: Test stand used in data collection. Actuator (A) length changes are transformed into shaft rotation (B) and collected by a potentiometer (C). Shaft counterweight ensures the string remains taught (D). Weights are hung incrementally on the end of the actuator (E).

Testing Procedure: The actuator begins at 0 gauge pressure and the inlet valve is opened for 10 ms from a 650 kPa air supply, and then allowed to rest for 1 sec-

ond. Each data point is associated with actuator dimensions, weight, pressure, and length at time of recording. The data is collected by a single board reconfigurable input\output device (sbRIO) and transferred to the computer. This process is repeated until the actuator pressure is greater than 620 kPa. At this point the exhaust valve is opened for 10 ms repeatedly with data taken at each increment until the actuator returns to 0 gauge pressure. This is repeated for a total of 300 data recordings. This procedure is performed with a hanging weight of 0-25 lbs. (0-11.34 kg) in 1 lb. (0.45 kg) increments.

Actuator Model

The Festo air muscle is a McKibben type actuator with a cross weave of fibers woven into the bladder membrane. Many physics based models have been developed ([Kelasidi et al., 2011] for review), however there are often still errors resulting from initial actuator length inaccuracy, internal actuator friction, and end effects. Another approach is to fit a large parameter set with multiple polynomial terms [Hošovský and Havran, 2012], however this makes it difficult to understand the important factors involved and can result in over fitting of the data. The approach used in this work was to analyze the data and make intelligent equation choices which would fit data trends with the fewest number of parameters.

Initial inspection of the data(Fig. 4.6) showed that end effects were significant at both low and high pressure zones such that pressure is proportional to the tangent of the strain. This curve exists for all actuator lengths, however because end effects are more significant with shorter actuators, the width of the curve depends strongly on the initial actuator length (Fig. 4.6). Maximum strain was used in the equation instead of resting length as it is able to account for differences in attachment mechanisms which resting length could not. Because of this, the maximum strain is the only parameter which must be calculated experimentally for new systems. This maximum
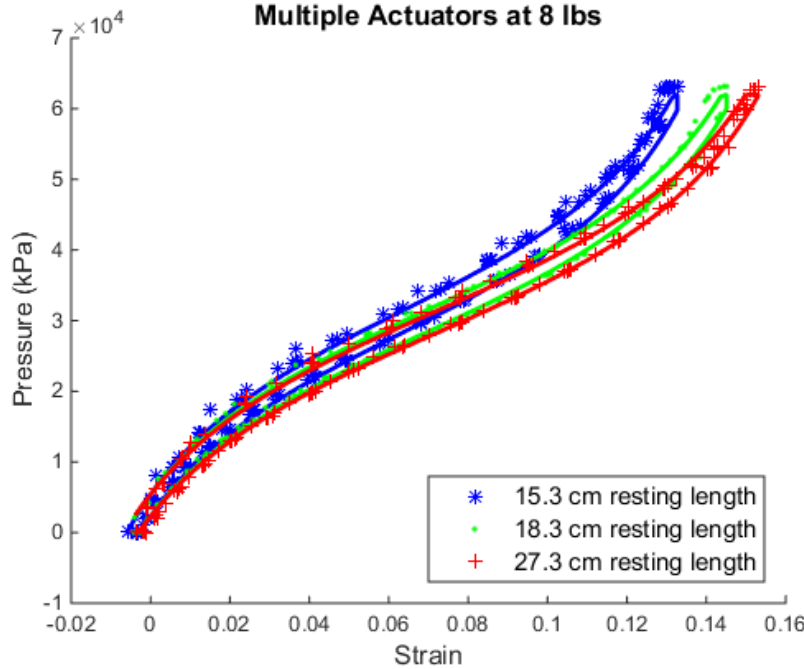
Figure 4.6: Multiple actuators with the same diameter and same weight attached to the end. Although most models do not account for actuator length it is apparent that initial actuator length has a significant effect on the strain of the actuator. This effect is accounted for in my model.

strain is the strain the actuator experiences under no load at 650 kPa.

Force has two major effects on the pressure vs. strain curve. The first is a linear proportionality. The second is a contracting of the tangent curve with increased end effector force and is observable in Fig. 4.7. Finally, the hysteresis from internal friction results in a constant offset based on filling or emptying of the actuator.

Therefore, the actuator data fit has 3 control inputs (force, strain, and filling state (+1 for filling and -1 for emptying) and 1 output (Pressure). There are also offsets associated with the tangent function leading to a model of pressure as a function of strain (k), load (F), and state (S):

$$P = a_1 + a_2 * F + a_3 * S + a_4 * \tan\left(a_5\left(\frac{k}{a_6 * F + max(k)} + a_7\right)\right) \qquad (4.3)$$

Model Fit Compared with Collected Data
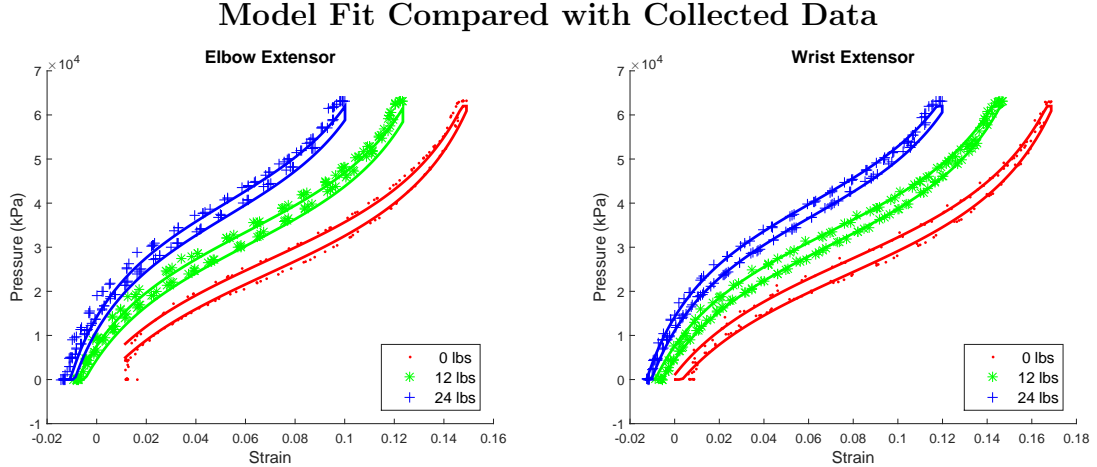
Figure 4.7: Two comparisons of the model fit with the collected data. The solid lines are from the model and the points are from measurements. The elbow extensor actuator was used in developing the model while the wrist extensor was not. The elbow extensor fit has the most error compared to all other actuators compared. The largest error is due to the kink which greatly effects the combined low pressure, low force case.

where $a_1 - a_7$ are the unknown parameters to be fit to the data. An initial fit of the equation was found by plugging in initial conditions for a tangent curve centered on the data with no force correction ($a_5 = 2$, $a_6 = 0$ and $a_7 = -0.5$) and performing a least squares linear regression for terms $a_1 - a_4$. Parameter fitting was performed on three of the actuators (15.31, 19.50, and 28.09 cm lengths) and validated on the other three (18.28, 18.94, and 27.27 cm lengths). All air muscles have a diameter of 10 mm.

After the initial fit was found, a Nelder-Mead simplex method was used to refine the parameters [Nelder and Mead, 1965]. The initial fit values were used as an initial point as well as random perturbations of each value of up to 100% for the additional points in the simplex. The optimized error attempted to reduce the rms between the calculated pressure and experimentally determined pressures. The Nelder-Mead method was run until either the linear distance in the simplex or the normalized error were less than machine epsilon. The process was repeated 5 times with the previous best fit as the new starting point.

Table 4.1: Parameters in Equation 4.3. First row is after least squares fit and second row is after Nelder-Mead optimization.

$a_1 kPa$	$a_2 \frac{kPa}{mN}$	a_3 kPa	a_4 kPa	a_5	$a_6 \frac{1}{mN}$	a_7
376.3	329.3	22.1	207.3	2.0	0	-0.5
254.3	1.230	15.6	192.0	2.0265	-0.331	-0.461

After the least squares fit, parameter values for $a_1 - a_7$ in Eq. 4.3 are shown in the first row of 4.1. This fit had a total rms error of 51.24 kPa with a maximum error of 159.3 kPa. With an operating range of 0-620 kPa, this is an rms error of 8.3% and a maximum error of 25.7%. The Nelder-Mead method resulted in values for Eq. 4.3 shown in the second row of Table 4.1. This fit has an rms error of 11.17 kPa and a maximum error of 75.8 kPa. This reduces the rms error to 1.8% with a maximum error of 12.2%. Fig. 4.7 shows the model fit with the data collected at 0, 12, and 24 lbs. on the wrist and elbow extensor. The average and maximum errors for each individual actuator are show in Table 4.2.

Actuator collection code, raw data files, and model fitting can be found with the on-line material at http://biorobots.case.edu/hunt-dissertation-files/.

Robot Testing and Control

The actuator fit was applied to the actuators on the front leg of Puppy (Fig. 4.4), a four legged robot with three planar degrees of freedom per leg first introduced

Table 4.2: Model Fit Compared to Collected Data

Length (cm)	RMS (kPa)	Max Error (kPa)
15.31	16.9	75.8
18.28	11.4	75.8
18.94	7.4	48.0
19.50	14.5	65.5
27.27	8.3	39.3
28.09	8.6	71.4

in [Aschenbeck et al., 2006]. Each joint has two antagonistic actuators. Each actuator has separate input and exhaust valves with a pressure sensor in parallel with the actuator. The developed controller is demonstrated on each of the joints on the front right leg. The actuators used for the fit are the elbow flexor, elbow extensor, and shoulder extensor. The same model was then applied to the wrist extensor, wrist flexor and shoulder flexor.

The geometry of the robot was measured and equations were developed which represent the strain of each actuator as a function of joint angle as well as equations for the transformation of torque into individual actuator force based on angle. Maps for these functions as well as the feed-forward actuator controller were written in Labview 2014 and run on the sbRIO. As shown in Fig. 4.8, the computer commands angles (α) with desired torques (T) which are transformed into desired actuator strain (k) and force (F) and are used along with individual actuator maximum strain as input into the general controller developed with the developed equation. This control module provides the desired pressure to the valve controller which is run on an FPGA. The valve controller then opens the required valves until the desired pressure (within a specified range) is reached. The smallest usable buffer for valve control is approximately ± 15 kPa due to the speed of air flow, and delays in air pressure readings and control.

For testing, each joint is provided a series of command angles from the computer and the angles from the sensors are recorded as the controller works to provide the desired pressures based on the actuator model. This is repeated for desired torques of 0, 1, and 2 N-m. The desired torque is commanded from both actuators around a single joint at the same time. This increases the force that each actuator is applying to the joint.

The FPGA valve control speed is able to control the pressure within the actuators to within approximately ± 15 kPa. This is above the rms error in all but one of

Control Flow for Testing Actuator Model
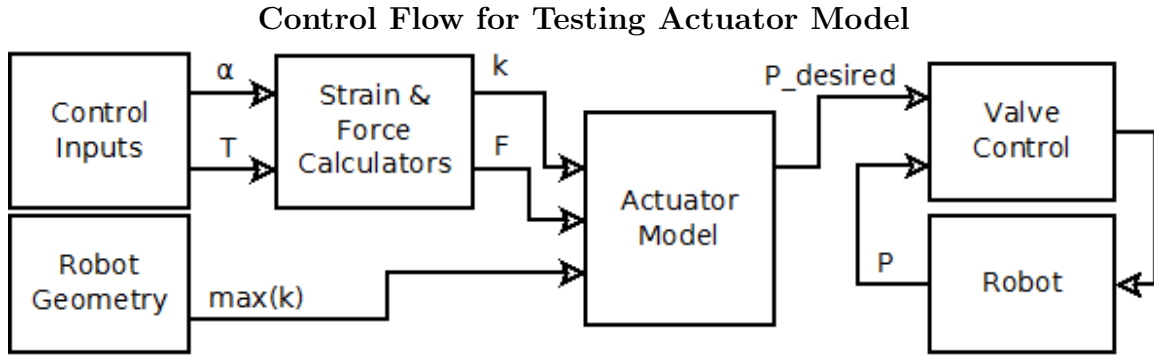
Figure 4.8: Control flow diagram for actuators. The computer sends desired angle and torque commands for the different joints, these are transformed to desired strain and force for the individual actuators based on robot and actuator geometry. These values are then used with each actuators maximum strain value to determine actuator pressure from the developed actuator model. On the FPGA, this desired pressure is compared to the current pressure and the appropriate valves are opened and closed until the measured pressure is within ±17 kPa of the desired pressure.

the actuators in the model. To compensate, a ±17 kPa no-control buffer zone is used around the desired pressure of each actuator. That is, if the measured pressure is within 17 kPa of the commanded pressure, no control action takes place. This value was found through trial and error. Both actuators in the elbow were used in the control model, and one actuator in the shoulder. For all three joints, when commanded to a series of specific angles, the controller is able to stably control the robot to different control angles within 2 degrees of accuracy under no torque (Fig. 4.9). When torque is commanded, control of the elbow drifts in more flexed positions. This is expected from inspecting the model of the elbow extensor and seeing that the model predicts lower pressures than was collected at specific strains. The shoulder control remains within 3 degrees under load, though more drifting occurs at more extended angles. Though the wrist has no actuators which were used in determining the model, it has the most accurate control.

The ability of the controller to respond to dynamic signals is also tested. Because there is no inertia model built into the controller, the wrist joint is shown to minimize effects of lag and overshoot because it has the lowest inertial load. Different frequency

Semi-Static Control of Front Leg Joints
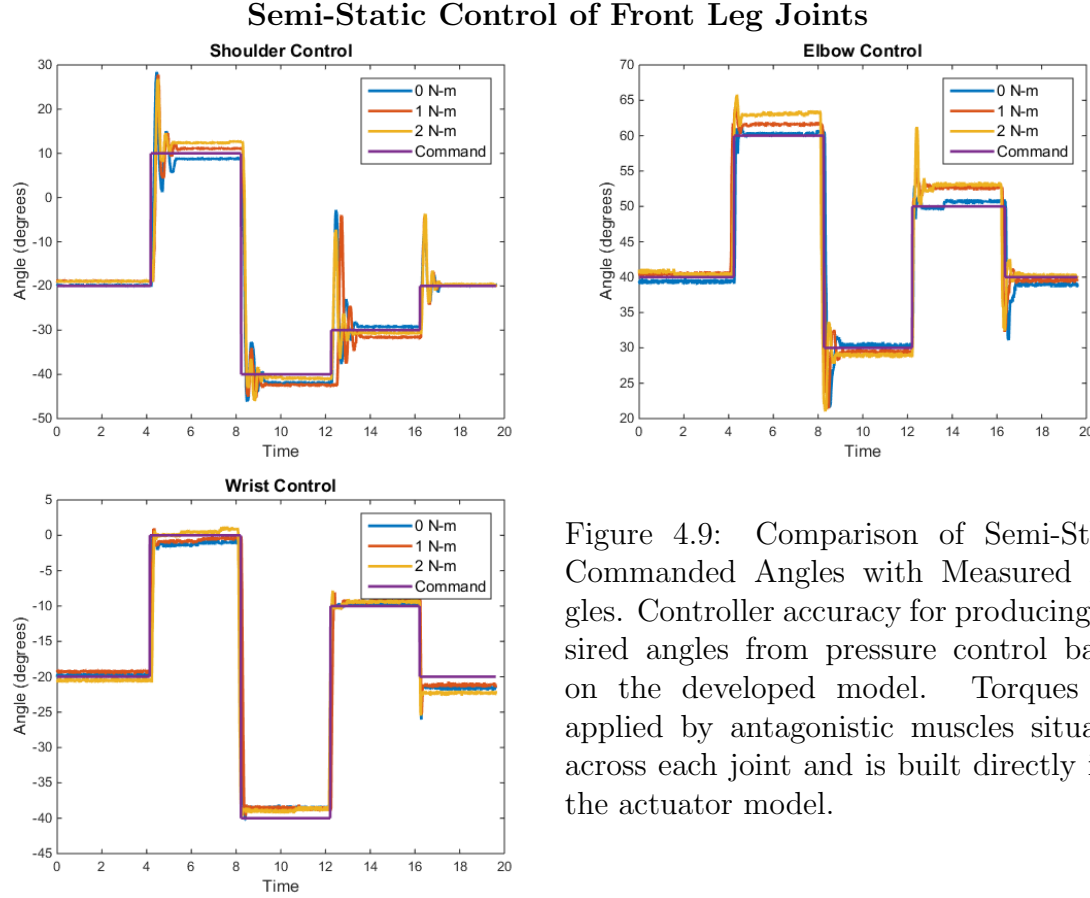
Figure 4.9: Comparison of Semi-Static Commanded Angles with Measured Angles. Controller accuracy for producing desired angles from pressure control based on the developed model. Torques are applied by antagonistic muscles situated across each joint and is built directly into the actuator model.

sine waves are commanded to the wrist angle and the ability of the controller to follow the commands is shown in Fig. 4.10.

In the actuator model, the fill-empty state is used as a complete offset which is independent of speed. Attempts at implementing the model during dynamic control this way proved unstable, causing vibrations in the pressure control signal. Instead, this signal was turned in to a continuous signal based on the velocity of the joint. The joint velocity was smoothed using a Butterworth filter with a cutoff frequency of 0.01 Hz, and scaled to be on the order of ± 1 when moving at maximum velocity.

Actuator Model Discussion

The actuator model fits the data within a few kPa over most ranges. The model is able to capture the effect that the resting length and attachment hardware has on
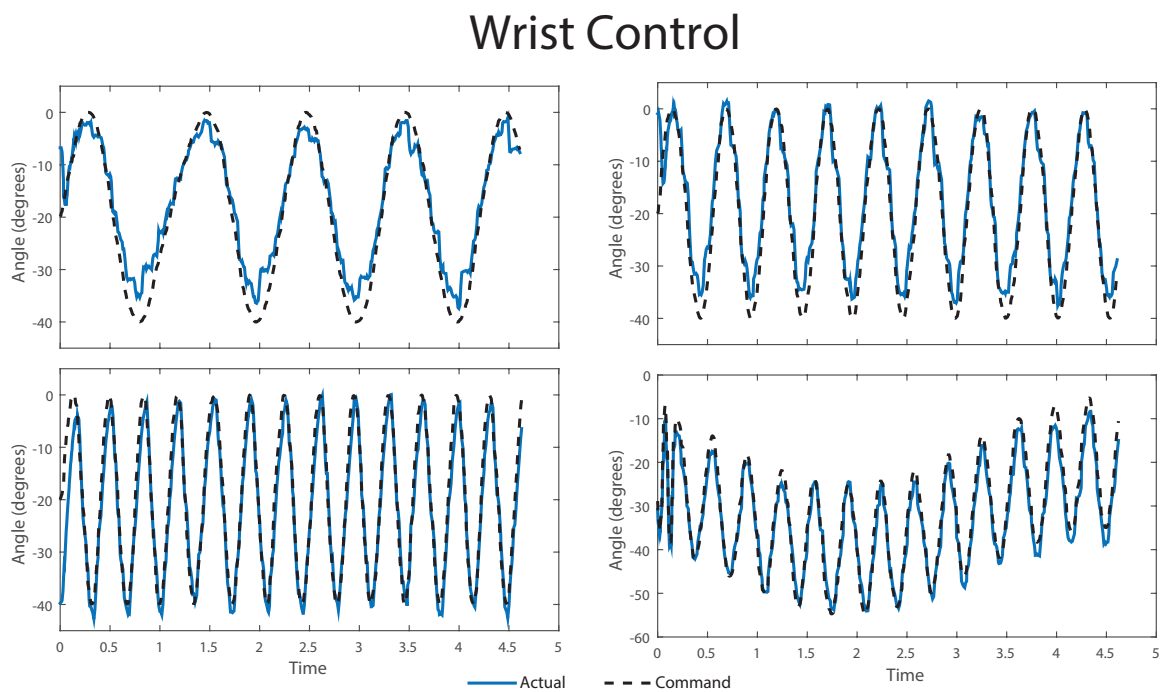
Figure 4.10: Wrist control for following different frequency sine waves. As speed is increased, error is decreased when the actuators spend less time dwelling at specific pressures. Because the actuators do not fully empty, the controller is able to trace sine waves at varied mean points up to approximately 3 Hz.

actuator strain (Fig. 4.6) with the inclusion of a maximum strain variable into the equation. This ability makes controlling newly designed hardware easy to implement without developing a new model for each actuator. Fig. 4.7 shows two example fits, and it can be seen that even the worst fit (elbow extensor) matches the data shape well.

The model is least accurate when there is combined low pressure and low force. This is an artifact of the particular actuators used in experimentation which have permanent kinks in them (Fig. 4.4). These kinks keep them from stretching out fully in this state. This is most readily visible with the elbow extensor where there is no change in length in the collected data under 500 kPa. This has little effect over the control of the robot as the actuators spend little to no time in this range during walking.

Control of semi-static joint positioning is accurate within three degrees, and is well within the range of joint variation seen during walking in animal systems. This accuracy has multiple advantages for control. It enables the implementation of a low impedance controller. When the current angle is fed back into the robot as the desired angle, human operators can move the joints by hand with little resistance from the robot. No joint torques or force on the arm need be computed for this to occur. The actuator compliance allows for small changes in angle with little force. These new angles are then transformed into new desired pressures to keep the actuators at the desired length for the new angles. When the operator is done moving the robot arm, the joints maintain their position and do not drift.

This ability of the actuators to follow joint movements without applying torques decreases actuator response times to new commands in opposite directions. A previous controller on the robot required that an actuator be fully emptied to ensure it did not provide counter torques to a movement. When the actuator is required to provide a force, time must be spent filling up the empty actuator before it can provide

the commanded force. With the developed actuator model, responses to directional changes can be performed more rapidly. This is clear in Fig. 4.10 where the controller is able to cycle 30 degrees of rotation at 3 Hz over a range of mean set points.

There are two main reasons for the angle overshoot. The first, most readily seen in the shoulder control, is that of angular momentum. No dynamic model is built into the controller, therefore no attempt is made to slow the arm down or create a smooth trajectory. This is not seen as a problem as the final controller will inherently account for the dynamics through the neural control network. Second, foam is placed in the air line in series with the pressure sensors. This foam evens out pressure readings, however it creates a delay in the actual pressure readings. This delay causes the valves to stay open longer than desired, needing a corrective action from the opposing valve to bring the actuator to the correct pressure. This problem was mitigated through the reduction of the amount of foam in the line to the minimum amount of foam needed to keep the system stable.

These basic tests of the model and low level control have proven to be satisfactory in enabling effective force control of the muscles. The system is able to reliably respond to dynamic demands of a higher level controller and remain stable. Now that we have the desired kinematics and dynamics, and we have developed a model capable of providing desired force output, it is time to determine the actuator tensions and motor neuron activations.

4.2.3 Calculating Muscle Tension and MN activation

Calculation of the tension and MN activation for the muscles on Puppy were done similarly to that of the rat simulation. To take advantage of already written code, the developed Festo actuator model was adapted to the Hill muscle model. The series spring element was assumed to be extremely stiff ($10^{12}N/m$). To match the length-tension relationship, the maximum output force of 509 N was set at the muscle's

maximum length and 0 N at its minimum length. The peak velocity of the muscles was estimated to be twice the speed of the average joint rotation speed. All other parameters were kept the same as the rat model.

4.3 Results and Discussion

4.3.1 Rat

Active, passive, and total muscle forces for the hip, knee and ankle are shown on the left of Fig. 4.11. For the hip, passive muscle properties work against motion, causing the muscle to develop more active tension to overcome passive muscle forces from itself and the antagonist. However, passive properties in the knee and ankle extensors have assistive effects during stance, helping provide force rather than reduce it. This is because both the knee and ankle go through eccentric contractions at the beginning of stance, even though the extensors are active. The joints flex due to the weight of the rat, causing energy to be stored in the spring elements of the extensors and providing additional force through the rest of stance. This stored energy continues to affect the system, resisting flexion motion at the beginning of swing, and providing some additional extension just before touchdown.

Muscle activations are found on the right side of Fig. 4.11. Activation of the hip muscles is directly in time with changes from stance to swing. Ankle flexor activation occurs with the onset of swing. Both ankle and knee extension begin well before ground contact, extending the leg in search of the ground and providing support immediately upon ground contact. Desired knee activation has a biphasic nature to it, where the flexor activates at both the beginning of stance and the beginning of swing. Activation at the beginning of swing acts to lift the foot off the ground, however active knee flexion during stance has a less clear motivation. One possible reason for this could be the role of the hamstring muscles in providing both hip
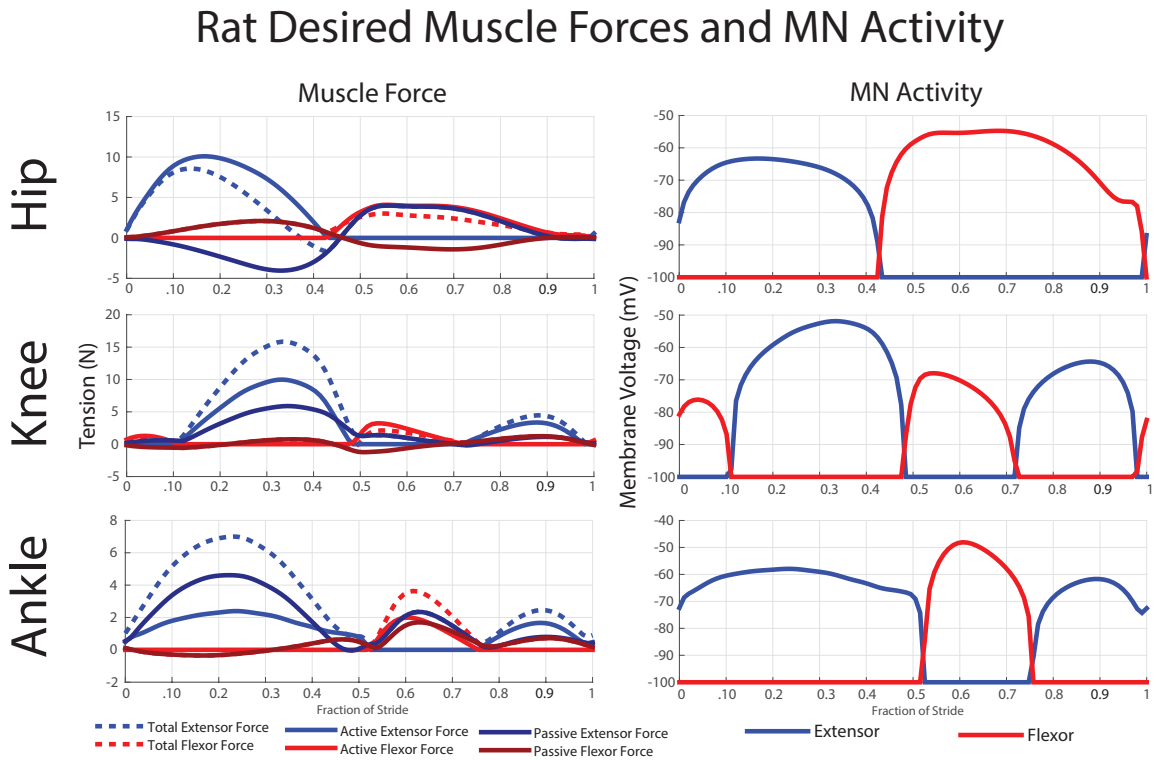
Figure 4.11: Desired muscle forces and MN activity for the hind leg of the rat simulation. Hip activity is in time with stance and swing transitions, while the ankle and knee exhibit more nuanced behaviors midswing and at the beginning of stance.

extension and knee flexion. The hamstring could serve to stiffen the joint during stance, and could be manifested as an initial flexing force in the knee during stance. Because of this, knee flexion activation at the beginning of stance is ignored during initial training and is accommodated later through a 'hamstring' synapse from the hip extensor MN to the knee flexor MN.

The code for producing these can be found in the 'Matlab Code/Rat Model Development' at http://biorobots.case.edu/hunt-dissertation-files/.

4.3.2 Puppy

The resultant tension for the hind and foreleg joints can be seen in Fig. 4.13. Muscle force requirements in the robot are significantly higher than that of the simulated rat. For the hip and knee, the ratio of peak muscle force for puppy to the rat is

approximately 17:1, and the ankle is approximately 47:1. This is a little higher than initial estimates which scale peak forces approximately proportional to body mass, which is about 10:1 for the robot to the rat. The hip and knee are only 70% greater than the theoretical ratio, and differences in kinematics and effective moment arms could reasonably account for these differences. The significantly higher ankle forces might be a function of under-calculated ankle torques in the rat as described later.

Activation profiles for the robot require much higher activations than as seen with the rat. This is not an indicator that dogs must work harder than rats while walking (though we did notice higher than predicted muscle forces in the previous paragraph), but is instead an indicator that the Festo muscles might be underpowered to produce the desired walking speed. This was most evident when the training of the network (described next in Chapter 5) first produce saturated MNs, indicating the desired torques required the maximum possible muscle force during the majority of walking. With decreased, or partially supported weight of the robot, the Festos can provide sufficient forces for walking. The muscles' capability for providing force also becomes much smaller as they get shorter, requiring higher activations near the end of swing and end of stance. This requirement is opposite the CPG shape, which tends to peak higher and then reduce over time.

Additionally, the knee for Puppy does not seem to exhibit the same bi-phasic activation profile that the rat does. This is likely a result of desired kinematic behavior. Compared to dogs, rats walk with much more crouched gaits in which the knee stays moderately flexed during stance. Desired knee kinematics for Puppy are approximately 30 degrees more open than for the rat.

The code for producing these can be found in the 'Matlab Code/Puppy Kinematics and Dynamics' at http://biorobots.case.edu/hunt-dissertation-files/.
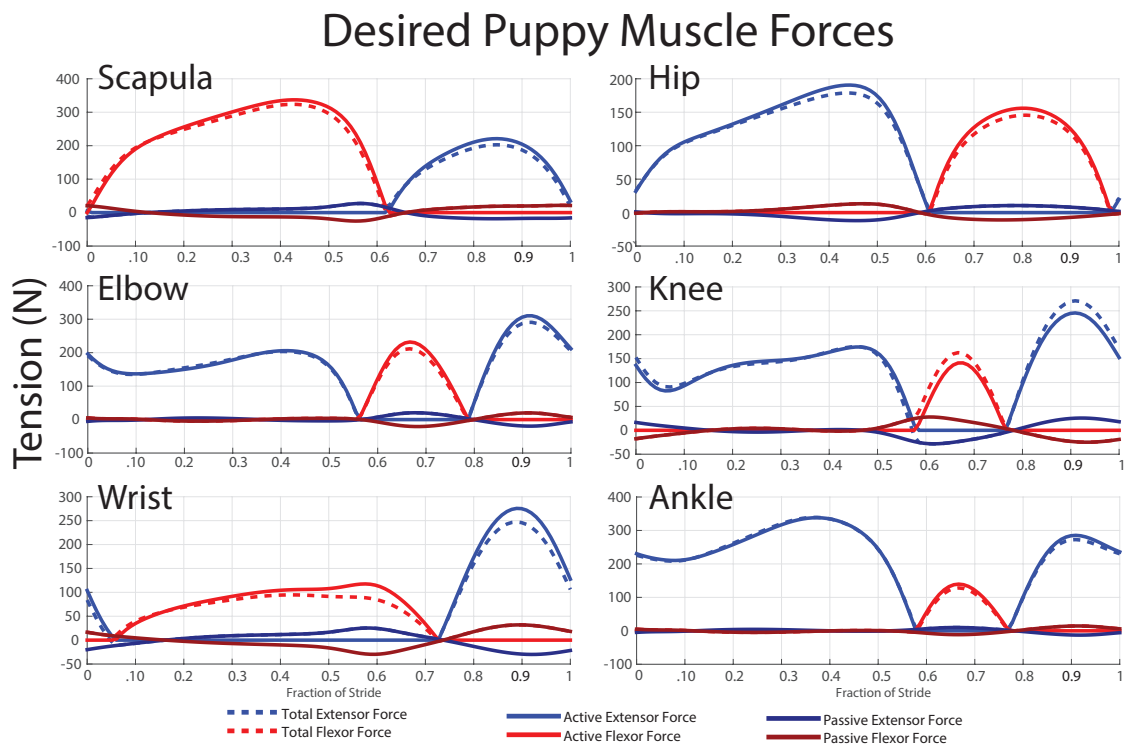
Figure 4.12: All desired muscle forces for forward walking of the puppy robot. Hind leg forces have the same shapes as the rats' with knee and ankle extensors building tension before stance. Additionally, the knee and ankle flexors begin to lift the leg just before the hip flexors at the beginning of swing. Front leg muscle tensions are significantly different compared to the rat due to the fewer number of joints. The multiple significantly different tension profiles would later prove troublesome when applied to the robot.
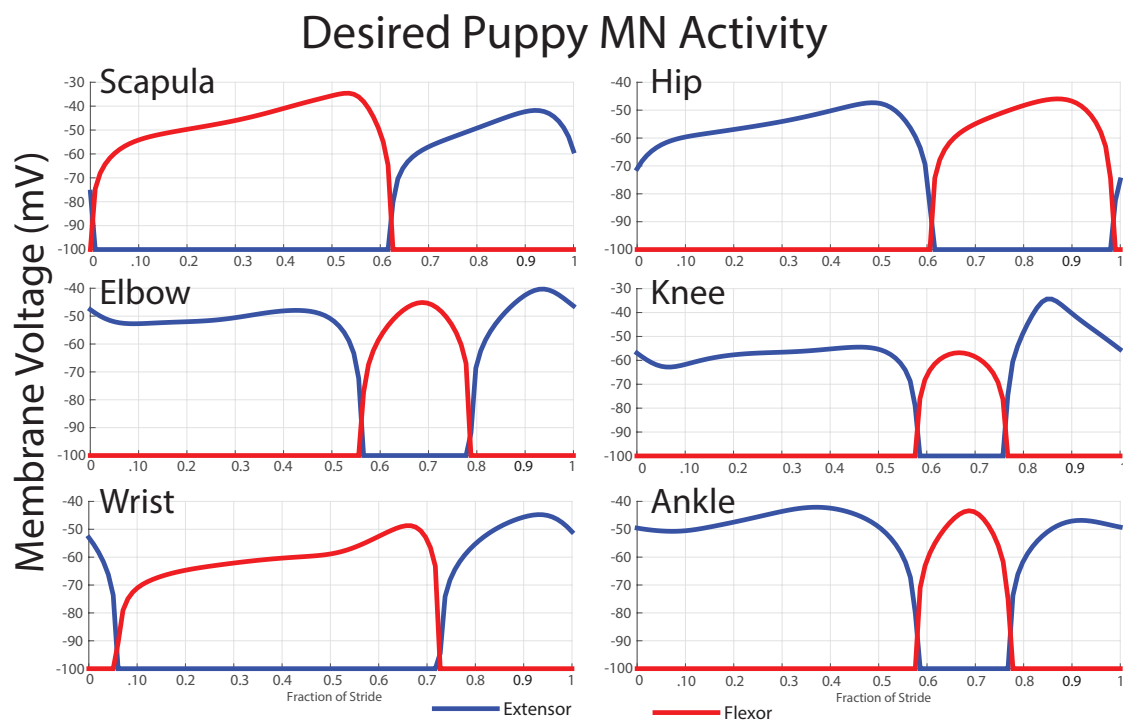
Figure 4.13: All desired MN activations for forward walking of the puppy robot. Activations are higher than compared to the rat activations, often increasing over time. This is an effect of the muscles being able to provide less force at shorter lengths when compared to the simulated rat muscles. The increase in activations is also opposite to what the current feed forward CPG synapses can provide, and additional shaping of the curve occurs through lower level feedback pathways.

Chapter 5

Training CPG Network Output

Now that the desired MN activation patterns are determined, the network training procedure for both the simulated rat, and Puppy are the same. The trained network need not know anything about the specifics of the system it is actuating, only the desired MN activation patterns and the feedback patterns it expects to encounter while performing the desired motion. Each joint is trained individually and then combined together and tested with the simulation or physical robot.

The developed procedure is used to set neuron and synapse parameters to achieve the desired functionality - walking. This procedure is performed in four steps based on functional analysis of the system. For effective walking, the CPG system must oscillate independently at approximately the same time scale as the walking model, and this oscillation frequency must be adjustable by sensory feedback to entrain the CPG to the dynamics of the system. Therefore, the first step in setting the parameters involved further analysis of the CPG system and setting its parameters to achieve these desired functionalities.

The next step involves training the system to oscillate with the correct joint timings based on sensory feedback. This involves determining which feedback pathways synapse where onto the CPG, and setting the parameters in these synapses such that

the activation of a particular half-center corresponds with the desired activation of the corresponding motor neuron. These values are set using a genetic search algorithm followed by a Nealder-Mead minimizer.

After the CPG is entrained to the predicted dynamics of the system, the output synapses from the CPG to the MNs are set to provide significant activation for the production of walking. A quick genetic search followed by a Nealder-Mead optimization is able to set the weights of these synapses to produce MN activation peaks which are equal to desired peak heights.

Finally, the final Ia and Ib feedback parameters are set for the system. Ia inhibitory feedback from antagonistic muscles encourages the leg to slow down when swinging too quickly, and self-excitatory Ib feedback helps the leg produce more force when the leg is in a less mechanically-advantageous position or is overcoming obstacles. These are also set using a genetic search and Nealder-Mead minimizer.

After the parameters for each joint have been found using Matlab, they are written into the Animatlab file and the simulation or robot is run for testing. The current setup requires no additional training with all joints together, and is capable of running immediately. The following sections will describe each of these steps in more detail.

5.1 Designing CPGs

The connectivity of the Zhong locomotor model ([Zhong et al., 2012]) was chosen as the basis for the neural control system of the low level control model. The implemented model was simplified to a single network for each joint with a pattern formation layer and lower level afferent feedback networks (Fig. 5.1). This allows us to concentrate our efforts on how feedback can be used to shape motor neuron activation level and timing. The integrator layer of neurons described earlier is removed and direct connections are made to the interneurons of the CPGs. The implemented
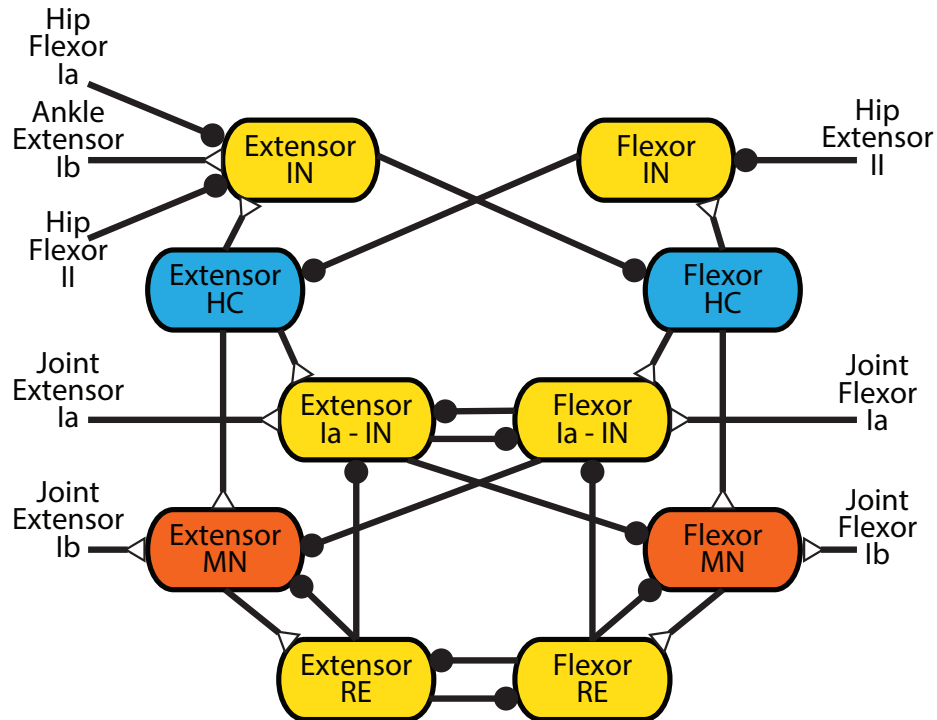
Figure 5.1: Network architecture for a single joint in the hind leg. Blue neurons are CPG half-centers with additional sodium currents. Red neurons are motor neurons used to provide activation to the muscles in the rat simulation or the Festos in the robot. Yellow neurons are interneurons. Feedback from the entire leg is applied directly to the CPG of each joint in the form of hip flexor Ia and II, hip extensor II, and ankle extensor Ib feedback. Extensor and flexor Ia and Ib feedback from each joint feed directly back onto the joint control through Ia interneurons or directly onto the motor neuron.

connections are derived from the overall inhibitory or excitatory effects of the Ia, Ib, and II pathways. This removal of the integrator layer reduces the number of parameters in the neural system, simplifies the training process, and reduces computational time.

Each leg network (which includes three joints) consists of 82 neurons with 12 parameters each, and 134 synapse connections with 4 parameters each. Many parameters were set using basic heuristics such as resting voltage (-60 mV), time constant (5 ms), and relative size (1). Even after these simplifications, approximately 90 parameters per leg, mostly synapse strengths, still needed to be set. Because of the

large number of possible local solutions, the design and training of the CPG network was done over the course of several iterations in which more and more detail was added to the simulation. The network was built and trained without a physics-based simulation and then the results were tested with the physical model or physics-based simulation.

I started by designing a CPG for the pattern formation layer of a single joint which is capable of producing the desired phase transitions in response to sensory feedback. In work with Nick Szczecinski, we used numerical methods and eigenvalue analysis to characterize a computational model of a CPG our collaborators have been using for modeling stick insect walking in Cologne [Daun-Gruhn et al., 2009]. The system is composed of two mutually inhibitory neurons called half-centers (HCs), each with persistent sodium channels (Eq. 2.4). These channels provide decaying positive reinforcement to membrane voltage fluctuations, which make sustained oscillation possible. Mutual inhibition is implemented via nonspiking interneurons (INs). Each HC excites an IN, which inhibits the other HC, as shown in Fig. 5.2. Though this CPG is composed of only 4 non-spiking neurons, it exhibits many of the same shapes, behaviors, and responses to perturbations that are seen in the average spiking frequency of four pools of spiking neurons. It has the same network architecture as the neural pools used in the Zhong locomotor model, and the oscillatory dynamics are also governed by a slowly activating and deactivating persistent sodium current.

Szczecinski's analysis finds nullclines and equilibrium points for the system, characterizes their stability, and examines how oscillation is achieved. To simplify analysis, we assume that the parameters of each HC, its IN, and the synapses that connect them are symmetrical. In addition, since $\tau_m < \tau_V << \tau_h$, we assume $m = m_\infty$, which lets us visualize one neuron's phase portrait in two-dimensional space.

This model may either have one or two equilibrium points, depending on the applied drive. When there are two, we categorize these points by their state relative
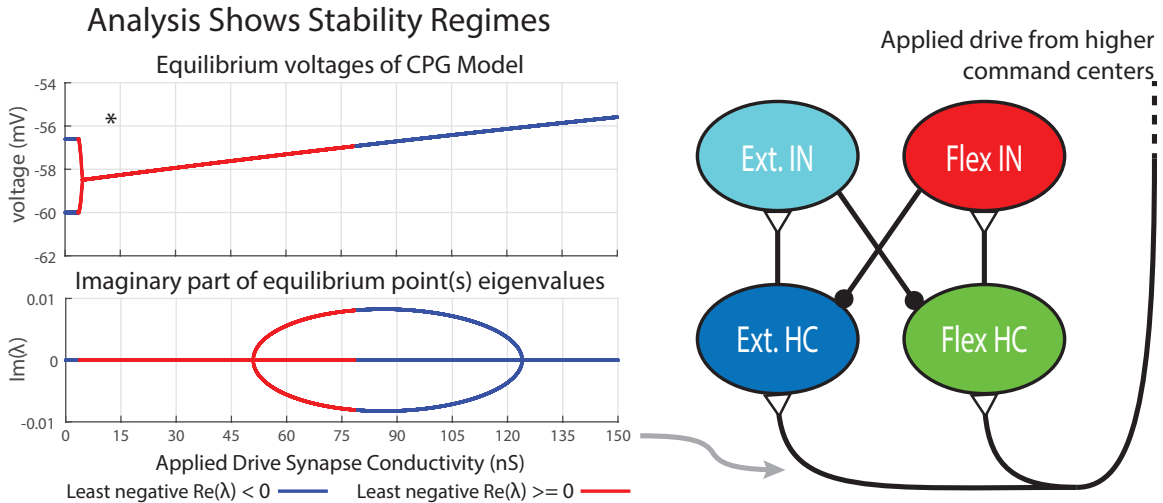
Figure 5.2: Plots showing the equilibrium voltages of the neurons in a CPG and their eigenvalues as the conductivity of an excitatory pathway to both HCs is varied. This changes the INEV, resulting in a variety of eigenvalues and thus behaviors. The * denotes the system configuration used in this study.

to the other, yielding an excited neuron equilibrium voltage (E_{exc}) and an inhibited neuron equilibrium voltage (E_{inh}). E_{exc} is the steady state voltage of the neuron when it has no inputs, and E_{inh} is the steady state voltage of the opposite HC when inhibited by its counterpart resting at E_{exc}. E_{inh}'s value relative to synaptic threshold E_{lo} (Eq. 2.2) was revealed to be important for determining the existence and nature of oscillation. For example, if E_{inh} is below the synaptic threshold, no endogenous oscillation will occur, because the inhibited HC has no means of escape. Applying excitation via descending commands increases E_{inh} and E_{exc}, and when $E_{inh} > E_{lo}$, the system oscillates. However, in this case E_{inh} and E_{exc} no longer correspond to actual equilibrium states of the system; with enough applied drive, the system will possess only one unstable equilibrium point, about which a limit cycle forms. Fig. 5.2 shows a full sweep of applied drives, revealing a number of bifurcations. However, high-drive scenarios were not applied to my model.

Perturbation response was also studied by numerically generating phase response surfaces (PRSs). These PRSs are different from the typical phase response curve in that the duration of a stimulus (a square pulse) is plotted along with the phase of

stimulus onset. We chose this method because our inputs are in the form of sustained signals from afferent receptors, not impulses.

PRSs for inhibitory stimuli to the HC and the IN, for the first or second cycle following the stimulus are shown in Fig. 5.3. The PRS for stimulus to the IN shows that it is comprised of three planar regions. If inhibition arrives while that IN is active, the CPG advances phase proportional only to the phase of its arrival. If it arrives while the IN is inactive, the CPG phase is delayed only if the stimulus duration is longer than the remaining time in that cycle.

The CPG's response to stimuli applied to the HC is more complicated. The response is linear along the stimulus phase for stimulus durations longer than 10% of the period. It is also linear along the stimulus duration, which suggests that the phase shift depends on the timing of both the application and removal of the stimulus. When the stimulus is removed, a rapid upward change in V following release is reinforced by m, causing the neuron to overshoot E_{lo}, inhibit the other HC, and create a secondary transition. This rebound effect can also be achieved by exciting the presynaptic IN, which we choose to do in our model.

A CPG was designed by setting the equilibrium point of the low neuron to 0.001 mV below threshold, adding a synaptic drive of 13 nS towards 0 mV, and adjusting the slope of $m_\infty(V)$, h_∞, and G_{Na} until a CPG was formed with a peak height approximately 20% above the high equilibrium point and a period of two times the final desired oscillation period.

5.2 CPG Entrainment

The next step in choose parameters for the network to produce the desired output was to entrain the CPGs to the sensory feedback such that it oscillates in conjunction with the calculated alternating motor neuron activations. Training the network to

Stimuli to the CPG Interneurons Produces Favorable Responses
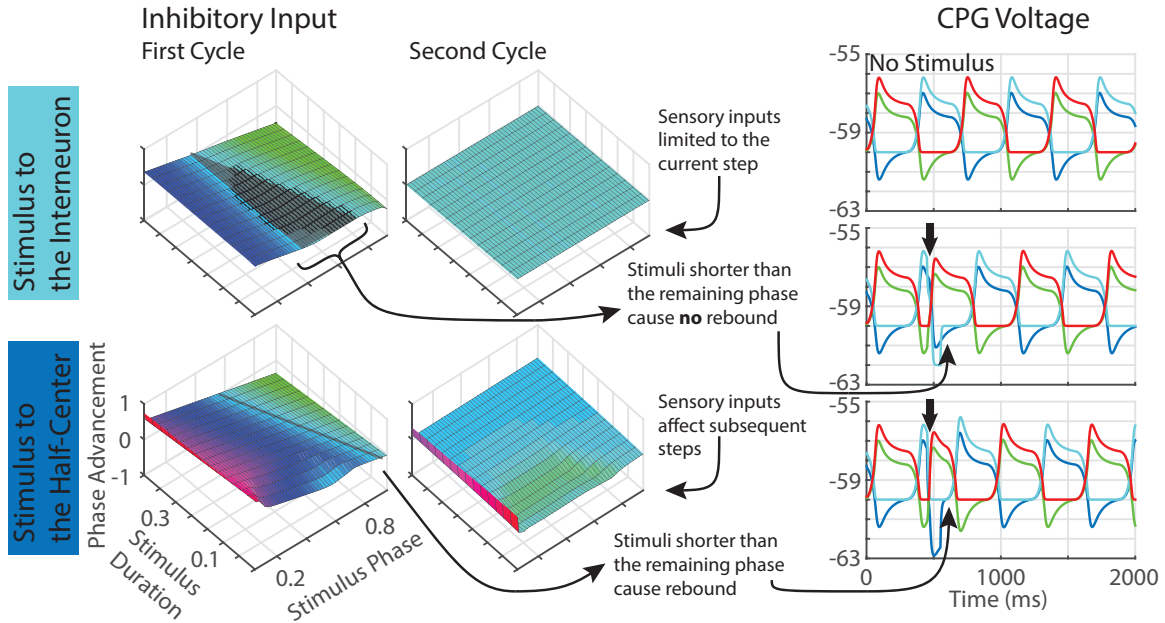
Figure 5.3: Phase response surfaces from inhibitory inputs, and their interpretation explained by simulation output. All axis labels for the surfaces are the same, in units of % of the period. When an inhibitory input is applied to the interneuron, while the interneuron is active, the phase is advanced according to the time at which the input is applied (blue). If the inhibition is applied while the neuron is inactive, the phase is delayed only if the duration of the input extends beyond when the CPG would have transitioned otherwise (green). Otherwise there is no effect on the CPG (gray\cyan). When an inhibitory input is applied to the active half-center, the phase is advanced according to when the input is applied. If an inhibitory input is continued to be applied, or is applied when the half-center is inactive, the phase is advanced when the stimulus is removed from the neuron.

produce these results necessitates that feedback be provided as though the correct stepping motions are taking place. Types Ia, Ib and II feedback are calculated as follows in AnimatLab 2:

$$\text{Ia} = k_a x_{series} \qquad \text{Ib} = k_b T \qquad \text{II} = k_c x_{parallel} \qquad (5.1)$$

where k_a, k_b, and k_c are gain parameters set by the user, and the expressions in Eq. 5.1 specify the current injected into sensory neurons. Ia feedback encodes both length and velocity of muscle movement. Ib encodes the muscle tension, and II

encodes the length of the parallel elastic element $x_{parallel}$. The gains were set such that the feedback injects between 0 and 20 nA of current into a designated sensory neuron over the full possible range of tension and lengths for each muscle. Using the kinematics and expected muscle tensions calculated earlier, we are then able to calculate the afferent feedback of the AnimatLab 2 simulation for walking with the projected kinematics.

This feedback is used as input into the CPG according to rules discovered in vertebrates, previously described in Chapter 3. Additionally, analysis of the CPG system enabled the elimination of the integrator layer of neurons with the direct application of the feedback onto the CPG system. Hip flexor stretch encourages a transition from stance to swing in decerebate cats [Pearson, 2008], and hip extensor stretch contribute to termination of swing [McVea et al., 2005, Akay et al., 2014]. To obtain the proper CPG response, these feedback pathways are implemented as inhibitory synapses to the CPG INs. Research also shows that stance can be prolonged in spinal cats with continued stimulation of ankle Ib feedback [Pearson, 2008]. This is implemented as an excitatory connection to the extensor IN to ensure stance when force is detected and obtain the rebound effect described earlier when force is removed.

The strength, synaptic thresholds, and driving current of these four synapses onto the CPG were first trained using a genetic algorithm with a population of 1500 samples for 5 generations, and then refined using a Nelder-Mead simplex method. Penalties to the objectives were period, CPG rise times in relation to desired MN rise times, and the synaptic strengths. The fitness function being minimized is as follows:

$$f_1(x) = (P - P_o)^2 + (Se - Se_o)^2 + (Sf - Sf_o)^2 + \sum(G_{syn}) \qquad (5.2)$$

where P is the calculated period, Se and Sf are the calculated extensor and flexor activation times, P_o, Se_o, and Sf_o are the desired period, and extensor and flexor activation times, and G_{syn} is the maximum synaptic conductance of the input synapse

onto the CPG.

5.3 CPG Output

Subsequently, the CPG output synapse strength was trained to produce activations of the motor neurons with a peak height that matches each desired motor neuron activation and a minimum of no activation at some point in the cycle using a genetic population of 300 samples for 5 generations and further refinement by Nelder-Mead. The fitness function is:

$$f_2(x) = (\max(\boldsymbol{E}) - \max(\boldsymbol{E_o}))^2 + (\max(\boldsymbol{F}) - \max(\boldsymbol{F_o}))^2 + \min(\boldsymbol{E}) + \min(\boldsymbol{F}) \quad (5.3)$$

where $\boldsymbol{E}$ and $\boldsymbol{F}$ are the full extensor and flexor motor neuron patterns and $\boldsymbol{E_o}$ and $\boldsymbol{F_o}$ are the desired patterns.

5.4 Afferent Influence of MN Activation

Afferent feedback was trained to help shape the MN output and provide additional force if necessary to overcome changes in foot placement (excitatory Ib feedback), or reduced force if the leg is moving too quickly (inhibitory Ia feedback). All neurons and pathways involved in these networks were designed to be completely continuous over all possible ranges. Though sensory feedback could be modulated by thresholds in the animal, I did not train thresholds because the input is only expected input and training thresholds causes the system to become overly dependent on exact threshold points and small changes in feedback strength had significant effects on behavior. The

fitness function for the final training is:

$$f_3(x) = (\max(\boldsymbol{E}) - \max(\boldsymbol{E_o}))^2 + (\max(\boldsymbol{F}) - \max(\boldsymbol{F_o}))^2 +$$
$$\min(\boldsymbol{E}) + \min(\boldsymbol{F}) + (\boldsymbol{E} - \boldsymbol{E_o})^2 + (\boldsymbol{F} - \boldsymbol{F_o})^2$$

(5.4)

The final fits of the training for the rat hind legs, and the puppy front and hind legs can be seen in Fig. 5.4.

For the rat, the hip and ankle fit well, while the bi-phasic nature of the knee provided some problems. Extensor output is much higher than desired at the end of swing, and does not see a full dip down at the beginning of stance. Flexor output at the beginning of stance was ignored during training and later produced through a 'hamstring' connection in which hip extensor activation also activates knee flexion. Despite this problem, the desired timing of activations for all joints is directly in line with desired transitions between stance and swing and back.

For Puppy, hip extensor output at the beginning of stance is a little high, but final extensor output is within 5% of desired output. This initial extra activation is a result of training the CPG output synapse on the highest desired peak of MN activity, and could be improved by training the output strength based on the highest point in the first 25% of MN activity. Additionally, knee extensor output is initially within a few percent, however it maintains much higher output during stance than is desired. Additional feedback pathways may be required to limit the activity during stance. Trained ankle output for flexor and extensor activity follows the desired shape and is within a few percent of the desired output. Hip flexor MN activity begins a little early, however the height is within 10% of the desired activity while the knee and ankle transitions are at the correct time during the stride.

The code for performing the training for both Puppy and the Rat can be found in 'Matlab Code/Optimizer' with the on-line material at http://biorobots.case.edu/hunt-
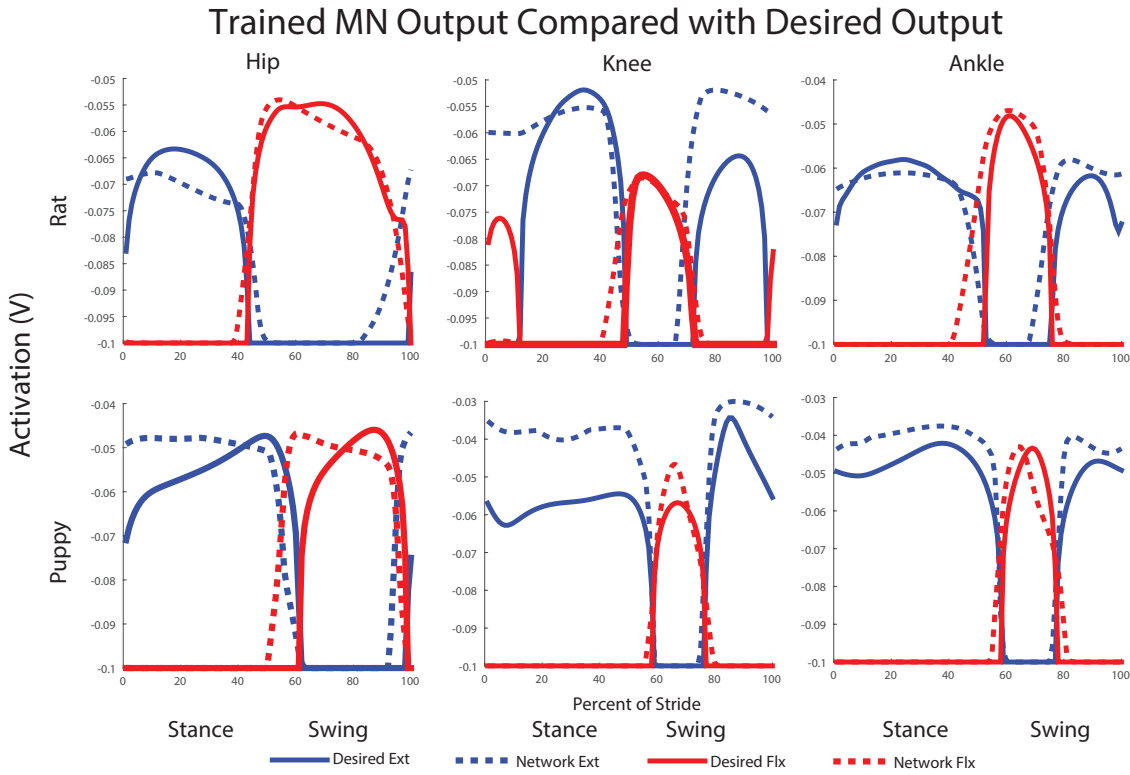
Figure 5.4: Trained Network Output compared with desired motor neuron activations. Top row is rat hind leg while bottom row is the Puppy robot hind leg. For the rat, the hip and ankle fit very well, while the bi-phasic nature of the knee posed some problems. Extensor output is much higher than desired at the end of swing, and does not see a full dip down at the beginning of stance. Flexor output at the beginning of stance was ignored during training and later produced through a 'hamstring' connection in which hip extensor activation also activates knee flexion. For Puppy, hip extensor output at the beginning of stance is a little high, but final extensor output is within 5% of desired output. Hip flexor MN activity begins a little early, however the height is within 10% of desired value for over 90% of the cycle. Knee and ankle transition timing are exactly timed with desired transitions. Knee extensor output is initially within 5%, however it maintains much higher output during stance than is desired. Desired ankle output is within 5-10% for both extensor and flexor activity.

dissertation-files/.

Chapter 6

Resultant Simulation and Puppy Walking

The developed training procedure is capable of producing coordinated, hind leg walking in both the simulated rat and Puppy robot. The rat simulation required one additional modification to ensure sustained walking, while the robot is capable of sustained walking at a variety of treadmill belt speeds and with a range of body weights.

6.1 Rat

6.1.1 Additional Modification

Initial observations of the rat kinematics showed joint timing between stance and swing transition match the desired timings, however the ankle was never flexed enough to complete swing, causing the toe to catch the ground and stay in a relatively extended position such that the top of the foot faced the ground at all times. This inspired the addition of an additional feedback pathway to encourage more ankle flexion. Type II feedback was added to the ankle flexor which would provide addi-
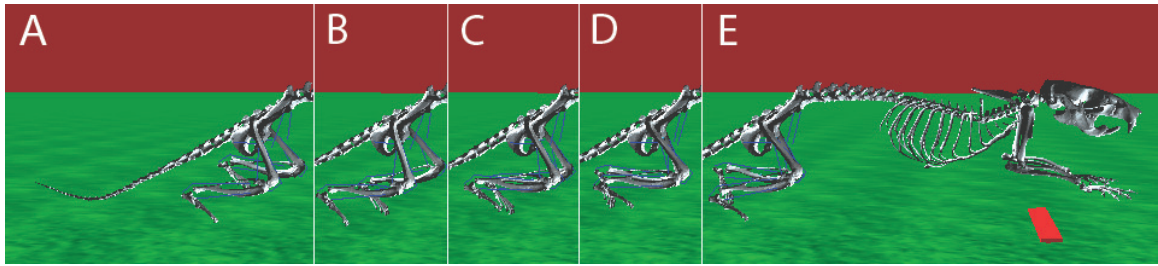
Figure 6.1: Series of screen shots demonstrating hind leg walking in the rat simulation. (A) Left leg is in swing and the right leg is in stance. (B) Double support phase. (C) As the left leg takes up more weight, and the right leg moves further back, it begins to enter swing. (D) When the forward swing position is reached, the right leg begins extension. (E) When the right leg touched down and begins to bear load the left leg enters swing and the process is repeated.

tional MN activation and force if the ankle flexor was longer. This causes the foot to swing faster to avoid ground contact, and provides additional activation roughly proportional to ankle angle. This additional pathway provided ground clearance, encouraged the ankle to be more flexed, and enabled the leg to make full, propulsive steps.

6.1.2 Walking Results

A multiframe depiction of the walking hind legs are shown in Figure 6.1.

To test the network, motor neurons in the hind leg were stimulated in two ways and kinematics were compared with the animal data. In the first method the motor neurons were stimulated by a sequence of currents which produces steady state activation equal to the average activation of 1/10 of the step. This provides motor neuron activation roughly equal to predicted motor neuron activity based on work done in Chapter 4. In the second method the motor neurons were stimulated by the CPG network with all feedback pathways connected. These two results are compared with the desired muscle forces and kinematics in Fig. 6.2.

The CPG network is significantly more capable of producing steps than direct stimulation of the motor neurons without any feedback. When using direct stimu-

lation, the simulation was sensitive to friction values and pelvis height and did not produce kinematic motions beyond a few degrees, despite having input the calculated desired muscle activations.

This may be a result of incorrect torque calculations stemming from one of two areas. The first possible area is from the application of estimated torques from averaged rat data to a specific rat model. Though the torques in our collaborators work are normalized to body weight, there may be additional modifications to torque values based on rat sizes and limb lengths that were not accounted for when applied to my model in Animatlab. Additionally, applied frictions and muscle properties in the model may be different from what the rats experienced in the experiments. This
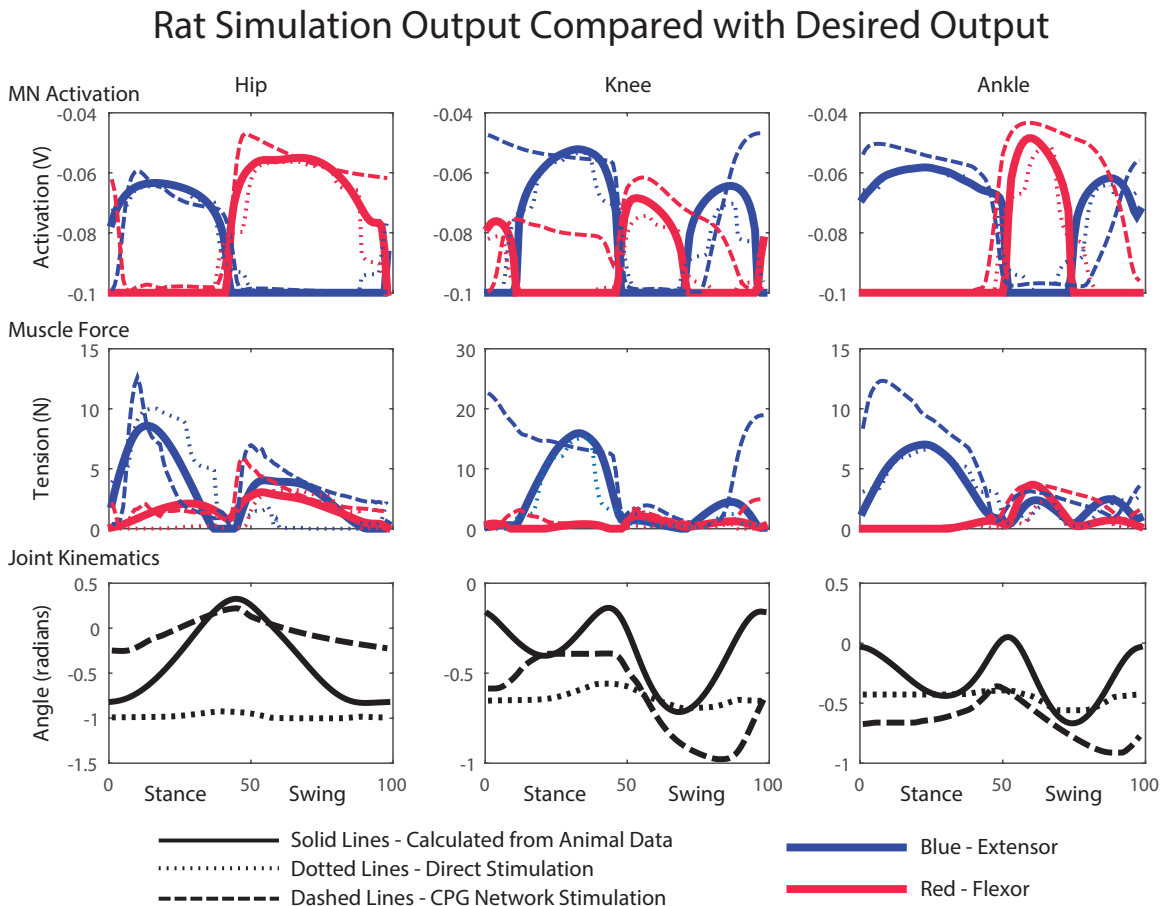
Figure 6.2: Comparison of desired motor neuron activations, muscle tensions, and joint kinematics with those produced by direct stimulation of the motor neurons and stimulation of the motor neurons by the CPG network.

would change the required torques and muscle forces but not be fully captured in the model.

Another indication that the calculated torques may be too low is evidenced with the CPG network movements and tensions. Here, most produced tensions are larger than the calculated tensions, however joint movements are not as large as in the real animal.

The CPG network does not have any connections between the legs, and is not capable of producing sustained alternating stepping. Because the leg is not catching the weight of the rat, the first half of stance for the knee and ankle do not undergo early flexion followed by extension; however the power stroke of the leg raises the pelvis from the ground during each step, indicating the muscles are receiving activations capable of supporting and propelling the rat.

Though joint kinematics and muscle forces have some errors, the neuron network is capable of maintaining the necessary rhythms despite not having been trained with the full physical simulation. The careful construction of the CPG model and subsequent training of the coordinating currents is successful in producing the transition from stance to swing. The timing of this transition for all three joints is properly coordinated with the end of ground contact.

The flexion period of the knee and ankle during swing last too long relative to the extension period. Observations of the simulation indicate this may be a result from the foot contacting the ground more quickly in simulation than in the animal. This earlier contact could be because the hip does not flex as fast as the other joints and does not raise the knee high enough. Another cause could be higher activations of the knee extensor during swing cause the tibia to extend faster and create early ground contact, shortening the extension period of swing.

The simulation file, data, and videos of the walking rat can be found with the on-line material here.

6.2 Puppy

6.2.1 Hind Legs

To test the control of the neural network, a support system was built to constrain the robot to planar motion (Fig. 6.3). This system consists of a Teflon covered support bar attached to the robot which slides in between two clear plastic sheets. This enables longitudinal, vertical, and pitch movements while constraining lateral, roll, and yaw. For specific testing of the hind legs, the front of the robot is tied to the bar above, and a 5 lb counterweight is hung through a pulley system and attached to the center of the robot. The robot's rear legs contact a treadmill belt that can be varied in speed while the front legs are suspended.

With the applied trained network (Section 5.4), the hamstring and ankle flexion pathway (Section 6.1.1), and the commisural inter-leg network 3.1.2, the hind legs perform sustained, alternating stepping at about 1.2 steps per second per leg, or a stepping period of .83 seconds. This stepping is able to adjust to different treadmill belt speeds, and maintains the alternating pattern when the belt is switched off. It is also able to adjust to changes in weight including the removal of the counterweight during medium speeds. A screen capture of step sequence is show in Fig. 6.4

The average MN activations, muscle tensions, and joint kinematics for 38 right and left steps with the counterweight at medium speeds can be seen in Fig. 6.5.

The walking robot had much closer to 50%-50% stance to swing duty cycle compared to the training data of 60%-40%. This transition timing was independent of belt speed, and most often occurred with the onset of stance in the other leg. This suggests that the robot's transition to swing is more strongly dependent on Ib feedback than may be true in the animal.

Average extensor MN activations have peaks which are within 10% of desired peak heights, while flexor activity peaks lower, but overall activity is more spread out than
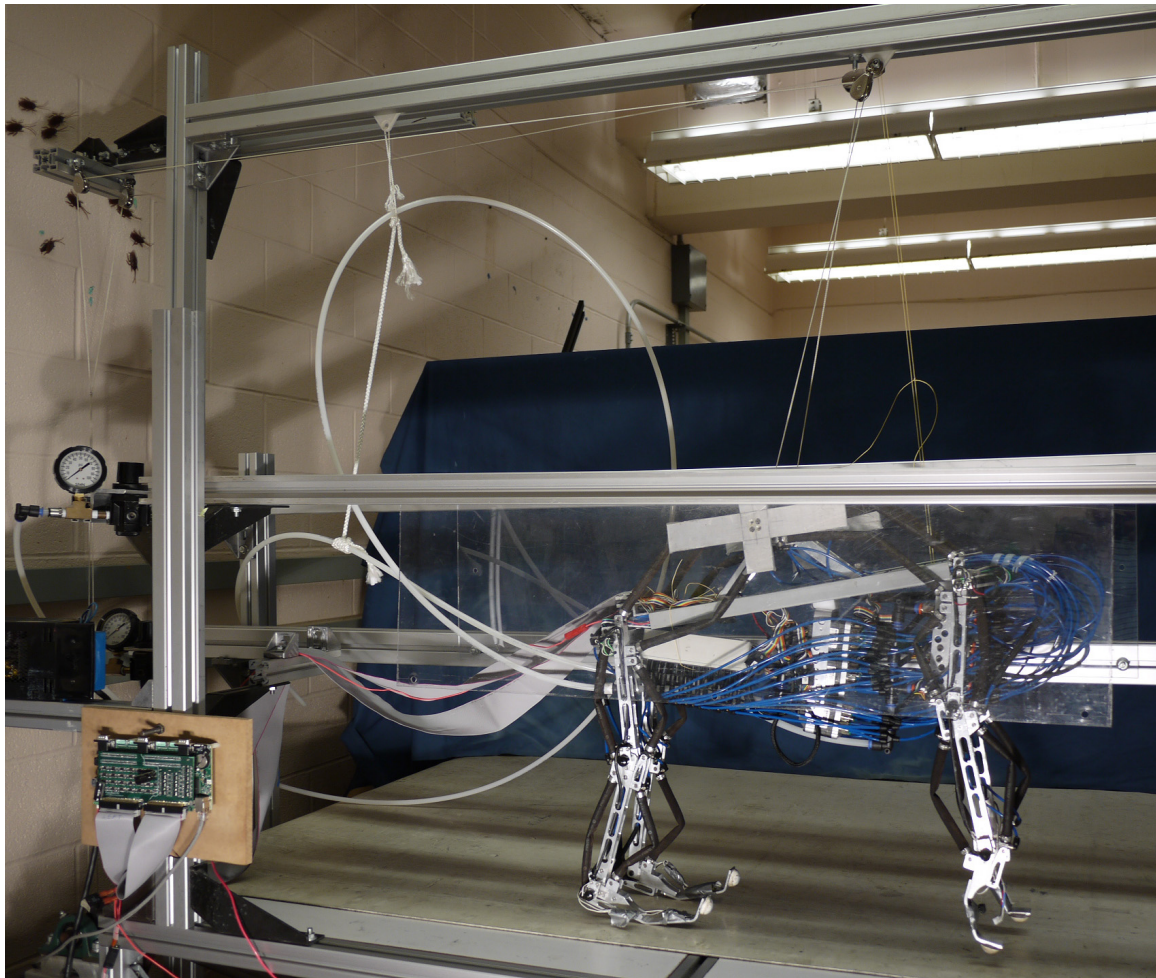
Figure 6.3: The robot is constrained to planar motion and a counterweight pulley system is used to reduce the effective weight of the robot and encourage a center position on the belt.
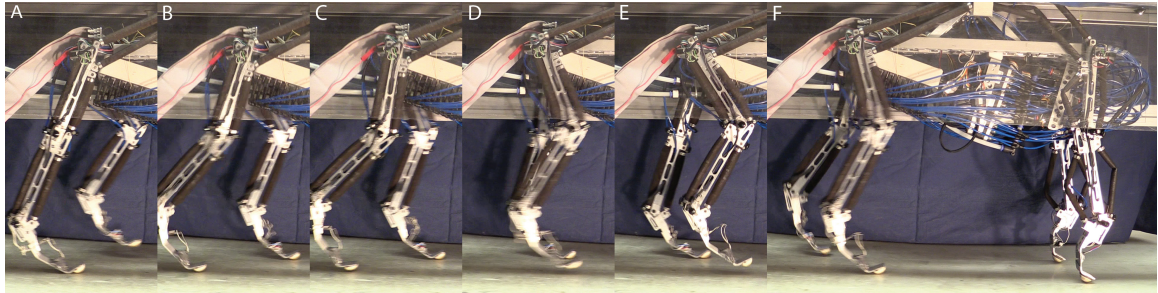
Figure 6.4: Series of screen shots demonstrating hind leg walking in Puppy. (A) Left leg is in swing and the right leg is in stance. (B) Double support phase. (C) As the left leg takes up more weight, and the right leg moves further back, it begins to enter swing. (D) While the right leg swings, the left leg bears the weight of the robot. (E) When the forward swing position is reached, the right leg begins extension. (F) When the right leg touched down and begins to bear load the left leg enters swing and the process is repeated.

desired activations. Relative timing between the joints is accurate, with hip, knee, and ankle flexors transitioning to swing at about the same time, and knee and ankle extensors activating mid-swing before the hip extensors at the beginning of stance.

Recorded Festo muscle tensions are significantly less than desired tensions, and don't seem to fully represent the MN activity and motions that occur. There are several possible explanations for this error. There are a few errors which emerge due to inaccuracies in the actuator model. The first is due to inaccuracies and delays in the model of tension in the actuators. The recorded tensions are based on lookup tables for the Festo actuators in which current angle and pressure are used to estimate the force. If this estimated force is incorrect, even if the actuator is producing the correct force, it will not appear that way in the data. Second, inaccuracies in the model based on adapting the Festo model to the linear Hill model may have created tension demands which were unachievable by the physical actuator. The actuator may have much larger, and variable delays in developing force due to the speed at which air can enter and exit the artificial muscle.

Despite these errors in the tension profiles, the robot continuously steps on the treadmill. All joint peak angles are within 5-15 degrees of accuracy. The largest errors
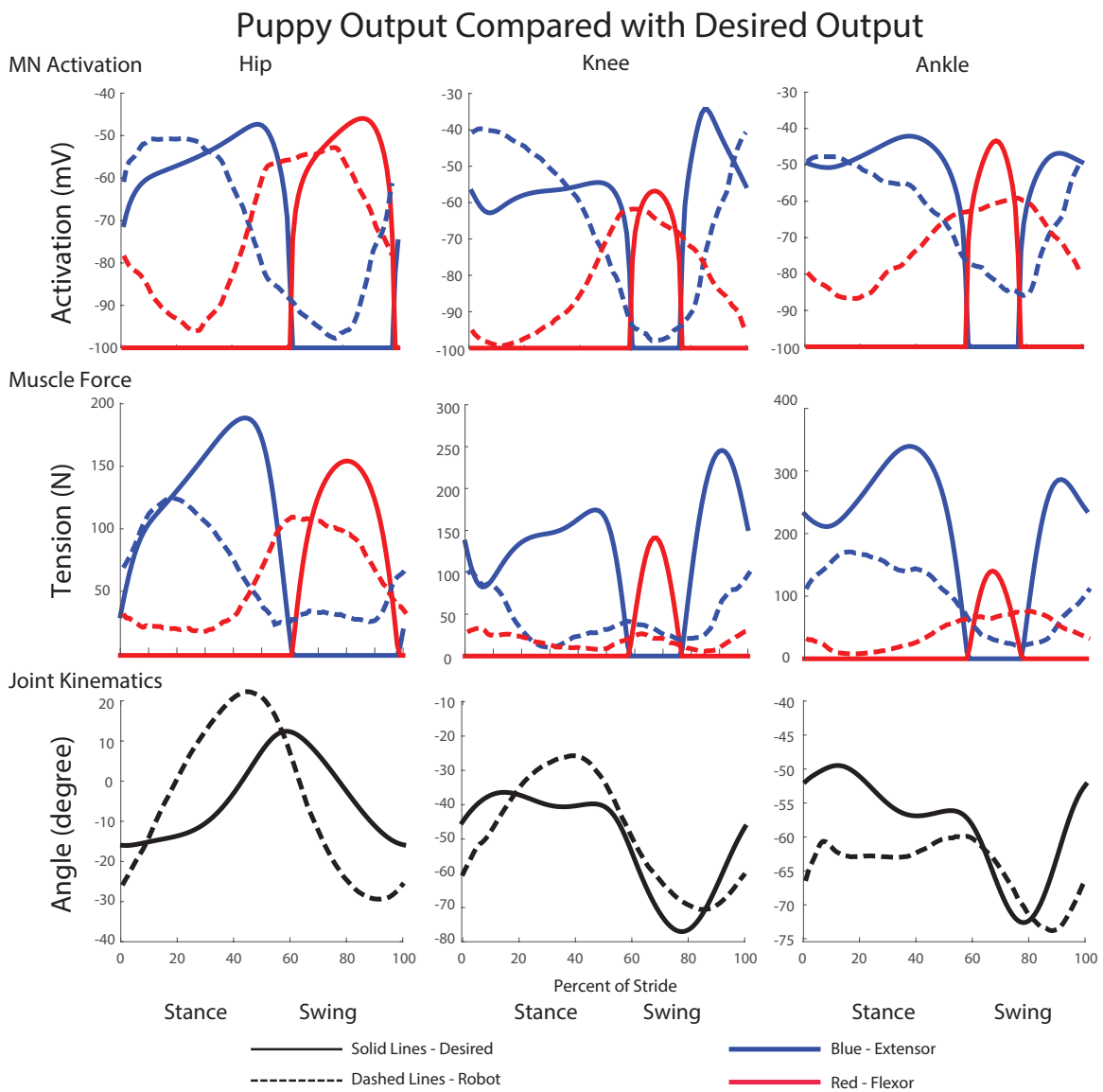
Figure 6.5: Comparison of desired motor neuron activations, muscle tensions, and joint kinematics with those produced during walking motions in the robot.

occur with the hip. Errors in hip peaks are possibly due to the delays in communication between Animatlab and Labview and the robot. The hip is the only joint to provide feedback on position, and this delay would impact the sensory signal which causes transitions in the neural system to be behind real time of the robot. The response of the robot would then be additionally delayed by the returning communication. There is no such delay built into the training of the neural system. Ankle movement was the most susceptible to changes in belt speed and counterweight.

Comparisons between the right and left leg show activations, tensions, and joint angles with similar shapes and peak amplitudes within a few percent of each other, except with a small phase delay (Fig. 6.6). One possible explanation for this asymmetry could be a result of movement in the ankle. It is noted that the left ankle maintains a more flexed position than the right, especially during stance. This difference could be a result of a problem in the robot controller at the low level, turning the MN activations into pressures in an uneven manner. Another explanation is that the controller is such that when a phase delay occurs, it continues to occur based on the overall kinematics and dynamics of the system. This could be determined through more extensive testing of the robot in different initial conditions and determining if the lag always occurs on the same side of the robot.

Observations of individual step data reveal larger variation occurring on a step by step basis. Observations of activations during a single step show sharper transitions and higher peak heights in MN activity than is noticeable in the average data. This indicates that the neural system is adapting the stride and adjusting its control continuously.

The raw data and a video of the walking robot can be found with the on-line material at http://biorobots.case.edu/hunt-dissertation-files/.
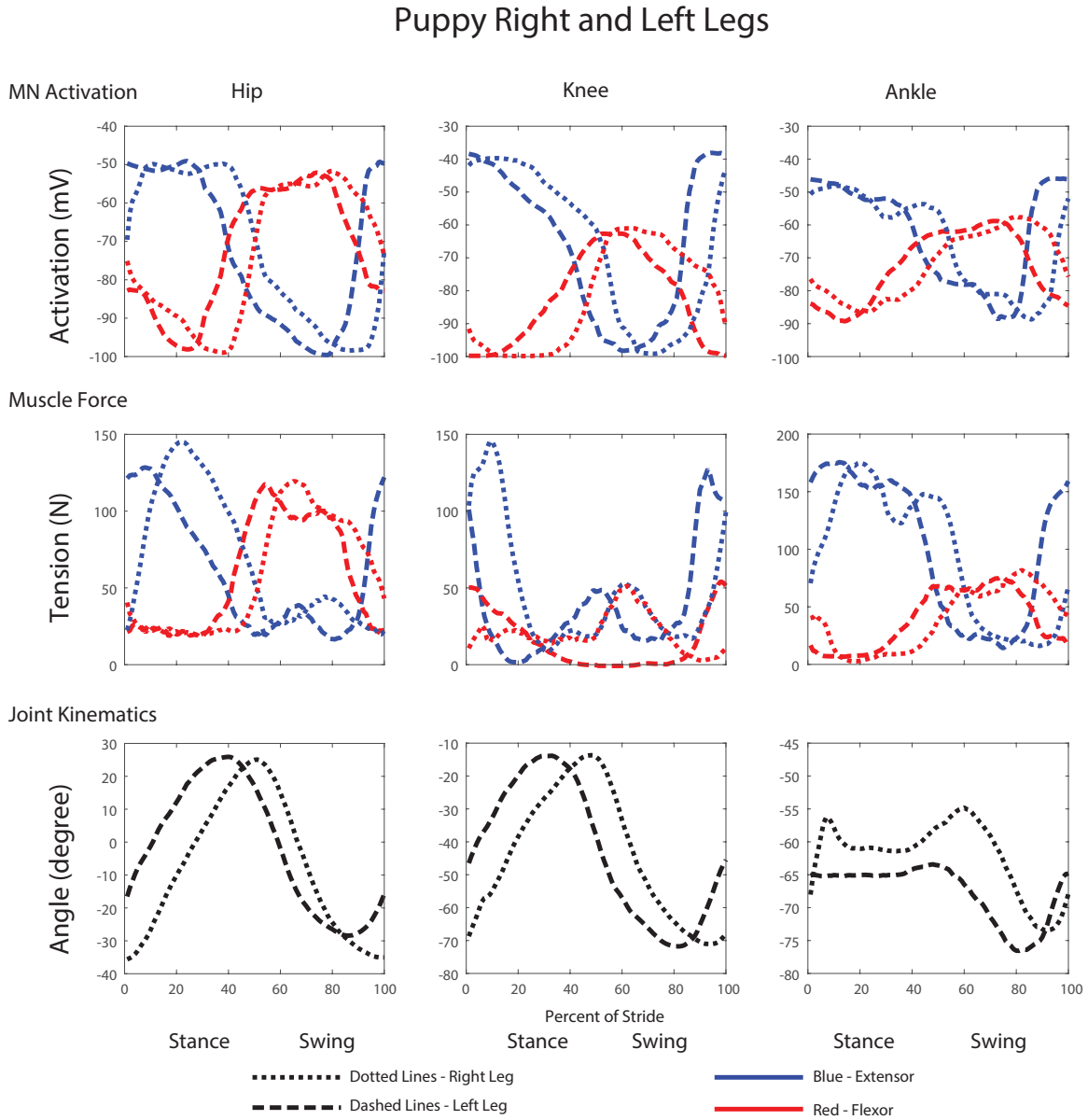
Figure 6.6: Comparison of motor neuron activations, muscle tensions, and joint kinematics between the left and right legs of the robot.

6.2.2 Forelegs

To test the forelegs, the hind part of the body was tied to the overhead support bar, with a 5 lb counterweight attached to the middle of the body. The fore legs were unable to produce continued stepping behavior, often tripping with legs stuck underneath the body. If a single leg was run, and the front of the robot was manually picked up when the leg was at the end of stance, continued stepping could occur.

Our collaborator Dr. Fischer has previously investigated on how the Z configuration of the leg maintains stability during stance and enables sufficient ground clearance during swing [Fischer and Blickhan, 2006], and help to explain why the hind legs of the robot are able to maintain stepping while the front legs are not. For the hind legs, the knee and ankle control the length of the leg while the hip provides propulsion and return motions. When swing occurs, the joints are configured such that flexion of either the knee or ankle will lift the foot away from the ground. If the foot stays on the ground longer than normal, this requires the knee and ankle of the robot to become more extended, and flexion movements from the knee at the beginning of swing cause even more foot clearance than in shorter steps.

The fore legs of the robot are configured in a Σ shape. The upper joint (shoulder) also provides the power and return stroke, while the lower two joints (elbow and wrist) are used to extend and retract the leg. However, as stance is extended, flexion at the elbow produces more longitudinal movement than vertical movement. This makes it more difficult to pick up the paw as stance continues, instead of easier as with the hind legs. This explains the importance of the scapula in quadruped locomotion, and why the data shows that the scapula joint mimics the hip joint, the shoulder mimics the knee, and the elbow mimics the ankle.

Chapter 7

Conclusions and Future Work

The work presented provides insights into how sensory feedback can be used to coordinate joints and limbs in trotting tetrapods, and represents the most complete neuro-mechanical model of mammalian intra-leg and inter-leg pathways to date. This model is developed with dynamic neurons in which structure and function play an important role. This careful attention to structure enables focused training of the network, and allows for expandability of function with additional subnetworks and connectivity.

This work is the first network in which all known mammalian hind leg coordinating influences have been combined with a central pattern generator model and applied to a mechanical model to produce forward stepping. The developed model shows the sufficiency of this neural system for timing the joints and producing the necessary kinematic motions. Additionally, I have shown how this network is readily applied to the front legs by substituting joints and pathways with their front leg equivalents, where the hip maps to the scapula, the knee maps to the shoulder, and the ankle maps to the elbow.

I seamlessly connect these networks using inter-leg pathways hypothesized from research performed on cats and mice, and show that the proposed pathways are suf-

ficient for producing coordination as is observed in the animal. I conducted deletion and pathway strength modulation experiments on the model and developed hypotheses for the roles each performs in maintaining coordination between fore and hind legs. I found that a mechanism in which elbow flexion encourages hind leg stance is sufficient and necessary to produce coordination in the proposed scheme. Additionally, the mechanism in which the end of hip flexion initiates swing of the front limb is not sufficient for producing coordination because the hind legs are not coupled contralaterally. However, its removal from the network reduces the likelihood of walking coordination in the model. Having hip and knee flexion encouraged by elbow extension is also not capable of producing symmetrical coordination by itself, however, this connection appears to be important in controlling the timing and reducing deviations in walking coordination. In fact, changes in this synapse strength produce changes in phase timing by up to 17%.

Though rats primarily locomote with a trot, many other animals use different gaits and phase timing, and these different gaits often require only slight changes in the timing between fore and hind legs, such as the difference between a trot and a gallop. An interesting area of future work could be in studying the ability of the implemented networks to produce different gait structures through modulation of synapse strengths within the network. Work done by my collaborator Nick Szczecinski has shown how descending commands can elicit gait changes in a cockroach model [Szczecinski et al., 2013] and it would be interesting if similar animal-like gait changes could be produced in the rat model.

It would also be interesting to study how additional reflex pathways could be added to the network, and how that could influence the timing and resetting of patterns within a leg as well as across legs. Pathways such as the elevator reflex if a paw were to contact and obstacle mid-swing, or an early step if a current stance leg were to slip could readily be tested with the current network.

The developed controller shows promise in several areas for being useful for robotic applications. This controller is able to coordinate four limbs in a trotting gait effectively. This gait is also adjustable, with smooth, continuous changes which affect limb coordination while maintaining individual joint coordination within the legs. The gait is also more drastically modifiable through the modulation of a single synapse coordinating the front legs, producing two different stable systems. Implementing a controller with these properties on a robotic system may enable more flexible changes in speed or even more drastic gait changes while maintaining control over individual leg functions.

For the goal of implementing such a controller, I developed a method for setting network parameters which is faster and more reliable than the hand tuning that was done during the exploration of the network architecture. This involved first determining the neural activations which are required to produce walking. For the rat, I was able to use kinematic and dynamic data collected by our collaborators in Dr. Martin Fischer's lab in Jena, Germany, and build a complete rat model based on biological data. Backtracking from desired motions for the robot to MN activations for the robot was more complicated, requiring the construction of a detailed actuator model as well as desired kinematic and dynamic data from simulations in SimMechanics.

Next, with my colaborator Nick Szczecinski, we learned more about the CPG response to different inputs and parameters, and used it to build a CPG which would respond to sensory inputs in a reliable manner. We then developed an optimization routine to set synapse parameters within the rest of the network to produce the desired MN activations which would theoretically produce walking, and applied this optimization to both the simulated rat and the robot.

The trained solutions were nearly sufficient to produce walking with the hind legs on their own, however two additional pathways were added which improved results significantly. The first pathway added activation to the knee flexors when the

hip extensors were active in order to simulate the role the hamstring muscles play during locomotion. Future work could explore replacing this pathway with an actual hamstring muscle and further expanding the muscle set from six to nine as has been done in the study of cat hind leg walking [Pearson et al., 2006]. This would complicate how desired torques are divided up into the different, redundant muscles, but could lead to some interesting results with exploration into how intra-leg CPGs might act not specifically on the individual joints, but across synergies of muscles which span multiple joints.

The Ib and Ia feedback pathways that modulate motor neuron output add significant control to the simulation and the robot. Positive Ib feedback adds additional MN activation when load is encountered on a muscle, enabling it to pull harder to overcome obstacles. Negative Ia feedback reduces MN activation when the joint is moving too quickly, slowing down stance or swing. However there is not enough available data on how these pathways affect walking to properly train and set weights off-line. It is estimated that additional low level pathways could contribute up to 30% of the forces used during walking, and further training of these pathways could prove fruitful. This further training could come from two separate sources. The first, which is being attempted right now, is to do optimization with the physics-based simulation in the loop. The optimizer could be trained on stability and or matching of animal kinematics. This would enable the system to learn low level feedback pathways which are able to make the subtle corrections necessary for the simulation to produce repetitive, self supporting walking which more closely matches the animal. The second method would require more data, using kinematics and dynamics for a series of steps in the training. These series would have different MN profiles for each step, and the optimizer could adjust the feedback pathways to better match the step by step information, and not just the average data.

When a more complete rat hind leg simulation is accomplished, the front legs

should be trained in the same manner such that a full simulation without external support could be tested. This would allow for testing of the inter-leg pathways under more realistic conditions where improper leg transitions could lead to complete failure of the system. These tests would determine if the hypothesized inter-leg pathways were sufficient for continuous, self-supported walking, or if additional pathways are needed. This would be especially interesting to observe in the context of gait transitions, where the timing between legs must be adjusted without falling over. This is currently an important area of study in robotics as there are very few robots which can dynamically change and adapt gait while moving.

In addition to training the full rat simulation, work to get Puppy to walk independently could provide additional insights into walking behaviors. First, it would be interesting to determine if the developed procedure could be applied to the front legs with new kinematics and different feedback pathways. There may prove to be a useful set of pathways and activation level which can maintain continuous walking behavior in the ⅄ configuration, we just have not found it yet. If work continues to find that the ⅄ configuration has trouble walking, it may be advantageous to redesign the front legs to be in a Z configuration and train the control network accordingly. After successful implementation of the control on the front legs, the inter-leg controller could be applied, and neural walking control could be fully explored in hardware, where physical perturbations to the system are easier to perform and observe.

Though the developed controller is able to produce walking with only feedback from muscles, animals take advantage of significantly more sensors than that while walking. It would be interesting to add more sensors to the system to see if walking can be made more robust and able to handle more diverse situations such as large perturbations or obstacle avoidance. Currently Puppy is equipped with sensors on the bottom of the feet which are able to sense force on the bottom of the foot. Inclusion of these sensors in the walking control system would add redundancy to

ground detection and would likely result in more stable behaviors.

Appendix A: Analysis of biological data: leg kinematics and dynamics of walking rats

A significant portion of this dissertation relied on the collection of animal data for both kinematic and dynamic analysis. A big thank you to Manuela Schmidt, Emanuel Andrada, and Martin Fischer at the University of Jena for providing this data and some of the analysis. Below are small experimental portions written by these collaborators.

Forelimb and hindlimb kinematics are the visible and measurable output of the nervous system in biological systems and reflect the role of muscles as mobilizers or stabilizers at a certain instant of a stride cycle. In order to test the validity of our model we analyzed the movements of leg elements and joints by means of a X-ray-based motion analysis on four adult rats. Animal care was in accordance with German animal welfare regulations, and experimental procedures were registered with the Thuringian Committee for Animal Research.

The animals were filmed while they walked along a horizontal track. High-resolution videoradiography was used to collect data in lateral projection. The X-ray system (Neurostar, Siemens AG, Erlangen, Germany) operates with high-speed cameras (SpeedCam Visario G2, Weinberger GmbH, Erlangen, Germany) with a maxi-

mum temporal resolution of 2000 Hz and a maximum spatial resolution of 1536 dpi x 1024 dpi. For our purposes a frame frequency of 500 Hz and the maximum spatial resolution were used. The movement of the leg elements was quantified by manually tracking previously defined landmarks using SimiMotion 3D (Simi Reality Motion Systems GmbH, Unterschleissheim). Scapula angle is defined relative to the horizontal plane, leg joint angles are measured on the flexion side of each joint. Temporal gait parameters and inter-leg coordination were determined with the aid of additional normal light cameras helping to identify left and right leg. The normal light cameras recorded the locomotion synchronously to the x-ray system. Further details of the method are published in [Niderschuh et al., 2015]. Data illustrated in Fig. 7 were obtained from six complete cycles. The cycles were adjusted to the same duration by means of linear interpolation before mean and standard deviation were computed.

Appendix B: OpenSim and Matlab

OpenSim is a mature modeling system that has been used extensively for modeling human movements [Delp et al., 2007], though it is not exclusive to human modeling and a rat hind leg with 23 muscles has already been built in this system [Johnson et al., 2008]. It allows the modeler to choose the desired level of fidelity vs. computational speed. The major modeling feature that OpenSim provides is flexible muscle modeling. It has the ability to model biarticulated muscles, the wrapping of muscles around bone, and more diverse joint kinematics than what is available in Animatlab.

The rat model developed in this system and seen in Fig. 1 has a reduced number of muscles compared to a live rat. However, these muscles more directly line up with the main muscle groups that are recorded during rat testing than is possible in Animatlab. The full rat with muscles was developed for two dimensional movements in SIMM and imported into OpenSim. The muscles wrap around the teal objects, allowing for much greater ranges of motion than were achievable in Animatlab. Constraints can be turned on and off, locking and unlocking joints and degrees of freedom, giving the pelvis additional support if necessary, and allowing joints to translate as well as rotate. Changes can be made to how joints move, or body components without needing to rebuild the entire model.

OpenSim 3.0 uses the Millard Acceleration Muscle model [Millard et al., 2013] as the default muscle type. In this model, more parameters than Animatlab are adjustable including the length of the tendon, which are based on biological data [John-
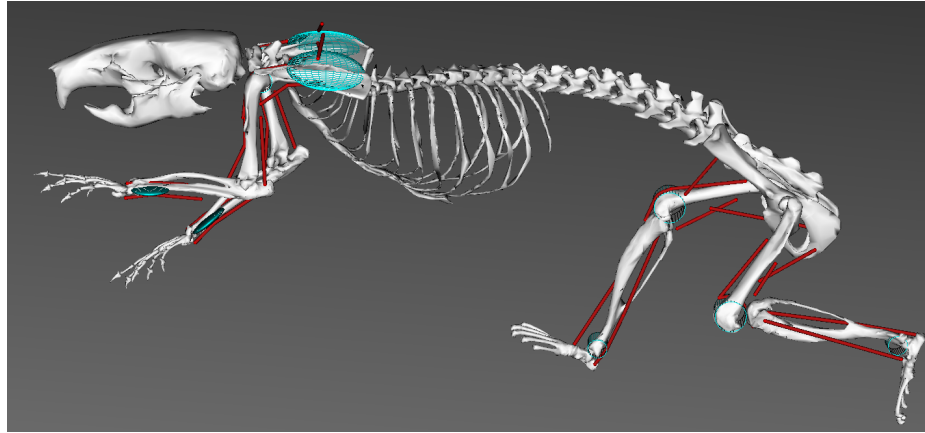
Figure 1: Skeletal model of rat assembled in OpenSim with spine flexion, and 3D joint kinematics. The red muscles wrap around the teal objects, controlling 4 joints in each front leg and 3 joints in each hind leg.

son et al., 2008] and more specific shapes of the force-length curves and force-velocity curves which are more biologically accurate than other models. And finally, the addition of the passive force-length allows for an effective limit on the length of the muscles, increasing force dramatically when muscles get stretched to their limit, similar to that of a true musculoskeletal system. The muscle model also significantly reduces vibrations during simulations compared to that of the linear-Hill muscle model.

While OpenSim was used for the mechanical modeling and simulation, Matlab and Simulink were used to model the neural system and provide integration parameters. A toolbox of neural system components were created in Simulink and can be found on-line here. This system includes different neuron types (Integrating, Integrate and spike), different synapse types (spiking and non-spiking), and muscle feedback equations (Ia, Ib, and II). Anyone wishing to do modeling of neural systems in Simulink may find this as a launching point.

Matlab/Simulink and OpenSim do not natively communicate with one another, and MEX code added to a Simulink file are needed to facilitate the communication. The original code was downloaded from SimTK.org and was provided by Misagh Mansouri [Mansouri and Reinbolt, 2012]. This code was written for OpenSim v2.3.1

and required a few days tweaking to enable communication between OpenSim 3.0 and Matlab 32 bit. I was unable to get it to work with 64 bit Matlab.

With this communication in place, a full neuromechanical simulation system was complete. A neural system was built and used to control a single leg in OpenSim. This system is also available on the website. Though I was ultimately successful in getting the entire system set up, I was still hand tweaking parameters at the time, and the slower simulation resulted in not achieving any substantial results.

Appendix C: Code, Simulations, and Videos

Copies of the Matlab and Labview code, Animatlab simulation files, raw data, and relevant videos can be found on-line at:

http://biorobots.case.edu/hunt-dissertation-files/

Bibliography

[Ahn and Thanh, 2005] Ahn, K. and Thanh, T. (2005). Nonlinear PID control to improve the control performance of the pneumatic artificial muscle manipulator using neural network. *Journal of mechanical science and technology*, 19(1):106–115.

[Akay et al., 2001] Akay, T., Bässler, U., Gerharz, P., and Büschges, A. (2001). The role of sensory signals from the insect coxa-trochanteral joint in controlling motor activity of the femur-tibia joint. *Journal of Neurophysiology*, 85(2):594.

[Akay and Büschges, 2006] Akay, T. and Büschges, A. (2006). Load signals assist the generation of movement-dependent reflex reversal in the femur-tibia joint of stick insects. *Journal of Neurophysiology*, 96(6):3532–3537.

[Akay et al., 2004] Akay, T., Haehn, S., Schmitz, J., and Büschges, A. (2004). Signals from load sensors underlie interjoint coordination during stepping movements of the stick insect leg. *Journal of Neurophysiology*, 92(1):42–51.

[Akay et al., 2006] Akay, T., McVea, D. A., Tachibana, A., and Pearson, K. G. (2006). Coordination of fore and hind leg stepping in cats on a transversely-split treadmill. *Experimental brain research. Experimentelle Hirnforschung. Expérimentation cérébrale*, 175(2):211–222.

[Akay et al., 2014] Akay, T., Tourtellotte, W. G., Arber, S., and Jessell, T. M. (2014). Degradation of mouse locomotor pattern in the absence of proprioceptive sensory feedback. *Proceedings of the National Academy of Sciences*, 111(47):16877–16882.

[Alexander, 2003] Alexander, R. M. (2003). *Alternative Land Locomotion in Principles of Animal Locomotion.*

[Andrada et al., 2013] Andrada, E., Mämpel, J., Schmidt, A., Fischer, M. S., Karguth, A., and Witte, H. (2013). From biomechanics of rats' inclined locomotion to a climbing robot. *International Journal of Design and Nature and Ecodynamics*, 8(3):191–212.

[Andrikopoulos and Nikolakopoulos, 2014] Andrikopoulos, G. and Nikolakopoulos, G. (2014). Piecewise affine modeling and constrained optimal control for a pneumatic artificial muscle. *IEEE Transactions on Industrial Electronics*, 61(2):904–916.

[Arbas and Calabrese, 1987] Arbas, E. A. and Calabrese, R. L. (1987). Ionic Conductances Underlying the Activity Control Heartbeat in the Medicinal Leech. *Journal of Neuroscience*, 7(December 1987):3945–3952.

[Aschenbeck et al., 2006] Aschenbeck, K. S., Kern, N. I., Bachmann, R. J., and Quinn, R. D. (2006). Design of a Quadruped Robot Driven by Air Muscles. *The First IEEE/RAS-EMBS International Conference on Biomedical Robotics and Biomechatronics*, pages 875–880.

[Bässler, 1974] Bässler, U. (1974). Vom femoralen Chordotonalorgan gesteuerte Reaktionen bei der Stabheuschrecke Carausius morosus: Messung der von der Tibia erzeugten Kraft im aktiven und inaktiven Tier. *Kybernetik*, 16(4):213–226.

[Bässler, 1988] Bässler, U. (1988). Functional principles of pattern generation for walking movements of stick insect forelegs: the role of the femoral chordotonal organ afferences. *Journal of Experimental Biology*, 136:125–147.

[Bässler and Büschges, 1998] Bässler, U. and Büschges, A. (1998). Pattern generation for stick insect walking movements–multisensory control of a locomotor program. *Brain Research Reviews*, 27(1):65–88.

[Beer et al., 1992] Beer, R. D., Chiel, H. J., Quinn, R. D., and Espenschied, K. S. (1992). A Distributed Neural Network Architecture for Hexapod Robot Locomotion. *Neural Computation*, 4:356–365.

[Beer et al., 1989] Beer, R. D., Chiel, H. J., and Sterling, L. (1989). Heterogeneous Neural Networks for Adaptive Behavior in Dynamic Environments. *Advances in Neural Information Processing Systems 1*, pages 577–585.

[Beer and Gallagher, 1992] Beer, R. D. and Gallagher, J. C. (1992). Evolving Dynamical Neural Networks for Adaptive Behavior. *Adaptive Behavior*, 1(1):91–122.

[Berns et al., 2001] Berns, K., Albiez, J., Kepplin, V., and Hillenbrand, C. (2001). Control of a Six-legged Robot using Fluidic Muscle.

[Bicanski et al., 2013] Bicanski, A., Ryczko, D., Knuesel, J., Harischandra, N., Charrier, V., Ekeberg, O., Cabelguen, J.-M., and Ijspeert, A. J. (2013). Decoding the mechanisms of gait generation in salamanders by combining neurobiology, modeling and robotics. *Biological cybernetics*, 107(5):545–64.

[Biewener, 2005] Biewener, A. A. (2005). Biomechanical consequences of scaling. *The Journal of experimental biology*, 208(Pt 9):1665–76.

[Blickhan, 1989] Blickhan, R. (1989). The spring-mass model for running and hopping. *Journal of biomechanics*.

[Borgmann et al., 2009] Borgmann, A., Hooper, S. L., and Büschges, A. (2009). Activation and Interaction of Central Pattern Generators in a Walking Insect. *Journal of Neuroscience*, 29(9):2972–2983.

[Boyd, 1980] Boyd, I. (1980). The isolated mammalian muscle spindle. *Trends in Neurosciences*, 3(11):258–265.

[Brooks, 1989] Brooks, R. (1989). A Robot that Walks; Emergent Behaviors from a Carefully Evolved Network. *Neural Computation*, 1(2):253–262.

[Brown, 1914] Brown, T. G. (1914). On the Nature of the Fundamental Activity of the Nergous Centres; Together with an Analysis of the Conditioning of Rhythmic Activity in Progression, and a theory of the evolution of function in the Nervous System. *Journal of Physiology - London*, (48):18–46.

[Brownstone and Bui, 2010] Brownstone, R. M. and Bui, T. V. (2010). Spinal interneurons providing input to the final common path during locomotion. *Progress in brain research*, (187):81–95.

[Bucher et al., 2003] Bucher, D., Akay, T., DiCaprio, R. A., and Büschges, A. (2003). Interjoint coordination in the stick insect leg-control system: the role of positional signaling. *Journal of Neurophysiology*, 89(3):1245–1255.

[Buchli and Ijspeert, 2008] Buchli, J. and Ijspeert, A. J. (2008). Self-organized adaptive legged locomotion in a compliant quadruped robot. *Autonomous Robots*, 25(4):331–347.

[Büschges and Borgmann, 2013] Büschges, A. and Borgmann, A. (2013). Network modularity: back to the future in motor control. *Current biology : CB*, 23(20):R936–8.

[Büschges et al., 1995] Büschges, A., Schmitz, J., and Bässler, U. (1995). Rhythmic patterns in the thoracic nerve cord of the stick insect induced by pilocarpine. *Journal of Experimental Biology*, 198(Pt 2):435–456.

[Caldwell et al., 1995] Caldwell, D. G., Medrano-Cerda, G. A., and Goodwin, M. (1995). Control of pneumatic muscle actuators. *IEEE Control Systems Magazine*, 15(1):40–48.

[Chiel and Beer, 1989] Chiel, H. and Beer, R. (1989). A lesion study of a heterogeneous artificial neural network for hexapod locomotion. *Neural Networks, 1989. IJCNN., International Joint Conference on.*

[Chou and Hannaford, 1996] Chou, C.-p. and Hannaford, B. (1996). Measurement and modeling of McKibben pneumatic artificial muscles. *IEEE Transactions on Robotics and Automation*, 12(1):90–102.

[Cofer et al., 2010] Cofer, D. W., Cymbalyuk, G., Reid, J., Zhu, Y., Heitler, W. J., and Edwards, D. H. (2010). AnimatLab: a 3D graphics environment for neuromechanical simulations. *Journal of neuroscience methods*, 187(2):280–288.

[Cohen et al., 1992] Cohen, A. H., Ermentrout, G. B., Kiemel, T., Kopell, N., Sigvardt, K. a., and Williams, T. L. (1992). Modelling of intersegmental coordination in the lamprey central pattern generator for locomotion. *Trends in neurosciences*, 15(11):434–438.

[Colborne et al., 2006] Colborne, G. R., Walker, A. M., Tattersall, A. J., and Fuller, C. J. (2006). Effect of trotting velocity on work patterns of the hind limbs of Greyhounds. *American Journal of Veterinary Research*, 67(8):1293–1298.

[Colbrunn and Nelson, 2001] Colbrunn, R. W. and Nelson, G. M. (2001). Design and control of a robotic leg with braided pneumatic actuators. *Intelligent Robots and Systems.*

[Colbrunn et al., 2001] Colbrunn, R. W., Nelson, G. M., and Quinn, R. D. (2001). Modeling of Braided Pneumatic Actuators for Robotic Control. In *International Conference on Intelligent Robots and Systems*.

[Cruse, 1990] Cruse, H. (1990). What mechanisms coordinate leg movement in walking arthropods? *Trends in Neurosciences*, 13(1990):15–21.

[Cruse and Warnecke, 1992] Cruse, H. and Warnecke, H. (1992). Coordination of the legs of a slow-walking cat. *Experimental Brain Research*, 89(1):147–156.

[Daun-Gruhn, 2010] Daun-Gruhn, S. (2010). A mathematical modeling study of inter-segmental coordination during stick insect walking. *Journal of computational neuroscience*, 30(2):255–278.

[Daun-Gruhn and Büschges, 2011] Daun-Gruhn, S. and Büschges, A. (2011). From neuron to behavior: dynamic equation-based prediction of biological processes in motor control. *Biological cybernetics*, 105(1):71–88.

[Daun-Gruhn et al., 2009] Daun-Gruhn, S., Rubin, J. E., and Rybak, I. A. (2009). Control of oscillation periods and phase durations in half-center central pattern generators: a comparative mechanistic analysis. *Journal of computational neuroscience*, 27(1):3–36.

[Daun-Gruhn and Tóth, 2010] Daun-Gruhn, S. and Tóth, T. I. (2010). An inter-segmental network model and its use in elucidating gait-switches in the stick insect. *Journal of computational neuroscience*.

[Delp et al., 2007] Delp, S. L., Anderson, F. C., Arnold, A. S., Loan, P., Habib, A., John, C. T., Guendelman, E., and Thelen, D. G. (2007). OpenSim: open-source software to create and analyze dynamic simulations of movement. *IEEE transactions on bio-medical engineering*, 54(11):1940–1950.

[Duysens et al., 2000] Duysens, J., Clarac, F., and Cruse, H. (2000). Load-regulating mechanisms in gait and posture: comparative aspects. *Physiological reviews*, 80(1):83–133.

[Duysens and Pearson, 1980] Duysens, J. and Pearson, K. G. (1980). Inhibition of flexor burst generation by loading ankle extensor muscles in walking cats. *Brain research*, 187(2):321–332.

[Dzeladini et al., 2014] Dzeladini, F., van den Kieboom, J., and Ijspeert, A. J. (2014). The contribution of a central pattern generator in a reflex-based neuromuscular model. *Frontiers in Human Neuroscience*, 8(June):1–18.

[Ekeberg, 1993] Ekeberg, O. (1993). A combined neuronal and mechanical model of fish swimming. *Biological Cybernetics*, 69(5-6):363–374.

[Ekeberg et al., 2004] Ekeberg, O., Blümel, M., and Büschges, A. (2004). Dynamic simulation of insect walking. *Arthropod structure & development*, 33(3):287–300.

[Ekeberg and Grillner, 1999] Ekeberg, O. and Grillner, S. (1999). Simulations of neuromuscular control in lamprey swimming. *Philosophical Transactions of the Royal Society of London - Series B: Biological Sciences*, 354(1385):895–902.

[Ekeberg and Pearson, 2005] Ekeberg, O. and Pearson, K. G. (2005). Computer simulation of stepping in the hind legs of the cat: an examination of mechanisms regulating the stance-to-swing transition. *Journal of neurophysiology*, 94(6):4256–4268.

[ElBasiouny et al., 2010] ElBasiouny, S. M., Schuster, J. E., and Heckman, C. J. (2010). Persistent inward currents in spinal motoneurons: important for normal function but potentially harmful after spinal cord injury and in amyotrophic lateral sclerosis. *Clinical neurophysiology : official journal of the International Federation of Clinical Neurophysiology*, 121(10):1669–79.

[Espenschied et al., 1996] Espenschied, K. S., Quinn, R. D., Beer, R. D., and Chiel, H. J. (1996). Biologically based distributed control and local reflexes improve rough terrain locomotion in a hexapod robot. *Robotics and Autonomous Systems*, 18(1-2):59–64.

[Farley et al., 1998] Farley, C. T., Houdijk, H. H., Van Strien, C., and Louie, M. (1998). Mechanism of leg stiffness adjustment for hopping on surfaces of different stiffnesses. *Journal of applied physiology (Bethesda, Md. : 1985)*, 85(3):1044–55.

[Ferris et al., 1999] Ferris, D. P., Liang, K., and Farley, C. T. (1999). Runners adjust leg stiffness for their first step on a new running surface. *Journal of biomechanics*, 32(March):787–794.

[Fischer, 1999] Fischer, M. S. (1999). Kinematics, EMG, and inverse dynamics of the Therian forelimb - a synthetic approach. *Zoologischer Anzeiger*, 238(1-2):41–54.

[Fischer and Blickhan, 2006] Fischer, M. S. and Blickhan, R. (2006). The trisegmented limbs of therian mammals: kinematics, dynamics, and self-stabilizationa review. *Journal of Experimental Zoology Part A: Comparative Experimental Biology*, 305(11):935–952.

[Fischer and Lilje, 2011] Fischer, M. S. and Lilje, K. E. (2011). *Dogs in Motion*.

[Fischer et al., 2002] Fischer, M. S., Schilling, N., Schmidt, M., Haarhaus, D., and Witte, H. (2002). Basic limb kinematics of small therian mammals. *The Journal of experimental biology*, 205(Pt 9):1315–1338.

[Flannigan et al., 1998] Flannigan, W. C., Nelson, G. M., and Quinn, R. D. (1998). Locomotion controller for a crab-like robot. In *Proceedings. 1998 IEEE International Conference on Robotics and Automation (Cat. No.98CH36146)*, volume 1, pages 152–156. Ieee.

[Gallagher et al., 1996] Gallagher, J. C., Beer, R. D., Espenschied, K. S., and Quinn, R. D. (1996). Application of evolved locomotion controllers to a hexapod robot. *Robotics and Autonomous Systems*, 19:95–103.

[Gay et al., 2013] Gay, S., Santos-Victor, J., and Ijspeert, A. J. (2013). Learning robot gait stability using neural networks as sensory feedback function for Central Pattern Generators. *2013 IEEE/RSJ International Conference on Intelligent Robots and Systems*, pages 194–201.

[Gaylord, 1958] Gaylord, R. (1958). Fluid Actuated Motor System and Stroking Device.

[Górska et al., 1999] Górska, T., Zmysowski, W., and Majczyski, H. (1999). Overground locomotion in intact rats: interlimb coordination, support patterns and support phases duration. *Acta neurobiologiae experimentalis*, 59(2):131–44.

[Goslow et al., 1981] Goslow, G. E., Seeherman, H. J., Taylor, C. R., McCutchin, M. N., and Heglund, N. C. (1981). Electrical activity and relative length changes of dog limb muscles as a function of speed and gait. *The Journal of experimental biology*, 94:15–42.

[Hägglund et al., 2013] Hägglund, M., Dougherty, K. J., Borgius, L., Itohara, S., Iwasato, T., and Kiehn, O. (2013). Optogenetic dissection reveals multiple rhythmogenic modules underlying locomotion. *Proceedings of the National Academy of Sciences of the United States of America*, 110(28):11589–94.

[Ham et al., 2009] Ham, V. R., Sugar, T. G., Vanderborght, B., Hollander, K. W., and Lefeber, D. (2009). Compliant actuator designs: Review of actuators with passive adjustable compliance/controllable stiffness for robotic applications. *IEEE Robotics and Automation Magazine*, 16(September):81–94.

[Hess and Büschges, 1999] Hess, D. and Büschges, A. (1999). Role of Proprioceptive Signals From an Insect Femur-Tibia Joint in Patterning Motoneuronal Activity of an Adjacent Leg Joint. *Journal of Neurophysiology*, 81(4):1856–1865.

[Hooper, 2012] Hooper, S. L. (2012). Body size and the neural control of movement. *Current Biology*, 22(9):R318—-R322.

[Hooper et al., 2009] Hooper, S. L., Guschlbauer, C., Blümel, M., Rosenbaum, P., Gruhn, M., Akay, T., and Büschges, A. (2009). Neural control of unloaded leg posture and of leg swing in stick insect, cockroach, and mouse differs from that in larger animals. *The Journal of neuroscience : the official journal of the Society for Neuroscience*, 29(13):4109–4119.

[Hošovský and Havran, 2012] Hošovský, A. and Havran, M. (2012). Dynamic Modeling of One Degree of Freedom Pneumatic Muscle-Based. *Tehnicki vjesnik*, 19:673–681.

[Hunt et al., 2014] Hunt, A. J., Schmidt, M., Fischer, M. S., and Quinn, R. D. (2014). Neuromechanical Simulation of an Inter-leg Controller for Tetrapod Coordination. In *Biomimetic and Biohybrid Systems*, volume 3, pages 142–153.

[Hunt et al., 2015a] Hunt, A. J., Schmidt, M., Fischer, M. S., and Quinn, R. D. (2015a). A biologically based neural system coordinates the joints and legs of a tetrapod. *Bioinspiration & Biomimetics*, 10(5):055004.

[Hunt et al., 2015b] Hunt, A. J., Szczecinski, N. S., Andrada, E., Fischer, M. S., and Quinn, R. D. (2015b). Using Animal Data and Neural Dynamics to Reverse Engineer a Neuromechanical Rat Model. In *Biomimetic and Biohybrid Systems*.

[Ijspeert, 2001] Ijspeert, A. J. (2001). A connectionist central pattern generator for the aquatic and terrestrial gaits of a simulated salamander. *Biological Cybernetics*, 84(5):331–348.

[Ijspeert, 2008] Ijspeert, A. J. (2008). Central pattern generators for locomotion control in animals and robots: a review. *Neural networks : the official journal of the International Neural Network Society*, 21(4):642–653.

[Ijspeert et al., 1999] Ijspeert, A. J., Hallam, J., and Willshaw, D. (1999). Evolving swimming controllers for a simulated lamprey with inspiration from neurobiology. *Adaptive Behavior*, 7(2):151–172.

[Jami, 1992] Jami, L. (1992). Golgi tendon organs in mammalian skeletal muscle: functional properties and central actions. *Physiological reviews*, 72(3):623–666.

[Jankowska, 1992] Jankowska, E. (1992). Interneuronal relay in spinal pathways from proprioceptors. *Progress in neurobiology*, 38(4):335–378.

[Jankowska, 2008] Jankowska, E. (2008). Spinal interneuronal networks in the cat: Elementary components. *Brain Research Reviews*, 57(1):46–55.

[Jindrich and Full, 2002] Jindrich, D. L. and Full, R. J. (2002). Dynamic stabilization of rapid hexapedal locomotion. *The Journal of experimental biology*, 205(Pt 18):2803–2823.

[Johnson et al., 2008] Johnson, W. L., Jindrich, D. L., Roland, R. R., and Edgerton, V. R. (2008). A three-dimensional model of the rat hindlimb: musculoskeletal geometry and muscle moment arms. *Journal of Biomechanics*, 41(3):610–619.

[Kelasidi et al., 2011] Kelasidi, E., Andrikopoulos, G., Nikolakopoulos, G., and Manesis, S. (2011). A survey on pneumatic muscle actuators modeling. *2011 IEEE International Symposium on Industrial Electronics*, pages 1263–1269.

[Kiebel et al., 2008] Kiebel, S. J., Daunizeau, J., and Friston, K. J. (2008). A hierarchy of time-scales and the brain. *PLoS Computational Biology*, 4(11).

[Kingsley et al., 2006] Kingsley, D. A., Quinn, R. D., and Ritzmann, R. E. (2006). A Cockroach Inspired Robot With Artificial Muscles. *2006 IEEE/RSJ International Conference on Intelligent Robots and Systems*, pages 1837–1842.

[Klein and Lewis, 2012] Klein, T. J. and Lewis, M. A. (2012). A physical model of sensorimotor interactions during locomotion. *Journal of neural engineering*, 9(4):46011.

[Kuznetsov, 1995] Kuznetsov, A. N. (1995). Energetical Profit of the Third Segment in Parasagittal Legs. *Journal Of Theoretical Biology*, 172(1):95–105.

[Loeb et al., 1999] Loeb, E., Brown, E., and Cheng, J. (1999). A hierarchical foundation for models of sensorimotor control. *Experimental Brain Research*, pages 1–18.

[Mansouri and Reinbolt, 2012] Mansouri, M. and Reinbolt, J. a. (2012). A platform for dynamic simulation and control of movement based on OpenSim and MATLAB. *Journal of Biomechanics*, 45(8):1517–1521.

[Markin et al., 2010] Markin, S. N., Klishko, A. N., Shevtsova, N. A., Lemay, M. A., Prilutsky, B. I., and Rybak, I. A. (2010). Afferent control of locomotor CPG: insights from a simple neuromechanical model. *Annals of the New York Academy of Sciences*, 1198:21–34.

[McCrea and Rybak, 2008] McCrea, D. A. and Rybak, I. A. (2008). Organization of mammalian locomotor rhythm and pattern generation. *Brain research reviews*, 57(1):134–146.

[McMahon and Cheng, 1990] McMahon, T. A. and Cheng, G. C. (1990). The mechanics of running: how does stiffness couple with speed? *Journal of biomechanics*, 23 Suppl 1:65–78.

[McVea et al., 2005] McVea, D. A., Donelan, J. M., Tachibana, A., and Pearson, K. G. (2005). A role for hip position in initiating the swing-to-stance transition in walking cats. *Journal of neurophysiology*, 94(5):3497–508.

[Meijer et al., 1998] Meijer, K., Grootenboer, H., Koopman, H., van der Linden, B., and Huijing, P. (1998). A Hill type model of rat medial gastrocnemius muscle that accounts for shortening history effects. *Journal of Biomechanics*, 31(6):555–563.

[Meyrand et al., 1994] Meyrand, P., Simmers, J., and Moulins, M. (1994). Dynamic construction of a neural network from multiple pattern generators in the lobster stomatogastric nervous system. *The Journal of neuroscience : the official journal of the Society for Neuroscience*, 14(2):630–644.

[Millard et al., 2013] Millard, M., Uchida, T., Seth, A., and Delp, S. L. (2013). Flexing computational muscle: modeling and simulation of musculotendon dynamics. *Journal of biomechanical engineering*, 135(2):021005.

[Minh et al., 2012] Minh, T. V., Kamers, B., Ramon, H., and Van Brussel, H. (2012). Modeling and control of a pneumatic artificial muscle manipulator joint Part I: Modeling of a pneumatic artificial muscle manipulator joint with accounting for creep effect. *Mechatronics*, 22(7):923–933.

[Mortin and Stein, 1989] Mortin, L. I. and Stein, P. S. (1989). Spinal cord segments containing key elements of the central pattern generators for three forms of scratch reflex in the turtle. *The Journal of neuroscience : the official journal of the Society for Neuroscience*, 9(7):2285–2296.

[Nakatsu et al., 2014] Nakatsu, S., Rosendo, A., Shimizu, M., and Hosoda, K. (2014). Realization of Three-dimensional Walking of a Cheetah-modeled Bio-inspired Quadruped Robot. pages 779–784.

[Nelder and Mead, 1965] Nelder, J. and Mead, R. (1965). A simplex method for function minimization. *Computing Journal*, pages 308–313.

[Niderschuh et al., 2015] Niderschuh, S., Witte, H., and Schmidt, M. (2015). The role of vibrissal sensing in forelimb position control during travelling locomotion in the rat (Rattus norvegicus, Redentia). *Zoology*, 118(1):51–62.

[Paskarbeit et al., 2015] Paskarbeit, J., Schilling, M., Schmitz, J., and Schneider, A. (2015). Obstacle crossing of a real, compliant robot based on local evasion movements and averaging of stance heights using singular value decomposition. In *IEEE ICRA*.

[Pearson, 2008] Pearson, K. G. (2008). Role of sensory feedback in the control of stance duration in walking cats. *Brain research reviews*, 57(1):222–227.

[Pearson et al., 2006] Pearson, K. G., Ekeberg, O., and Büschges, A. (2006). Assessing sensory function in locomotor systems using neuro-mechanical simulations. *Trends in neurosciences*, 29(11):625–631.

[Pratt and Williamson, 1995] Pratt, G. A. and Williamson, M. M. (1995). Series elastic actuators. In *Intelligent Robots and Systems 95.'Human Robot Interaction and Cooperative Robots', Proceedings. 1995 IEEE/RSJ International Conference on*, volume 1, pages 399–406. IEEE.

[Prochazka et al., 1997] Prochazka, A., Gillard, D., and Bennett, D. J. (1997). Positive force feedback control of muscles. *Journal of neurophysiology*, 77(6):3226–3236.

[Raibert et al., 2008] Raibert, M., Blankespoor, K., Nelson, G. M., and Playter, R. (2008). BigDog , the Rough-Terrain Quadruped Robot. In *17th World Congress, The International Federation of Automatic Control*, pages 6–9.

[Rollinson et al., 2013] Rollinson, D., Ford, S., Brown, B., and Choset, H. (2013). Design and Modeling of a Series Elastic Element for Snake Robots. In *ASME Dynamic Systems and Control*.

[Rutter et al., 2007] Rutter, B. L., Mu, L., Ritzmann, R. E., and Quinn, R. D. (2007). Transforming Insect Electromyograms into Pneumatic Muscle Control. *Neurobiology*, (April):10–14.

[Rutter et al., 2011] Rutter, B. L., Taylor, B. K., Bender, J. A., Blümel, M., Lewinger, W. A., Ritzmann, R. E., and Quinn, R. D. (2011). Descending commands to an insect leg controller network cause smooth behavioral transitions. *Intelligent Robots and Systems (IROS 2011)*.

[Rybak et al., 2013] Rybak, I. a., Shevtsova, N. a., and Kiehn, O. (2013). Modelling genetic reorganization in the mouse spinal cord affecting left-right coordination during locomotion. *The Journal of physiology*, 591(Pt 22):5491–508.

[Sarosi, 2012] Sarosi, J. (2012). New approximation algorithm for the force of Fluidic Muscles. *2012 7th IEEE International Symposium on Applied Computational Intelligence and Informatics (SACI)*, pages 229–233.

[Schilling et al., 2013a] Schilling, M., Hoinville, T., Schmitz, J., and Cruse, H. (2013a). Walknet, a bio-inspired controller for hexapod walking. *Biological cybernetics*, 107(4):397–419.

[Schilling et al., 2013b] Schilling, M., Paskarbeit, J., Hoinville, T., Hüffmeier, A., Schneider, A., Schmitz, J., and Cruse, H. (2013b). A hexapod walker using a heterarchical architecture for action selection. *Frontiers in Computational Neuroscience*, 7(September):1–17.

[Schmitz, 1986] Schmitz, J. (1986). Properties of the feedback system controlling the coxa-trochanter joint in the stick insect carausius morosus. *Biological Cybernetics*, 55:35–42.

[Semini, 2010] Semini, C. (2010). HyQ - Design and Development of a Hydraulically Actuated Quadruped Robot. *Darwin*, (April):210.

[Seok et al., 2015] Seok, S., Wang, A., Yee, M., Chuah, M., Hyun, D. J., Lee, J., Otten, D. M., Lang, J. H., and Kim, S. (2015). Design Principles for Energy-Efficient Legged Locomotion and Implementation on the MIT Cheetah Robot. 20(3):1117–1129.

[Szczecinski et al., 2013] Szczecinski, N. S., Brown, A. E., Bender, J. A., Quinn, R. D., and Ritzmann, R. E. (2013). A Neuromechanical Simulation of Insect Walking and Transition to Turning of the Cockroach Blaberus discoidalis. *Biological cybernetics*.

[Szczecinski et al., 2014] Szczecinski, N. S., Martin, J. P., Quinn, R. D., and Ritzmann, R. E. (2014). Modeling Mantis Prey Tracking with Head, Prothoracic, and Thoracic Movements. In *International Congress of Neuroethology*.

[Szepe, 2011] Szepe, T. (2011). Accurate force function approximation for pneumatic artificial muscles. *3rd IEEE International Symposium on Logistics and Industrial Informatics*, (1):127–132.

[Talpalar et al., 2013] Talpalar, A. E., Bouvier, J., Borgius, L., Fortin, G., Pierani, A., and Kiehn, O. (2013). Dual-mode operation of neuronal networks involved in left-right alternation. *Nature*, 500(7460):85–8.

[Thorson and Caldwell, 2011] Thorson, I. and Caldwell, D. (2011). A nonlinear series elastic actuator for highly dynamic motions. In *IEEE International Conference on Intelligent Robots and Systems*, pages 390–394.

[Ting et al., 1994] Ting, L. H., Blickhan, R., and Full, R. J. (1994). Dynamic and static stability in hexapedal runners. *The Journal of experimental biology*, 197:251–69.

[Tondu and Lopez, 2000] Tondu, B. and Lopez, P. (2000). Modeling and control of McKibben artificial muscle robot actuators. *Control Systems, IEEE*, pages 15–38.

[Tóth et al., 2012] Tóth, T. I., Knops, S., and Daun-Gruhn, S. (2012). A neurome-chanical model explaining forward and backward stepping in the stick insect. *Journal of neurophysiology*, 107(12):3267–3280.

[Tryba et al., 2006] Tryba, A. K., Peña, F., and Ramirez, J.-M. (2006). Gasping activity in vitro: a rhythm dependent on 5-HT2A receptors. *The Journal of neuroscience : the official journal of the Society for Neuroscience*, 26(10):2623–2634.

[Tytell et al., 2011] Tytell, E., Holmes, P., and Cohen, A. H. (2011). Spikes alone do not behavior make: why neuroscience needs biomechanics. *Current opinion in neurobiology*, pages 1–7.

[Van Damme et al., 2009] Van Damme, M., Vanderborght, B., Verrelst, B., Van Ham, R., Daerden, F., and Lefeber, D. (2009). Proxy-based Sliding Mode Control of a Planar Pneumatic Manipulator. *The International Journal of Robotics Research*, 28(2):266–284.

[Vanderborght et al., 2008] Vanderborght, B., Van Ham, R., Verrelst, B., Van Damme, M., and Lefeber, D. (2008). Overview of the Lucy Project: Dynamic Stabilization of a Biped Powered by Pneumatic Artificial Muscles.

[von Twickel et al., 2011] von Twickel, A., Büschges, A., and Pasemann, F. (2011). Deriving neural network controllers from neuro-biological data: implementation of a single-leg stick insect controller. *Biological cybernetics*, 104(1-2):95–119.

[Walter, 1950] Walter, G. W. (1950). An electro-mechanical animal. *Dialectica*, 4(3):206–213.

[Webster et al., 2014] Webster, V. A., Leibach, R., Hunt, A. J., Bachmann, R. J., and Quinn, R. D. (2014). Design and control of a tunable compliance actuator. In *Biomimetic and Biohybrid Systems*, volume 8608 LNAI, pages 344–355.

[Witte et al., 2002] Witte, H., Biltzinger, J., Hackert, R., Schilling, N., Schmidt, M., Reich, C., and Fischer, M. S. (2002). Torque patterns of the limbs of small therian mammals during locomotion on flat ground. *The Journal of experimental biology*, 205(Pt 9):1339–1353.

[Witte et al., 2001] Witte, H., Hackert, R., Lilje, K., Schilling, N., Voges, D., Klauer, G., Ilg, W., Albiez, J., Seyfarth, A., Germann, D., Hiller, M., Dillmann, R., and Fischer, M. S. (2001). Transfer of biological principles into the construction of quadruped walking machines. *Proceedings of the Second International Workshop on Robot Motion and Control. RoMoCo'01 (IEEE Cat. No.01EX535)*, pages 245–249.

[Zajac, 1989] Zajac, F. E. (1989). Muscle and tendon: properties, models, scaling, and application to biomechanics and motor control. *Critical reviews in biomedical engineering*.

[Zakotnik et al., 2006] Zakotnik, J., Matheson, T., and Dürr, V. (2006). Co-contraction and passive forces facilitate load compensation of aimed limb movements. *The Journal of neuroscience : the official journal of the Society for Neuroscience*, 26(19):4995–5007.

[Zhong et al., 2012] Zhong, G., Shevtsova, N. A., Rybak, I. A., and Harris-Warrick, R. M. (2012). Neuronal activity in the isolated mouse spinal cord during spon-

taneous deletions in fictive locomotion: insights into locomotor central pattern generator organization. *The Journal of physiology*, 590(Pt 19):4735–59.

[Zill et al., 2004] Zill, S. N., Schmitz, J., and Büschges, A. (2004). Load sensing and control of posture and locomotion. *Arthropod structure & development*, 33(3):273–286.